République Algérienne Démocratique et Populaire
Ministère de l'Enseignement Supérieur et de la Recherche Scientifique
Université Ahmed Draïa Adrar
Faculté des Sciences et de la Technologie
Département des Sciences et Technologie

THÈSE

En vue de l'obtention du diplôme de Doctorat LMD en génie électrique

Option : Commande Électrique

Présentée Par : **BELBALI Abdelkarim**

Thème

Réduction des ondulations du couple appliqué au moteur asynchrone par des commandes avancées

---

Soutenu publiquement le : 01/06/2023, **Devant le jury composé de :**

Pr. Hamouda Messaoud	Président	Université d'Adrar
Pr. Makhloufi Salim	Rapporteur	Université d'Adrar
Dr. Yaichi Ibrahim	Examinateur	Université d'Adrar
Dr. Mansouri Smaïl	Examinateur	Université d'Adrar
Dr. Lachtar Salah	Examinateur	URERMS-Adrar

2022/2023

People's Democratic Republic of Algeria
Ministry of Higher Education and Scientific Research
University of Ahmed Draia - Adrar
Faculty of Science and Technology
Department of Science and Technology

Thesis for obtaining the LMD doctorate in electrical engineering

Option: Electrical Control

***Presented by*:** Mr. BELBALI Abdelkarim

Thème

Reduction of torque ripples applied to the asynchronous motor by advanced controls

---

Presented in: 01/06/2023, **In front of the jury composed from:**

Pr. Hamouda Messaoud	Chairman	Adrar University
Pr. Mekhloufi Salim	Supervisor	Adrar University
Pr. Yaichi Ibrahim	Examiner	Adrar University
Pr. Mansouri Smaïl	Examiner	Adrar University
Pr. Lachtar Salah	Examiner	URERMS-Adrar

2022/2023

بسم الله الرحمن الرحيم

وما توفيقي إلا بالله

صدق الله العظيم

Dedication

*First, I would like to thank **ALLAH** for his help and the courage he gave me during the difficulties met in my years of study, as well as the stamina to finish this thesis.*

I dedicate this modest work to my mother and father's symbols of affection and love, who sacrificed all their time for my happiness and my success.

To all my friends and colleagues and to all those I love.

Abdelkarim belbali.

إهداء

*أولاً، أود أن أشكر **الله** على نعمه والقدرة التي منا علي بها لأجتاز الصعوبات التي واجهتها في سنوات دراستي، وكذلك القدرة على التحمل لإنهاء هذه الأطروحة*

أهدي هذا العمل المتواضع لرموز المودة والحب لأمي وأبي، الذين ضحوا بكل وقتهم من أجل سعادتي ونجاحي

إلى كل أصدقائي وزملائي ولكل من أحبهم

عبد الكريم بلبالي

Acknowledgments

*My sincere thanks go to **Pr. Makhloufi Salim**, the supervisor of this project whose experiences and ideas as well as his valuable advice were very useful for the development of this thesis for a Doctoral degree.*

*I want to express my deep gratitude to **Pr.Hammouda Messaoud** Teacher at UNIVERCITE D'ADRAR, who agreed to chair this jury, Mr. Yaichi Ibrahim, **Mr. Mansouri Smaïl**, and **Mr. Lachtar Salah** for accepting to examine my thesis. I would like to thank the laboratory directors; **Pr. Hamouda Messaoud** (LDDI lab director), and **Mr. Pr. Kalloum Slimane** (LEESI lab director) for providing me with the whole means to do this work.*

My sincere thanks also go to all those who participated from near or far in my formation and to all those who enriched me with their knowledge.

Résumé

La machine asynchrone est très utilisée dans les processus industriels grâce à sa simplicité de fabrication est son faible coût. Néanmoins la commande de cette machine est difficile à cause des couplages qui existent entre les grandeurs qui décrivent son comportement. Ceci rend les commandes classique peut performantes est inadaptées pour cette machine. Plusieurs solutions ont été proposées pour la commande de la machine asynchrone comme la commande par orientation du flux, la commande directe du couple ou des variantes améliorées de celle–ci. Cependant ces commandes présentes des inconvenants comme la variation de la fréquence de commutation et des ondulations qui apparaissent sur le couple appliqué à la machine. Récemment, le développement de commandes de moteurs électriques capables de fournir un couple fort avec des ondulations faibles, a gagné en importance surtout pour les applications d'entraînement direct, telles que les machines-outils, les convoyeurs, les ascenseurs, etc. Des commandes avancées comme DTC-SVPWM ont été proposées pour la réduction des ondulations du couple du moteur, mais les résultats ne sont pas toujours très satisfaisant et la recherche dans ce domaines est toujours ont cours. Le but de ce travail de cette thèse est de contribution au développement de commandes DTC-SVPWM pour la réduction des ondulations du couple du moteur asynchrone.

Mots clé : La machine asynchrone, ondulations du couple, DTC-SVPWM

Abstract

The induction machine is widely used in industrial processes thanks to its simplicity of manufacture and low cost. Nevertheless the control of this machine is difficult because of the couplings that exist between the quantities that describe its behavior. This makes the conventional controls can perform is unsuitable for this machine. Several solutions have been proposed for the control of the asynchronous machine such as flow orientation control, direct torque control or improved variants of it. However, these commands have unseemly effects such as the variation of the switching frequency and ripples that appear on the torque applied to the machine. Recently, the development of electric motor controls capable of providing high torque with low ripples, has gained importance especially for direct drive applications, such as machine tools, conveyors, elevators, etc. advanced controls like DTC-SVPWM have been proposed for the reduction of motor torque ripples, but the results are still not very satisfactory and research in this area is still ongoing. The aim of this thesis topic is to contribute to the development of DTC-SVPWM controls for the reduction of induction motor torque ripples.

Keywords: asynchronous machine, torque ripples, DTC-SVPWM

الملخص

تستخدم الآلة غير المتزامنة على نطاق واسع في العمليات الصناعية بفضل بساطتها في التصنيع وتكلفتها المنخفضة. ومع ذلك ، فإن التحكم في هذه الآلة صعب بسبب أدوات التوصيل الموجودة بين الكميات التي تصف سلوكها. هذا يجعل أدوات التحكم التقليدية غير فعالة وغير مناسبة لهذه الماكينة. تم اقتراح العديد من الحلول للتحكم في الماكينة غير المتزامنة مثل التحكم في اتجاه التدفق أو التحكم المباشر في عزم الدوران أو المتغيرات المحسنة منه. ومع ذلك ، فإن عناصر التحكم هذه تقدم عيوبًا مثل اختلاف تردد التبديل والتموجات التي تظهر على عزم الدوران المطبق على الجهاز. في الآونة الأخيرة ، اكتسب تطوير أدوات التحكم في المحرك الكهربائي القادرة على توفير عزم دوران مرتفع مع تموجات منخفضة ، أهمية خاصة لتطبيقات القيادة المباشرة ، مثل أدوات الماكينة ، والناقلات ، والمصاعد ، وما إلى ذلك ، وقد تم اقتراح عناصر تحكم متقدمة مثل DTC-SVPWM لتقليل تموجات عزم دوران المحرك ، لكن النتائج لا تزال غير محسنة للغاية ولا يزال البحث في هذا المجال قصيرا. الهدف من موضوع هذه الأطروحة هو المساهمة في تطوير ضوابط DTC-SVPWM لتقليل تموجات عزم دوران المحرك غير المتزامن.

الكلمات المفتاحية:. الآلة غير المتزامنة, تموجات عزم دوران DTC-SVPWM ,

Contents

Table of contents

Chapter I: The different control technique of an induction motor

Chapter II: Mathematical Modeling & Analysis of PWM Techniques for Induction Motor Drive

Chapter III : Mechanical Sensorless control

Chapter IV : Improving torque of induction motor using different DTC structures

List of figures

List Of Figures

Chapter I: The different induction motor control techniques

Chapter II: Mathematical Modeling & Analysis of PWM Techniques for Induction Motor Drive

Chapter III : Mechanical Sensorless Control

Chapter IV: Improving torque of induction motor using different DTC structures

List of the tables

Chapter I: The different induction motor control techniques

Chapter II: Mathematical Modeling & Analysis of PWM Techniques for Induction Motor Drive

Chapter IV: Improving torque of induction motor using different DTC structures

List of Symbols

P_{em} Electromechanical power.
Q_{es} Estimated reactive power.
$\psi_{s\alpha}, \psi_{s\beta}$ Stator flux components in α , β frame.
φ_{sd}, φ_{sq} Stator flux components in d , q frame.
φ_{rd}, φ_{rq} Rotor flux components in d , q frame.
$i_{sa}, i_{s,\beta}$ Stator currents components in α , β frame.
$V_{sa} V_{s\beta}$ Stator voltages components in α , β frame.
$V_{sd} V_{sq}$ Direct and quadratic stator voltage components.
$V_{rd} V_{rq}$ Direct and quadratic rotor voltage components.

ϕ_r Rotor flux.

$|\psi_s|$ Stator flux magnitude.
f_s Stator frequency.
ω_c Cutoff frequency.
$L_s L_r$ Rotor and stator inductances respectively.
$R_s R_r$ Rotor and stator resistances respectively.
σ Blondel's coefficient.
$T_s T_r$ Stator and rotor time constants.
ω_s Synchronous speed.

ω_r Rotor speed.

ω_r Mechanical speed.
p Number of poles pairs.
Γ_{em} Electromagnetic torque.

f Coefficient of friction.
V_{dc} Dc-bus voltage.

δ Load angle between the stator and rotor flux vectors.

θ_s Flux angle.

$K_p K_i$ Proportional and integral gains respectively.

η Efficiency.

List of Abbreviations

IM	Induction Motor/ Machine.
DTC	Direct Torque Control.
EMF	Electro-Motive Force.
PWM	Pulse Width Modulation.
SPWM	Sinusoidal Pulse Width Modulation.
SVPWM	Space Vector Pulse Width Modulation.
VSI	Voltage Source Inverter.
THD	Total Harmonics Distortion.
PI	Proportional-Integral.
FO-PI	Fractional Order-Proportional Integral.
MRAS	Model Reference Adaptive System.
HPF	High-Pass Filter.
LPF	Low-Pass Filter.
FOC	Field Oriented Control.
EKF	Extended Kalman Filter.

General introduction

General Introduction

Motors are widely used to drive most industrial processes. Depending on the applications, these motors are of different types because the performance requirements are widely variable. As a result, these motors must respond actually to set point variations (speed, position, torque), within a wide range of operating frequency variations. Therefore, we must have direct access to the torque, in order to control it successfully, and to adapt the motor more precisely to the imposed requirements. These requirements are fully achieved by the DC motor. This can be illustrated by the natural decoupling between flux and torque. However, the presence of the commutator and brushes limits the power and/or the speed and requires regular maintenance. This is why, nowadays, we are progressively using permanent magnet synchronous motors and induction motors.

The induction machine is particularly robust and low-cost, which makes it more useful in industrial applications. It is used in both simple and more complicated applications. Nevertheless, its control is more difficult to achieve than other electrical machines. Many strategies have been developed in order to make it a machine that exceeds others, even in controlled systems.

The scalar control was the first control introduced in the industry, this control is very widespread for its simplicity and its reduced cost, and it occupied a large part of industrial applications with variable speeds. However, requests for higher-performance applications have motivated the researchers to achieve appropriate controls, which satisfy industrial requirements.

Flux orientation vector control is based on effective control of the magnetic state. However, this design generally requires the insertion of a sensor on the shaft for the mechanical quantity knowledge. However, its sensitivity against the machine's parameter variations led to the search for other algorithms and the use of new control techniques appeared.

The concept called “direct torque control” has appeared to be competitive with vector control techniques. Unlike the latter, which are based on rigorous mathematical calculations, direct control techniques were originally based on qualitative and simplified knowledge of machine behavior. This control is mainly based on simple hysteresis regulators and commutation tables. Its main advantages are fast dynamic torque response and low dependence on machine parameters. However, two major drawbacks arise. On the one hand, the determination of the switching states is based on output information of the non-linear elements of the hysteresis type, on the other hand, the switching frequency is variable, which leads to torque and flux oscillations. In order to overcome the classical DTC control's drawbacks, another technique that reduces the torque and flux oscillations has appeared which imposes a constant modulation frequency. This technique is called DTC with space vector modulation DTC-SVPWM.

The work aim to improve the induction motor’s performance by reducing the torque’s ripples. Therefore, we proposed a new and simple estimation approach of stator flux that enhance torque at low speed.

This thesis is organized as follows:

In the first chapter, we will begin with an art state of the main control methods that industrially exist, in particular scalar vector control (FOC), and direct torque control (DTC), where we will present the progress in improving each control strategy.

The second chapter is devoted to the study of the different PWM techniques, and we finish this chapter with the simulation result of SPWM and SVPWM techniques. In addition, the three-phase induction machine modeling has been done. Then, simulation tests were presented to validate our model. MATLAB software and its SIMULINK environment were used to achieve this simulation.

The third chapter gives an overview of the different strategies used to estimate the unmeasured quantities of the motor, where we proposed an easy and simple estimation method to improve the motor response at low speed. This method has been validated by simulation and experimental tests.

The fourth chapter is devoted to direct torque control DTC, which is essentially based on the vector pulse width modulation technique. Where we used it with different control types such as; hysteresis controller, PI controller, fuzzy logic, and fractional order PI controllers. The simulation results given at the end of this chapter ensure that this control technique can be used to achieve high-performance torque control.

Chapter I

The different induction motor control techniques

I.1 Introduction

Electric machines are the most abundant actuators in industrial equipment and tertiary installations. Among all the types of existing machines, three-phase asynchronous motors and in particular squirrel-cage motors are by far the most used.

These machines are more robust and less expensive and especially require less maintenance intervention. However, although their control by contactor-based equipment is perfectly suited for a large number of applications, permanent developments in the fields of power electronics and digital control have enabled the development of variable-speed drives not only for this motor but also for all AC machines in most variable-speed drives. That is the case for controlling start and stop settings with a soft starter-stopper, or for precise speed adjustment with variable speed drives.

Considering that the induction machine is a multivariable nonlinear system, it remains a major challenge to master its dynamic behavior in speed and torque variation, because when high performance is required, quantitative knowledge of transient phenomena is assumed to be established. To this end, numerous controls have been designed to exploit the maximum performance of the machine at various operating points.

I.2 Different control strategies for induction motor

Typically, the induction motor has been powered at a fixed speed and frequency (50Hz/60Hz) directly from the AC power source. However, with the advancement of power electronic converters, it is now possible to use it with variable frequency by adding a converter between the motor and the AC power supply. This makes it possible to run this motor with variable speed [1][2].

The induction motor control is more difficult to achieve than other electrical motors. Many strategies have been developed to make it a machine that exceeds others, even in controlled systems. These technics are divided into two main categories, scalar control, and vector control. The most types of control used for the induction motor are [3]:

- Scalar control.
- Field oriented control.
- Direct torque control.

The various classifications of the control techniques for variable frequency drives are shown in Fig.1.1 below [4].

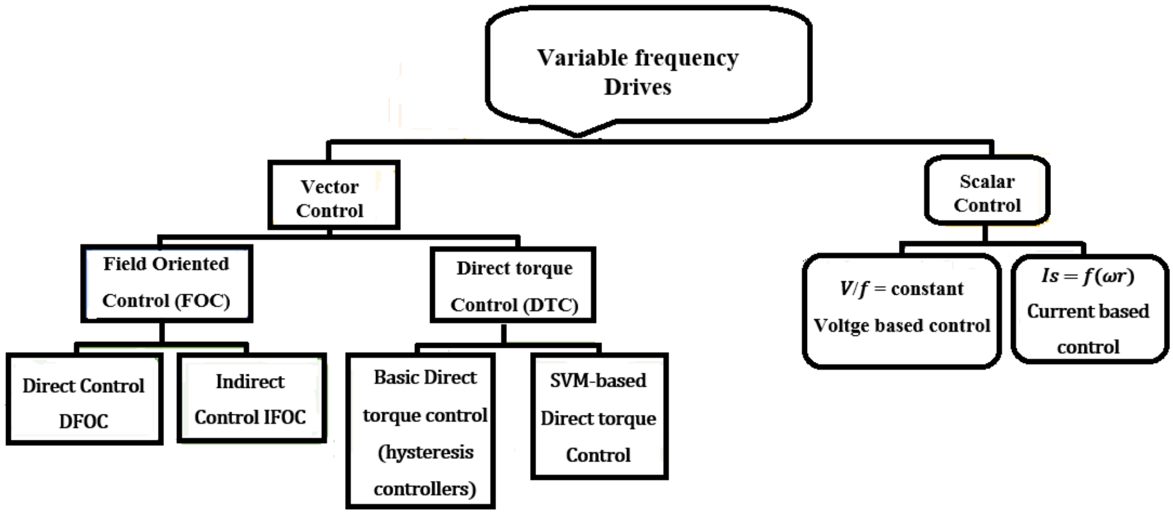

Figure I. 1: Different strategies of a variable frequency control for IM drive

I.2.1 Scalar control

The expressions obtained from the model of the machine in a steady state are used to construct the control laws specific to this kind of control. The torque is controlled in a steady state where the flux of the machine is maintained at a fixed value using V/f control [5] [11]. This type of control is especially suitable for the average operating performance of the induction motor [6]. Despite its performance shortcomings, this control is widely used in the industry due to its simplicity and relatively low cost [7]. However, some papers in the literature try to improve it by using innovative methods like fuzzy logic-based regulator optimization or the addition of stabilizing algorithms while still being easy to use [8].

There are various scalar control techniques, based on whether we adjust either the voltage or the current [8] [9]. They mainly depend on the actuator's topology (voltage or current inverter). In small and medium power applications, where the voltage inverters are most common [10] [12] [13].

At the output of the converter, we control [14]:

- Either the voltages/currents magnitude as well as their frequency (Figure I.2).

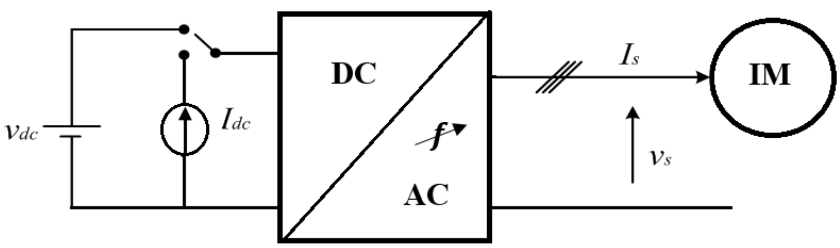

Figure I. 2: Ajustement principale

- Alternatively, using an autopilot control which controls the stator frequency f_s and either the voltage V_s or the current I_s by realizing $\omega_s = \omega_g + \omega_r$ using a mechanical speed sensor.

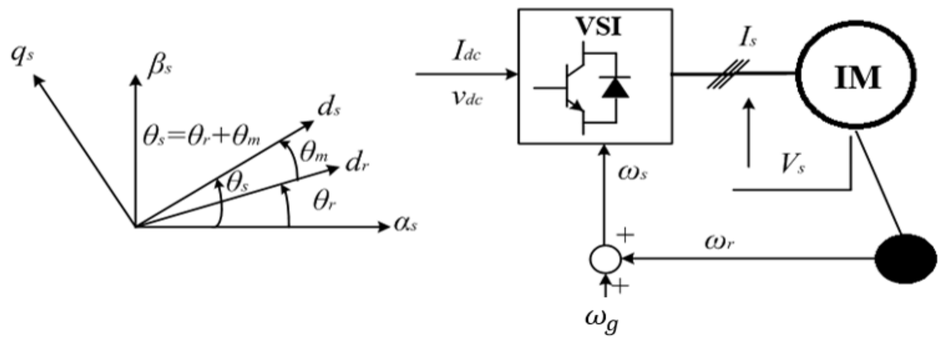

Figure I. 3: Tuning with Autopilot.

The stator flux and ω_s, as well as the torque, are required for the control of the rotor speed [15]. Furthermore, if we do not want to introduce a large error in the determination of ω_s, the speed ω_g must be measured with extreme precision to be added to that very low speed ω_r [16]. Therefore, it is recommended to estimate them through observers [17]. This autopilot can be associated differently with a current or voltage supply [18]. The frequency converter assemblies that are employed, as well as the adjustment and control circuits, are very diverse [19].

The control diagram below (Figure (I.4)) shows how to regulate the machine's speed by reconstructing the stator pulsation from the speed and the rotor pulsation. This latter arises from the speed regulator and represents the machine's torque image. When the motor is loaded, the speed tends to decrease, and the regulator will increase the torque to keep the speed stable [20]. Therefore, the stator pulse is modified to maintain this balance [20] where the voltage is calculated to ensure the V/f control mode of the machine [21].

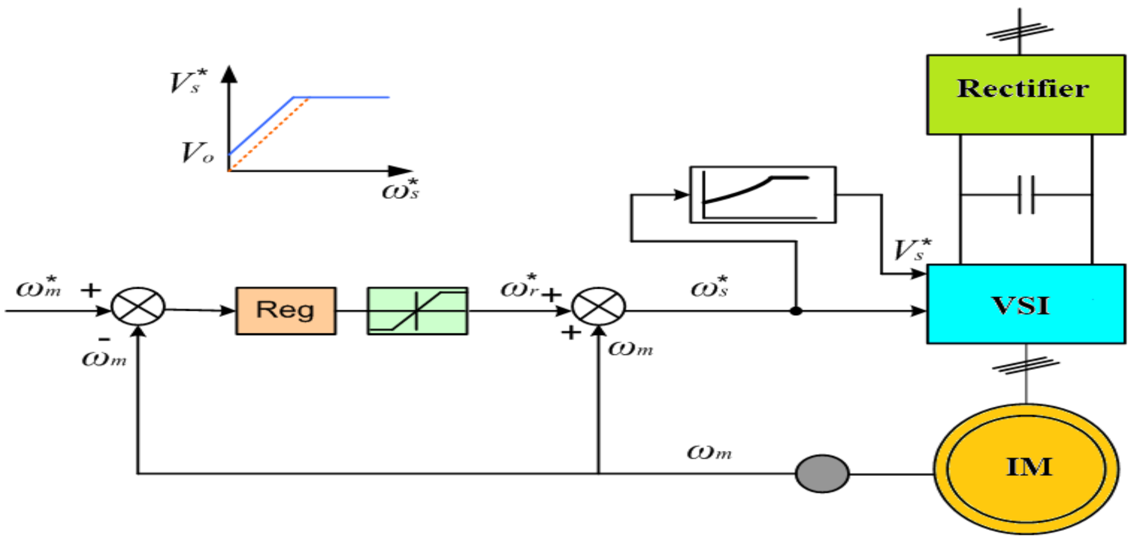

Figure I. 4: Voltage scalar control.

I.2.2 Field Oriented Control (FOC)

The vector control FOC (Field Oriented Control), with its two forms, direct DFOC (Direct Field Oriented Control) and indirect IFOC (indirect field oriented control) [22], which significantly outperforms the previous one in terms of its capacity for high-performance control and is still extremely competitive in the electrical machine control field [23]. Since Hasse and Blaschke's developed it in Germany towards the end of the 1960s (IFOC) and the beginning of the 1970s (DFOC), It is constantly updated to incorporate new developments [24]. The principle of the FOC is the independent control of the machine's flux and torque, similar to a separately excited DC machine [25]. Where the instantaneous stator currents are transformed in a rotating frame aligned with either the rotor, stator, or the air gap, in order to produce two components of the current, according to the axis d (the component which controls the flux), and that of the q axis (the component that controls the torque) [26]. The FOC technique's main issue is with the proportional-integral (PI) regulators that are highly sensitive to the machine's parametric properties, especially the rotor time constants T_r and stator time constants T_s [27]. Given this aspect, all researchers who have studied the FOC's fundamental forms have been interested to overcome this issue by enhancing its reliability and robustness against the inevitable parametric variations. Several works have been implemented, among them that suggested online identification of the stator time constant T_s and rotor time constant T_r for the proper slip angular speed calculation [28][29]. Actually, these works have made a significant contribution to the improvement of torque and speed dynamic response. To solve the problems of PI controller, sliding mode controller used with FOC control has demonstrated its robustness in the presence of uncertainties, particularly parametric variations and external perturbation, and since then, several works have sequentially followed one another, but with the issue of the phenomenon of chattering due to the discontinuity of controlling [30]. However, the inclusion of smooth integral control or the use of fuzzy logic-based techniques can overcome this phenomenon [31][32][33]. It is important to note that some researchers have combined the same control sliding mode regulators and proportional-integral PI regulators and introduced the space vector pulse-width modulation technique SVPWM [34][35][36]. The results obtained are satisfactory because the SVPWM (Space Vector Pulse Width Modulation) technique reduces the stator currents harmonics, and improves the steady state problem of torque, flux, and current ripples, while the sliding mode controller contributes to the system's robustness.

One difference between direct and indirect vector control is that, in direct vector control, we must have knowledge about the rotor flux to implement its regulation, whereas, in indirect vector control, we are freed from the knowledge of this flux by making some approximations [37]. This method requires a good knowledge of both the magnitude and the phase of the rotor flux, and this must be verified by whatever the dynamic stat is carried out.

A first possibility is to put flux sensors in the air gap, and directly measure the components $\phi_{r\alpha}$ and $\phi_{r\beta}$in order to deduce the magnitude and the phase [38]. The sensors are mechanically fragile, and subject to severe conditions due to vibrations and overheating. The rotor flux knowledge precision depends on the inductive parameters affected by the magnetic circuit saturation [39]. On the other hand, the caught signals are marred by noise generated by the notches and require adjustable filters.

Direct measurement allows knowing exactly the position of the flux [40]. Regardless of the operating point, this control mode ensures proper decoupling of flux and torque. However, it requires the use of a motor equipped with flux sensors, which considerably increases the cost of its manufacture and makes its application more delicate. (Figure I.5) [40].

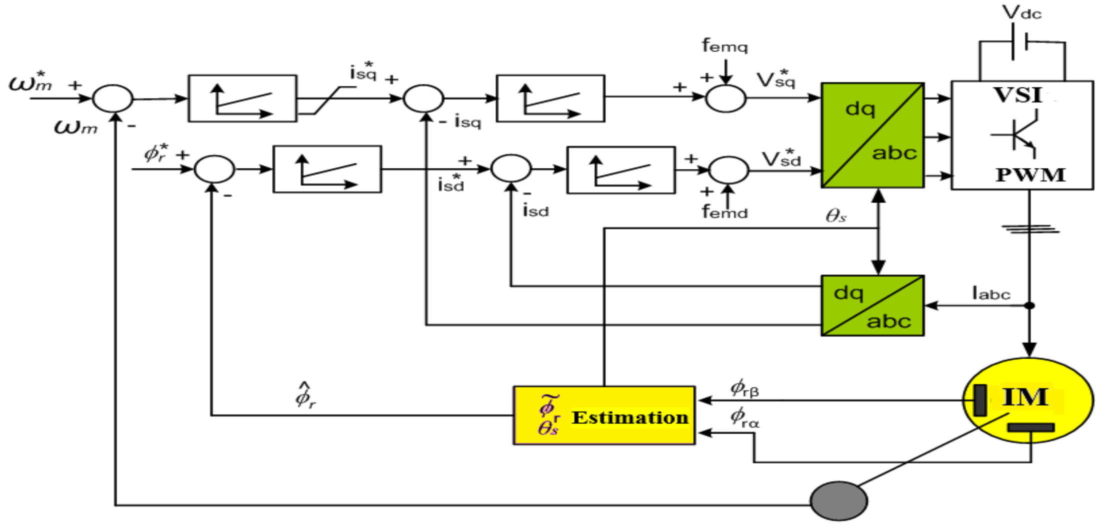

Figure I. 5: Direct vector control of an induction motor.

f_{emd} , f_{emq} : Compensation terms.

In the majority of applications, the usage of flux sensors is generally avoided. instead, we use estimators (open loop) or observers (closed loop) of the flux derived from conventional measurements (current, voltage, speed) that are easily accessible and carried out, figure (I.6).

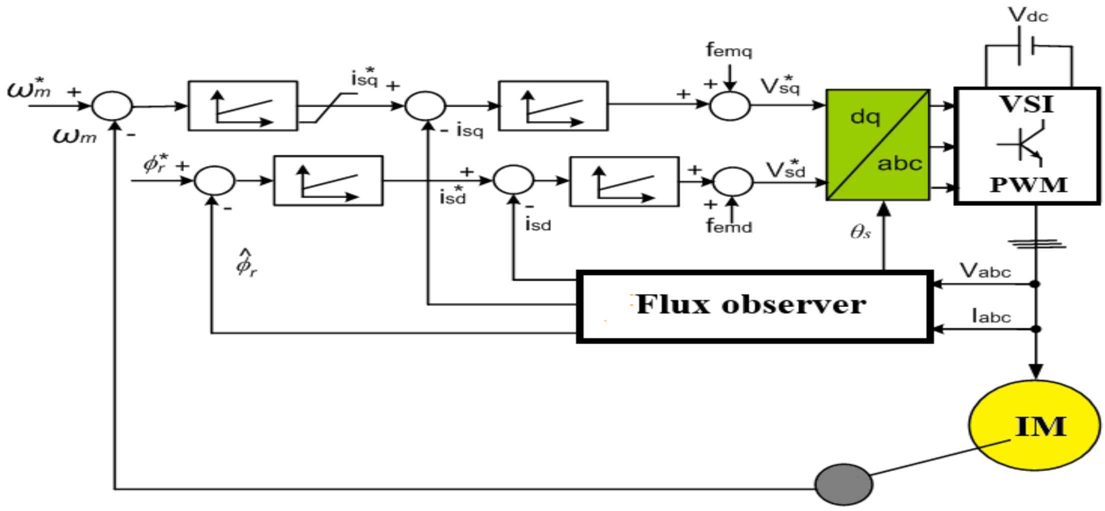

Figure I. 6: Direct vector control of an IM with rotor flux observer.

The idea behind indirect control is to just evaluate the flux's position rather than measuring (or estimating) its magnitude [41]. It involves estimating the flux vector's position and adjusting its magnitude in an open loop [42]. The voltages or currents ensuring flux orientation and decoupling are evaluated from the model machine in a dynamic state. This method has been favored by the development of microprocessors; it is very sensitive to the machine's parametric variations. It is important to highlight that the indirect method is the simplest to carry out and the most used than the direct method. However, the selection between the two approaches varies from application to application [43]. The principle of this control method is to ignore the rotor flux magnitude and only consider its position as obtained using the reference values [44]. The advantage of this approach is that a flux sensor is not required. However, the use of a rotor position sensor is unavoidable. This technique requires using an IFOC (Indirect Field Oriented Control) block to produce the supply voltages required to generate the desired flux and torque [45]. The IFOC control block generates the three command inputs v_{sd}^* , v_{sq}^* and ω_m^*, Based on the two reference inputs (i_{sq}^*, ϕ_r^*) which ensure the decoupling [46]. These control quantities generated by the IFOC, are used to control the direct i_{sd} and quadratic i_{sq} components of the stator current to obtain currents identical to the reference currents, and consequently, the flux and the torque are maintained at their reference values [47]. In our case, the voltages or currents ensure decoupling and flux orientation. When the machine is supplied with voltage, it is necessary to create the electrical model of the process to develop the necessary algorithms for determining the tuning variables $v_{sd}$and v_{sq} [48]. Considering the flux ϕ_r oriented on the d axis and taking into account the flux and voltage equations, we obtain [49]:

$$\begin{cases} v_{sd} = \left[R_s + L_s\sigma\frac{d}{dt}\right] i_{sd} - \omega_s L_s \sigma i_{sq} \\ v_{sq} = \left[R_s + L_s\sigma\frac{d}{dt}\right] i_{sq} + \omega_s L_s \sigma i_{sd} + \frac{L_m}{L_r}\omega_s\phi_r \\ T_r\frac{d\phi_r}{dt} + \phi_r = L_m i_{sd} \\ \frac{L_m}{T_r} i_{sq} = \omega_r\phi_r \\ \Gamma_{em} = p\frac{2}{3}\left[\frac{L_m}{L_r}\right]\phi_r i_{sq} \end{cases} \tag{I.1}$$

The goal is to limit the effect of an input to a single output. [50]. Then, we can model the process as a collection of mono-variable systems that develop in parallel with no interaction between the controls.

In steady state, we find the equations of the indirect vector control of the induction motor for the Park voltages v_{sd} and v_{sq} [51]:

$$\begin{cases} v_{sd} = R_s i_{sd} - \omega_s L_s \sigma i_{sq} \\ v_{sq} = \omega_s L_s i_{sd} + R_s i_{sq} \end{cases} \tag{I.2}$$

In addition, the steady-state flux equation becomes [52]:

$$\phi_r = L_m i_{sd} \Rightarrow i_{sd} = \frac{\phi_r}{L_m} \tag{I.3}$$

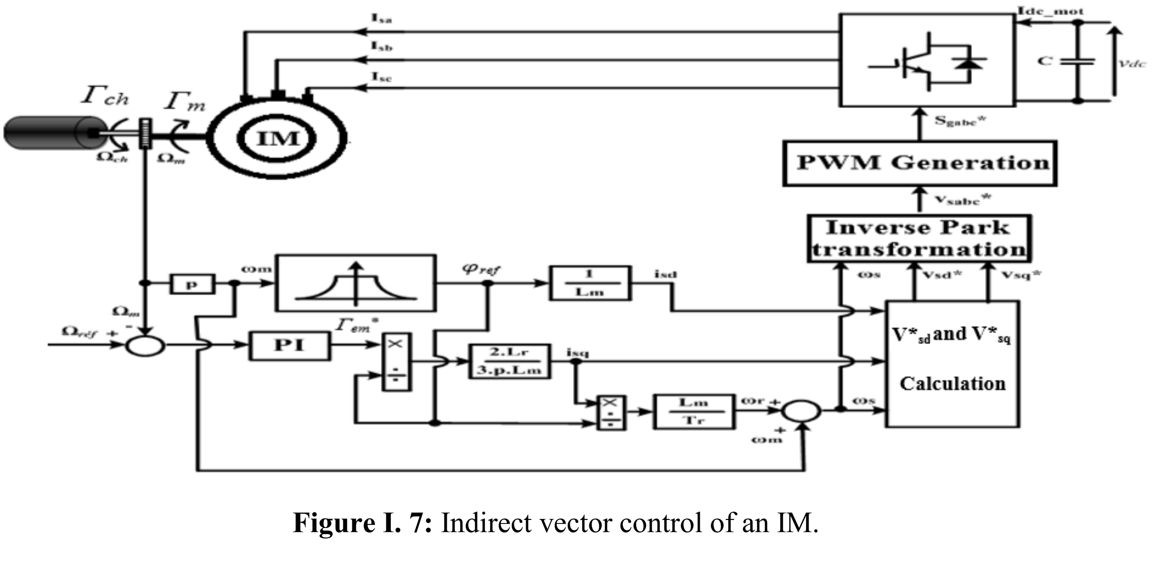

Figure I. 7: Indirect vector control of an IM.

The indirect vector control method for an induction motor with variable speed is shown in Figure (I.7). After sensing the rotational speed at the level of the motor rotor shaft, the latter will be compared to the reference speed.

I.2.3 Classical direct Torque Control

The control of the induction motor has been the subject of numerous studies in recent years to achieve an accurate and fast torque response while reducing the complexity of the flux-oriented vector control. Therefore, the creation of direct torque and flux control (DTC) by Takahashi (DTC) and Depenbroak (Direct Self Control-DSC) in the middle of the 1980s was recognized as an implementable approach to achieve those previous conditions [53].

The DTC has opened a new horizon in the control field; in fact, this technique's fundamental idea is to control the motor's flux and torque independently [54]. This is achieved through hysteresis comparators to reduce torque and flux errors within the hysteresis band limits, these comparators compare the reference values with the estimated values, then directly control the inverter's states. Without going through rigorous calculations of transformation between reference frames, fewer regulators are considered overly sensitive to parameter variations, and no requirement for a pulse width modulation (PWM) or (PWM) generator. The biggest drawback of the DTC is the ripple that the torque, flux, and current generate. This is caused by the fact that when the flux is outside the hysteresis band, the inverter's frequency changes and the flux follows an optimal path towards the desired value [55]. These have an effect on speed estimation and its response, and in the creation of acoustic noises as well [56].

Like the FOC, several works come from the two basic forms suggested by Takahashi and Depenbroak to overcome these persistent issues. Some have used the multilevel inverter, but this solution turns out to be complex and expensive. Others have used the SVM (Spatial Vector Modulation) technique [57]. Its main idea is to impose the appropriate voltage vector through space vector modulation [58]. As a result, ripples are significantly reduced, although not at a completely constant switching frequency, especially considering that this method had parametric dependencies, particularly on the stator resistance, and required extensive online calculations [59]. In some research, the truth table (Takahashi table) has been enlarged by applying a larger number of vectors than those applied in classical DTC using five-level comparators [60]. This technique, known as DSVM (discrete space vector modulation), has been implemented in simulation and carried out experimentally. The results showed the effectiveness of this method in processing ripples without adding complexity to the original DTC. Recently, other studies have used fuzzy logic; either to adapt the hysteresis band and have obtained satisfactory results even at low speeds or to optimize the Takahashi table with good torque and flux performance in the steady state [61][62]. Others have used the technique which combines SVM with fuzzy logic DTC control (FLDTC); ripples were significantly minimized at the nearly constant switching frequency [63] [64].

The objective of the DTC strategy is to achieve effective control, both steady state and dynamic state, by combining several switching strategies. Appropriate voltage vector selection, at each sample period, is made to keep torque and flux within the two-hysteresis bands [65].

In particular, the selection is made on the basis of the instantaneous flux error ϕ_s and the electromagnetic torque Γ_{em} [66]. Several voltage vectors can be chosen for a specific flux and torque combination. Each one has an impact on torque and current ripple, dynamic performance, and two- or four-quadrant operation, where the decision is based on a predetermined strategy.

Figure (I.8) shows the stator flux in the (α, β) frame, and the effect of the different states of a two-level VSI according to the torque and the variation of the stator flux magnitude.

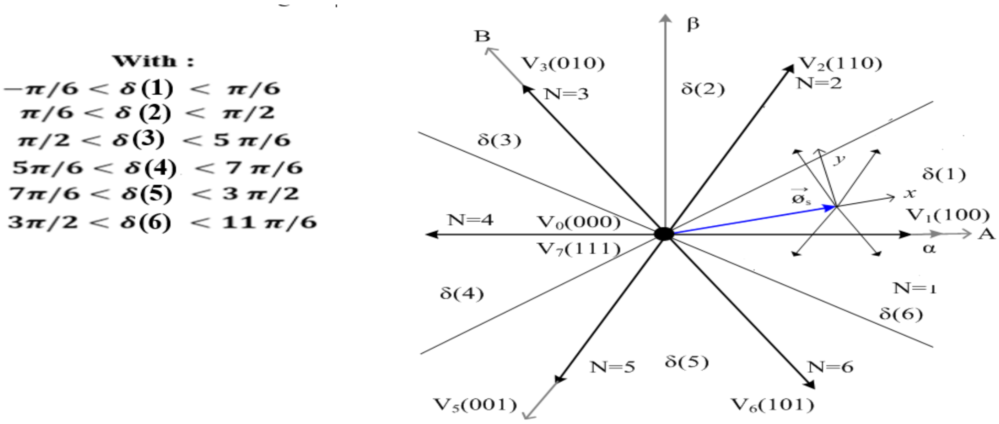

Figure I. 8: Influence of the chosen voltage vector on the variation of the stator flux magnitude and the torque.

The control table is built according to the variables state ($\Delta\varphi$) and ($\Delta\Gamma_{em}$), and the sector *N* of the flux position φ_s. Which takes the following form [67]:

Table I. 1: Takahashi's switching table.

	N	1	2	3	4	5	6
$\Delta\varphi$ =1	$\Delta\Gamma_{em}$=1	V_2	V_3	V_4	V_5	V_6	V_1
	$\Delta\Gamma_{em}$ =0	V_7	V_0	V_7	V_0	V_7	V_0
	$\Delta\Gamma_{em}$ =-1	V_6	V_1	V_2	V_3	V_4	V_5
$\Delta\varphi$ =0	$\Delta\Gamma_{em}$ =1	V_3	V_4	V_5	V_6	V_1	V_2
	$\Delta\Gamma_{em}$ =0	V_0	V_7	V_0	V_7	V_0	V_7
	$\Delta\Gamma_{em}$ =-1	V_5	V_6	V_1	V_2	V_3	V_4

The structure of classical DTC applied for induction motor is shown in Figure (I.9).

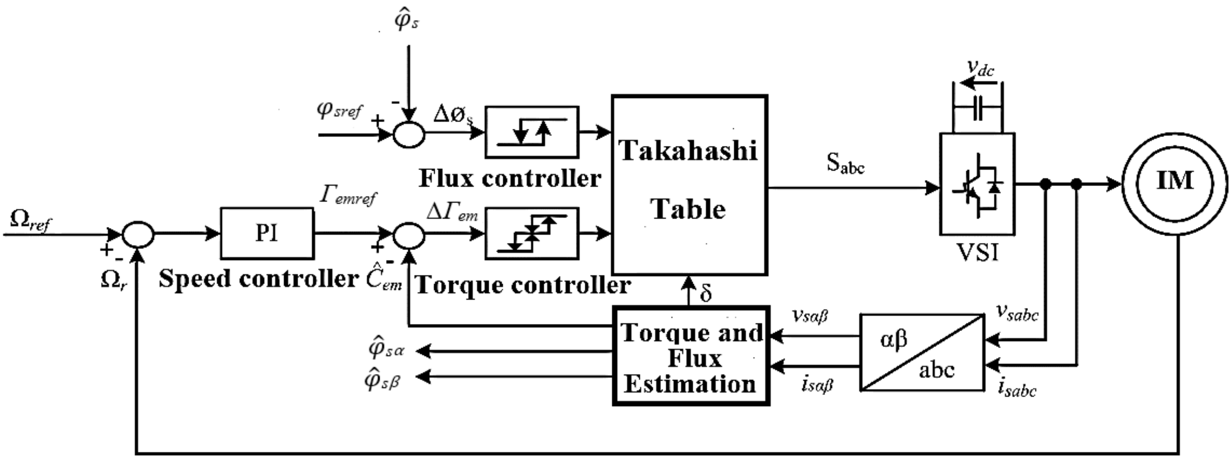

Figure I. 9: General structure of the Classical Direct Torque Control (CDTC).

The reference values for the stator flux magnitude and the torque are compared with the estimated values. The output provides the stator flux and electromagnetic torque errors that will be fed into a two-level flux magnitude and three-level torque hysteresis controller respectively as shown in Figure (I.9). The three-level comparator allows the machine to control in both rotational directions, in positive and negative torque.

I.2.3.1 Main features of the DTC technique [68]

- DTC is based on selecting the best inverter switching vectors.
- Indirect control of the machine's stator currents and voltages.
- Obtaining stator fluxes and currents close to sinusoidal forms.
- The machine's dynamic torque response is very fast.
- The presence of torque ripple is dependent on the hysteresis comparators' bandwidth.
- The switching frequency of the inverter depends on the hysteresis bands magnitude.

I.2.3.2 Advantages and drawbacks of DTC

I.2.3.2.1 Direct torque control advantages [69]

- It is not necessary to transform the coordinates, because the currents and the voltages are in a frame linked to the stator.
- Uses a simplified model of the induction motor.
- Elimination of calculating PWM modulation block.
- As in the case of vector control, it is not necessary to decouple the currents from the control voltages.
- It requires two hysteresis comparators and a single PI-type for the speed controller, while vector control requires two more PI regulators and a PWM modulator.
- It is not necessary to know the rotor position angle with great precision, because only the sector information in which the stator flux vector is located is necessary.
- The dynamic torque response is very fast.
- Robustness against parametric variations.
- Possibility of applying the system algorithms with acquisition cards.

I.2.3.2.2 Direct torque control drawback [70]

- The existence of problems at low speed due to the resistive term.
- The requirement for stator flux and torque estimations.
- The existence of torque oscillations.
- Variable switching frequency.

I.2.4 DTC with Space Vector Pulse Width Modulation SVPWM (DTC-SVPWM)

The switching frequency is not constant for conventional DTC control. This causes torque oscillations, which can excite mechanical resonances, and high harmonic content, both of which increase losses in the motor [71]. The use of more robust hysteresis regulators is a solution to the issue of tracking rapidly shifting trajectories. In this instance, the reference frame abc is used to regulate the currents [72]. The basis of the hysteresis regulation principle is to control the inverter switches such that the change in current in each machine's phase occurs within a band (±ΔI) around the current references.

Many methods have been presented to fix these problems. An overview of constant modulation frequency controls will be given here. Direct Torque Control Based on Space Vector Modulation [73]. They use space vector pulse width modulation (SVPWM), and the algorithm is then more complex, but torque and flux oscillations are reduced. Authors in [73] also presented an algorithm allowing to have a constant modulation frequency. Its main feature is the elimination of hysteresis regulators and the vector selection table, which eliminates the problems associated with them (the inconstant switching frequency). With this method of control, the inverter works at a constant frequency, where SVPWM modulation is applied to the output vector of the control. The objective of this method is to achieve direct control of the stator flux vector, in a reference frame linked to the stator (α, β). By projecting these two vectors into the (α, β) frame, their polar components can be determined. From these components, the desired stator flux vector at a given instant is calculated. The SVPWM modulation will be applied to this vector to obtain the switching states of the inverter. The algorithm is then more complex, but the torque and flux oscillations are reduced.

For the DTC control strategy with imposed switching frequency, the authors in [74] have proposed to move the voltage vector adjacently in the phase plane; these displacements make it possible to minimize the voltage derivatives. Under these conditions, the torque and flux ripple frequency is perfectly controlled and fixed. The obtained results in the simulation show that the performance is significantly better than that obtained with the classical DTC strategy (without frequency control).

In [75], the authors presented the DTC based on the neuron-fuzzy controller, which has advantages such as constant switching frequency, unipolar voltage, no distortion in the response on torque made by the changes of the sector, and no problems operation at low speed.

The block diagram of the control structure is shown in Figure (I.10). Two PI controllers are used to regulate flux and torque.

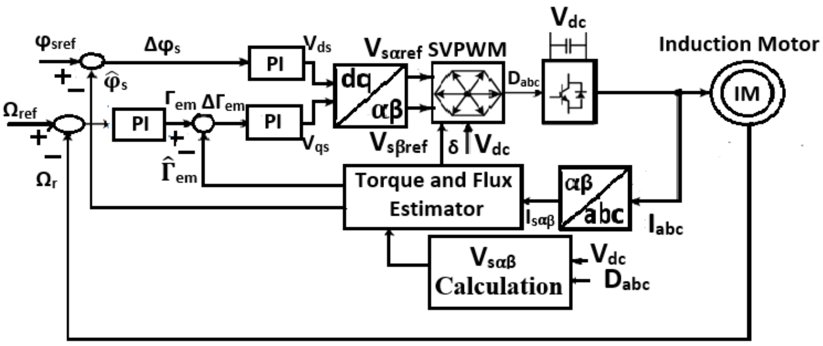

Figure I. 10: DTC-SVPWM direct torque and flux control of an induction motor.

In this arrangement, there are two proportional integral (PI) type controllers, which adjust the torque and stator flux magnitude instead of the hysteresis band. The two PI controllers produce a control voltage to control the inverter.

I.3. Conclusion

In this chapter, We started with the latest and most popular industrial control technologies, in particular scalar control, vector control (FOC), and direct torque control (DTC). Firstly, we illustrated the different scalar control techniques, based on the voltage or current inverter. Besides, we have studied the problems related to the use of FOC control such as parametric variations, where we presented the progress in terms of improvements of this control strategy against this problem. Moreover, the problems of classical DTC which are the presence of torque oscillations and variable switching frequency are also discussed, where we suggested using DTC-SVPWM to overcome these problems. The next chapter will be devoted to the mathematical modeling of the induction motor and the study of different pulse width modulation techniques (PWM) where we will choose the most adequate technique to combine it with DTC control applied to the induction motor.

References

[1] G. Grellet, G. Clerc “ Actionneurs électriques” , Editions Eyrolles, 1997.
[2] Flemming Abrahamsen “Energy Optimal Control of Induction Motor Drives” Ph.D. thesis, Aalborg University, Denmark, 2000.
[3] Mencou, S., Yakhlef, M. B., & Tazi, E. B. (2022, March). Advanced Torque and Speed Control Techniques for Induction Motor Drives: A Review. In 2022 2nd International Conference on Innovative Research in Applied Science, Engineering and Technology (IRASET) (pp. 1-9). IEEE.
[4] Pushparajesh Viswanathan and Manigandan Thathan (2016) Torque ripple minimization of direct torque controlled four phases witched reluctance motor using artificial intelligent controller World Journal of Modelling and Simulation,Vol. 12, pp. 163-174
[5] Boldea, I., Moldovan, A., & Tutelea, L. (2015, September). Scalar V/f and If control of AC motor drives: An overview. In 2015 Intl Aegean Conference on Electrical Machines & Power Electronics (ACEMP), 2015 Intl Conference on Optimization of Electrical & Electronic Equipment (OPTIM) & 2015 Intl Symposium on Advanced Electromechanical Motion Systems (ELECTROMOTION) (pp. 8-17). IEEE.
[6]Gupta, V. K., Tiwari, B., & Dewangan, B. (2015). Efficiency optimization of induction motor drive: a review. International Journal of Innovative Science, Engineering & Technology, 2(12), 650-665.
[7] Rahman, S., & Abidin, A. A. B. Z. (2016). A Review on Induction Motor Speed Control Methods. International Journal Of Core Engineering & Management (IJCEM), 3(5).
[8] Hannan, M. A., Abd Ali, J., Ker, P. J., Mohamed, A., Lipu, M. S., & Hussain, A. (2018). Switching techniques and intelligent controllers for induction motor drive: Issues and recommendations. IEEE access, 6, 47489-47510.
[9] Miveh, M. R., Rahmat, M. F., Ghadimi, A. A., & Mustafa, M. W. (2016). Control techniques for three-phase four-leg voltage source inverters in autonomous microgrids: A review. Renewable and Sustainable Energy Reviews, 54, 1592-1610.
[10] Boldea, I. (2008). Control issues in adjustable speed drives. IEEE Industrial Electronics Magazine, 2(3), 32-50.
[11] Souad Chaouch, “ Commande Vectorielle Robuste d'une Machine a Induction sans Capteur de Vitesse” , These de doctorat en science en électrotechnique l'université de Batna 03 Décembre
2005
[12] Abbondanti, A. (1975). U.S. Patent No. 3,909,687. Washington, DC: U.S. Patent and Trademark Office.
[13] Abbondanti, A., Westinghouse Electric Corp, 1976. Flux control system for controlled induction motors.
[14] Leonhard W.,“ Control of Machines with the Help of Microelectronics” , Third IFAC Symposium on Control in Power Electronics and Electrical Drives, Lausanne, Sept 1994, pp. 35-58.
[15] Abdelkoudouss FAQIR ‘’ Commande A Structure Variable D’un Entrainement A Machine Asynchrone Soumis A Un Environnement Mecanique Variable’’ Doctorat L’ Université de Picardie Jules Verne France écembre 2003.
[16] Miloudi Abdallah “ Etude Et Conception De Régulateurs Robustes Dans Différentes Stratégies De Commandes D’un Moteur Asynchrone’’ thèse Doctorat Es-Science Université Oran JUIN 2006.
[17] Wang, H., Yang, Y., Ge, X., Zuo, Y., Yue, Y., & Li, S. (2021). PLL-and FLL-based speed estimation schemes for speed-sensorless control of induction motor drives: Review and new attempts. IEEE Transactions on Power Electronics.
[18] Ludtke, I., Jayne M. G. “ A comparative study of high performance speed control strategies for voltage source PWM inverter fed induction motor drives” , Seventh International Conference on electrical Machines and Drives, 11-13 September 1995, University of Durham, UK
[19] Bose, B. K. (1993). Power electronics and motion control-technology status and recent trends. IEEE Transactions on Industry Applications, 29(5), 902-909.
[20] E.L. van cler Hooft.Scalar control of voltage fed induction machines van der Hooft, E. L. (Author). 31 Dec 1994
[21] Hannan, M. A., Ali, J. A., Mohamed, A., & Hussain, A. (2018). Optimization techniques to enhance the performance of induction motor drives: A review. Renewable and Sustainable Energy Reviews, 81, 1611-1626.
[22] Wang, Y., Shi, Y., Xu, Y., & Lorenz, R. D. (2015). A comparative overview of indirect field oriented control (IFOC) and deadbeat-direct torque and flux control (DB-DTFC) for AC Motor Drives. Chinese Journal of Electrical Engineering, 1(1), 9-20.

[23] Sakunthala, S., Kiranmayi, R., & Mandadi, P. N. (2018, February). A Review on Speed Control of Permanent Magnet Synchronous Motor Drive Using Different Control Techniques. In 2018 International Conference on Power, Energy, Control and Transmission Systems (ICPECTS) (pp. 97-102). IEEE.
[24] Tripathi, S. M., & Vaish, R. (2019). Taxonomic research survey on vector controlled induction motor drives. IET Power Electronics, 12(7), 1603-1615.
[25] Santisteban, J. A., & Stephan, R. M. (2001). Vector control methods for induction machines: an overview. IEEE Transactions on Education, 44(2), 170-175.
[26] Amezquita-Brooks, L., Liceaga-Castro, E., Liceaga-Castro, J., & Ugalde-Loo, C. E. (2015). Flux-torque cross-coupling analysis of FOC schemes: Novel perturbation rejection characteristics. ISA transactions, 58, 446 461.
[27] Novotny, D. W., &Lipo, T. A. (1996). Vector control and dynamics of AC drives Oxford university press. (Vol. 41)
[28] G. Guidi, H. Umida "A Novel Stator Resistance Estimation Method for Speed-Sensorless Induction Motor Drives", IEEE Transactions on Industry Applications, Vol. 36, No. 6, Nov/Dec 2000.
[29] A. Mezouar, M. K. Fellah, S. Hadjeri, 0. Touhami, Y. Sahalim "Robust Direct Field Oriented Control of Induction Motors Using Adaptive Observer", IEEE ISIE 2006, July 9-12, 2006, Montreal, Quebec, Canada.
[30] A. Sabanovic, B. V. Izozimov "Application of sliding modes to induction motor control", IEEE Trans. Idust. Applic. Vol.IA 13. N°.1, pp.41, 1981.
[31] Mohamed M. Negm "Integral VSC and Preview Control of Efficiency and Speed for a DC Drive" Power System Technology, 2002. Proceedings. International Conference on Volume 4, Issue , 2002.
[32] Mahieddine-Mahmoud S., Ramanou R., Kefsi L., Chrifi-Alaoui L. "Sliding mode control: a new contribution using an integral action in the boundary layer", Industrial Technology. IEEE International Conference on Volume, Issue, pp.681-686, Dec. 2006
[33] A. Hazzab, I. K. Bousserhane, P. Sicard "Fuzzy Soft-Switching Law of an Adaptive Sliding Mode Controller for Induction Motor Speed Control", IEEE ISIE, Montreal, Quebec, Canada, Jul. 2006
[34] Tian-Jun Fu, Wen-Fang Xie "A novel sliding-mode control of induction motor using space vector modulation technique", The Instrumentation, Systems, and Automation Society (ISA) Transactions 44. pp. 481–490, 2005.
[35] Zhiwen Ma, Trillion Zheng, Fei lin, Xiaojie You "A New Sliding-mode Current Controller for Field Oriented Controlled Induction Motor Drives", Industrial Electronics Society (IECON). 31st Ann. Con. of IEEE Publication Nov. 2005.
[36] Alkorta P., Barambones O., Garrido A. J., Garrido I. "SVPWM Variable Structure Control of Induction Motor Drives", Industrial Electronics, ISIE. IEEE International Symposium on Volume, Issue, pp.1195 – 1200, June 2007.
[37] Dominic, D. A., & Chelliah, T. R. (2014). Analysis of field-oriented controlled induction motor drives under sensor faults and an overview of sensorless schemes. ISA transactions, 53(5), 1680-1694.
[38] Barrero, F., & Duran, M. J. (2015). Recent advances in the design, modeling, and control of multiphase machines—Part I. IEEE Transactions on Industrial Electronics, 63(1), 449-458.
[39] Xue Yanhong, Xu Xingyi, Habetler Thomas G, Divan Deepakraj M. A stator flux-oriented voltage source variable-speed drive based on DC link measurement. IEEE Trans Ind Appl 1991;27(5):962–9.
[40] Chaikhy, H., Khafallah, M., Saad, A., Es-Saadi, M., & Chikh, K. (2011). Evaluation des performances des commandes vectorielles de la machine à induction. Revue de génie industriel, 6, 23-32.
[41] Gordillo, F., Salas, F., Ortega, R., & Aracil, J. (2018). Indirect Field-Oriented Control of Induction Motors: A Hopf Bifurcation Analysis. Chaos in Automatic Control, 481-502.
[42] Iffouzar, K., Amrouche, B., Cherif, T. O., Benkhoris, M. F., Aouzellag, D., & Ghedamsi, K. (2017). Improved direct field oriented control of multiphase induction motor used in hybrid electric vehicle application. international journal of hydrogen energy, 42(30), 19296-19308.
[43] Toliyat, H. A., Levi, E., & Raina, M. (2003). A review of RFO induction motor parameter estimation techniques. IEEE transactions on Energy conversion, 18(2), 271-283.
[44] Krishnan, R., & Bharadwaj, A. S. (1991). A review of parameter sensitivity and adaptation in indirect vector controlled induction motor drive systems. IEEE Transactions on Power Electronics, 6(4), 695-703.
[45] De Klerk, M. L., & Saha, A. K. (2021). A comprehensive review of advanced traction motor control techniques suitable for electric vehicle applications. IEEE Access.
[46] Bazanella, A. S., & Reginatto, R. (2000). Robustness margins for indirect field-oriented control of induction

motors. IEEE transactions on automatic control, 45(6), 1226-1231.
[47] Singh, G. K., Nam, K., & Lim, S. K. (2005). A simple indirect field-oriented control scheme for multiphase induction machine. IEEE Transactions on Industrial Electronics, 52(4), 1177-1184.
[48] Amezquita-Brooks, L., Liceaga-Castro, J., & Liceaga-Castro, E. (2013). Speed and position controllers using indirect field-oriented control: A classical control approach. IEEE transactions on Industrial Electronics, 61(4), 1928-1943.
[49] Hiware, R. S., & Chaudhari, J. G. (2011, November). Indirect field oriented control for induction motor. In 2011 Fourth International Conference on Emerging Trends in Engineering & Technology (pp. 191-194). IEEE.
[50] Masiala, M., Vafakhah, B., Salmon, J., & Knight, A. M. (2008). Fuzzy self-tuning speed control of an indirect field-oriented control induction motor drive. IEEE Transactions on Industry Applications, 44(6), 1732-1740.
[51] Garcia, G. O., Stephan, R. M., & Watanabe, E. H. (1994). Comparing the indirect field-oriented control with a scalar method. IEEE Transactions on Industrial Electronics, 41(2), 201-207.
[52] Shrawane, P. (2010, August). Indirect field-oriented control of induction motor. In 12th IEEE International Power Electronics Congress (pp. 102-105). IEEE.
[53] Swierczynski, D. A. R. J. U. S. Z., Kazmierkowski, M. P., & Blaabjerg, F. (2002, July). DSP based direct torque control of permanent magnet synchronous motor (PMSM) using space vector modulation (DTC-SVM). In Industrial Electronics, 2002. ISIE 2002. Proceedings of the 2002 IEEE International Symposium on (Vol. 3, pp. 723-727). IEEE.
[54] Cao, B., Grainger, B. M., Wang, X., Zou, Y., Reed, G. F., & Mao, Z. H. (2020). Direct torque model predictive control of a five-phase permanent magnet synchronous motor. IEEE Transactions on Power Electronics, 36(2), 2346-2360.
[55] Zidani, F., & Said, R. N. (2005). Direct torque control of induction motor with fuzzy minimization torque ripple. JOURNAL OF ELECTRICAL ENGINEERING-BRATISLAVA-, 56(7/8), 183.
[56] Bouhoune, K., Yazid, K., & Boucherit, M. S. (2014). ANN-based DTC scheme to improve the dynamic performance of an IM drive.
[57] Escalante, M. F., Vannier, J. C., & Arzandé, A. (2002). Flying capacitor multilevel inverters and DTC motor drive applications. IEEE Transactions on Industrial Electronics, 49(4), 809-815.
[58] Ozkop, E., & Okumus, H. I. (2008, March). Direct torque control of induction motor using space vector modulation (SVM-DTC). In 2008 12th International Middle-East Power System Conference (pp. 368-372). IEEE.
[59] Shehata, E. G. (2013). Speed sensorless torque control of an IPMSM drive with online stator resistance estimation using reduced order EKF. International Journal of Electrical Power & Energy Systems, 47, 378-386.
[60] Pal, A., Srivastava, G. D., & Kulkarni, R. D. (2019, January). Simulation of Sensorless Speed Control of Induction Motor Using Direct Torque Control Technique Employing Five Level Torque Comparator and Twelve Sector Method. In 2019 International Conference on Nascent Technologies in Engineering (ICNTE) (pp. 1-6). IEEE.
[61] Hafeez, M., Uddin, M. N., Rahim, N. A., & Ping, H. W. (2013). Self-tuned NFC and adaptive torque hysteresis-based DTC scheme for IM drive. IEEE transactions on industry applications, 50(2), 1410-1420.
[62] Kazemi, M. V., Moradi, M., & Kazemi, R. V. (2014). Fuzzy logic control to improve the performance of the direct power control based DFIG. COMPEL: The International Journal for Computation and Mathematics in Electrical and Electronic Engineering.
[63] Suresh, M. C. V., & Nagaiah, M. (2013). FUZZY LOGIC-DIRECT TORQUE CONTROL OF INDUCTION MOTOR USING SVM TECHNIQUE. Global J. of Engg. & Appl. Sciences, 3(2).
[64] Chen, L., Fang, K. L., & Hu, Z. F. (2005, August). A scheme of fuzzy direct torque control for induction machine. In 2005 International Conference on Machine Learning and Cybernetics (Vol. 2, pp. 803-807). IEEE.
[65] D.casadei, G. Grandi ,G serra, A. Tani, " Effects of flux and torque hysteresis band amplitude in direct Torque of induction machines' ' Industrial Electronics, Control and Instrumentation, IECON apos; Vol 1, Issue, 5-9 Sep 1994 Page(s):299 – 304.
[66] D. Casadei, F. Profumo, G. Serra, and A. Tani, "FOC and DTC: Two viable schemes for induction motors torque control," IEEE Trans. Power Electron., vol. 17, no. 5, pp. 779–787, 2002.
[67] Y. A Chapuis, " Contrôle Directe du Couple d'une Machine Asynchrone par L'orientation de son Flux Statorique", Thèse Doctorat INPG, génie électrique.
[68] Sellah, M., Kouzou, A., Mohamed-Seghir, M., Rezaoui, M. M., Kennel, R., & Abdelrahem, M. (2021). Improved DTC-SVM based on input-output feedback linearization technique applied on DOEWIM powered by

two dual indirect matrix converters. Energies, 14(18), 5625.
[69] Malla, S. G. (2016, March). A review on Direct Torque Control (DTC) of induction motor: With applications of fuzzy. In 2016 International Conference on Electrical, Electronics, and Optimization Techniques (ICEEOT) (pp. 4557-4567). IEEE.
[70] Hassan, A. A., & Shehata, E. G. (2012). High performance direct torque control schemes for an IPMSM drive. Electric Power Systems Research, 89, 171-182.
[71] Aroussi, H. A., Ziani, E., Bouderbala, M., & Bossoufi, B. (2020). Improvement of direct torque control applied to doubly fed induction motor under variable speed. International Journal of Power Electronics and Drive Systems, 11(1), 97.
[72] Errami, Y., Ouassaid, M., Cherkaoui, M., & Maaroufi, M. (2015). Variable structure sliding mode control and direct torque control of wind power generation system based on the PM synchronous generator. Journal of Electrical Engineering, 66(3), 121.
[73] Zang, C., & Cao, X. (2009, August). Direct torque control based on space vector modulation with adaptive neural integrator for stator flux estimation in induction motors. In 2009 Fifth International Conference on Natural Computation (Vol. 6, pp. 355-359). IEEE.
[74] Rahman, M. F., Zhong, L., & Lim, K. W. (1998). A direct torque-controlled interior permanent magnet synchronous motor drive incorporating field weakening. IEEE Transactions on Industry Applications, 34(6), 1246-1253.
[75] Kiran Kumar, B., Siva Reddy, Y. V., & Vijaya Kumar, M. (2021). Neuro Fuzzy Controller for DTC of Induction Motor Using Multilevel Inverter with SVM. Journal of Circuits, Systems and Computers, 30(14), 2150250.

Chapter II

Mathematical Modeling & Analysis of PWM Techniques for Induction Motor Drive

II.1 Introduction

A mathematical model is used to represent or reproduce a given real system. The interest of a model is the analysis and prediction of the static and dynamic behavior of the physical system. This chapter's goals are to provide an overview of both the three-phase induction machine modeling (using state equations for voltage control) and choosing an adequate Pulse Width Modulation (PWM) strategy to deal with the motor.

In this chapter, we will present the three-phase induction machine`s mathematical model and its transformation into the two-phase (α, β) Concordia system. Moreover, we will study various techniques of the PWM used for controlling the inverter. Then we will set up the simulation results of the induction machine powered by the three-phase network.

II.2 operating principle

To operate the machine in motor mode, the rotor must be rotated in the direction of the rotating magnetic field, at a speed lower than the synchronous speed (the speed of the rotating field), which is expressed by the following equation [1].

$$\Omega_s = \frac{60\,f}{p} \qquad \text{(II.1)}$$

With:
Ω_s: Synchronism speed;
f: Electric Network Frequency (ENF);
p: Number of pole pairs.

The speed at which this machine begins to operate (motor mode operation) when it is linked to the electrical network is just a little bit slower than the speed of the stator magnetic field [2]. If the rotational speed of the rotor becomes the same (synchronous) as that of the magnetic field, no induction appears in the rotor, therefore no interaction happens with the stator (motor stopped) [3]. Finally, if the rotation speed of the rotor is slightly higher than that of the stator magnetic field (generator mode operation); an electromagnetic force similar to that obtained with a synchronous generator will be developed **[4]**. The difference between the rotation speed of the rotor and that of the magnetic field is called the slip [5], practically its value does not exceed few percent.

However, from a certain rotational speed, a noticeable decrease in the motor`s stator flux occurs, which requires more current for a similar torque. After reaching a maximum torque value, a reduction in torque and consequently electrical power is observed.

Figure (II.1) illustrates the induction motor components [6].

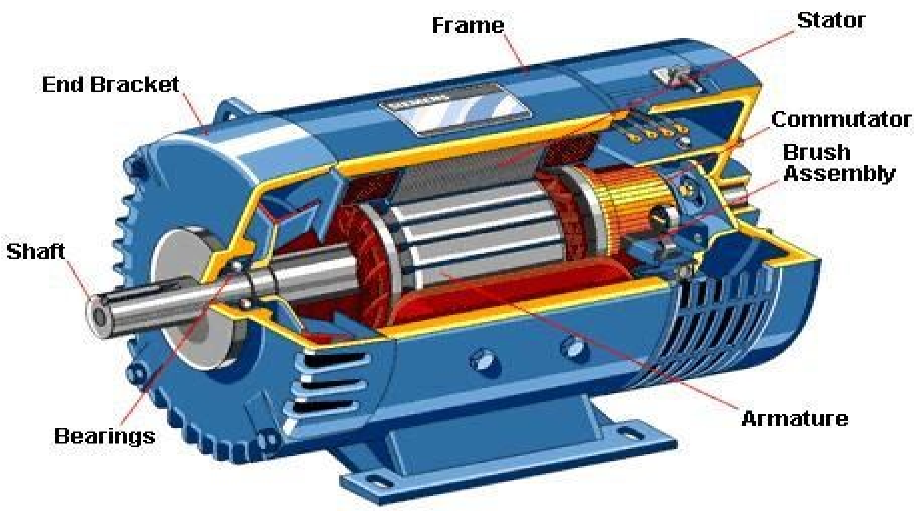

Figure II. 1: Induction motor components [6].

II.3 Induction Machine Modeling

II.3.1 Mathematical model of the induction motor

Modeling of any physical system is necessary in the research field because it allows researchers to predict how the system can be improved against various phenomena, thus, learning more about the mechanisms that control it. The induction machine can be modeled by different methods, depending on the desired purposes. The following models are developed in this chapter:

- ✓ Models in abc frame, resulting from differential equations controlling the operation of the machine. They are used mainly for the steady-state study [8] [9].
- ✓ The models resulting from Concordia's transformation are commonly used for the dynamic-state study and direct torque control (DTC) [10].

II.3.2 simplifying assumptions

An induction machine, with its windings distribution and geometry, is so complex that it cannot be analyzed, taking into account its exact configuration. Then, it is necessary to adopt simplifying assumptions **[11][12]**:

- ➢ The constant air gap;
- ➢ The neglected notching effect;
- ➢ Sinusoidal spatial distribution of magneto-motor air forces;
- ➢ Unsaturated magnetic circuit with constant permeability;
- ➢ Negligible ferromagnetic losses;
- ➢ The skin effect and warming effect on the characteristics are not taken into account.

Among the important consequences of these assumptions are:

- ➢ The association of flux.
- ➢ The self-inductances constancy;
- ➢ The invariance of stator resistances and rotor resistances;

- The sinusoidal variation law of the mutual inductances between the stator and rotor windings in terms of the electric angle of their magnetic axes,

The induction machine is represented schematically in Figure (II.2). It has six windings:

- The machine stator consists of three fixed windings shifted by 120° in space and crossed by three variable currents.
- The rotor can be modeled by three identical windings shifted in space by 120°. These windings are short-circuited and the voltage across them is zero.

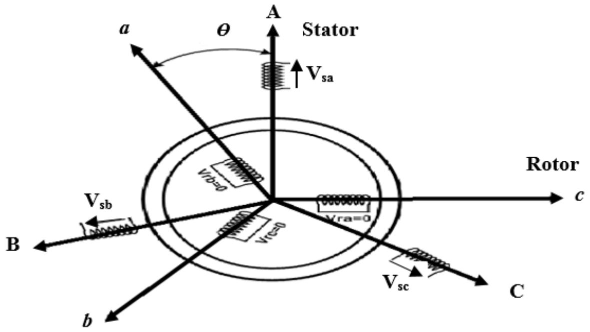

Figure II. 2: Representation of the induction machine.

II.3.3 Induction Machine Modeling

As mentioned above, to ensure motor operation, the IM's rotation speed must be lower than the synchronization speed (positive slip). Unlike the synchronous machine, the IM does not have a separate inductor. Therefore, it requires a reactive power input for its magnetization. When it is connected directly to the grid, the latter provides the required reactive power. On the other hand, in autonomous operation, it is necessary to bring this energy either by a battery of capacitors or by a controlled static converter (an inverter).

A mathematical model is necessary for the analysis of the IM's operation in both motor and generator modes. The analytical modeling will be presented in the section below.

II.3.3.1 Electrical equations of the asynchronous machine in the three-phase reference

The induction machine is of three phase nature. Taking into account the assumptions mentioned above, and using the diagram shown in Figure (II.2), the induction machine's basic equations are **[13] [14]**:

$$[v_{sabc}]^T = [R_s][i_{sabc}]^T + \frac{d}{dt}[\varphi_{sabc}]^T \tag{II.2}$$

$$[v_{rabc}]^T = 0 = [R_r][i_{rabc}]^T + \frac{d}{dt}[\varphi_{rabc}]^T \tag{II.3}$$

With:

v_{sabc} : The voltages applied to the three-stator phases.
i_{sabc} : The currents that cross the three-stator phases.
φ_{sabc} : The total flux through these windings.
R_s : The stator resistance.
R_r: The rotor resistance.

Each flux comprises an interaction with the currents of all the phases including its own.

$$\begin{bmatrix}\varphi_{sa}\\ \varphi_{sb}\\ \varphi_{sc}\\ \varphi_{ra}\\ \varphi_{rb}\\ \varphi_{rc}\end{bmatrix}=\begin{bmatrix} l_s & m_s & m_s & m_1 & m_3 & m_2\\ m_s & l_s & m_s & m_2 & m_1 & m_3\\ m\_s & m_s & l_s & m_3 & m_2 & m_1\\ m_1 & m_2 & m_3 & l_r & m_r & m_r\\ m_3 & m_1 & m_2 & m_r & l_r & m_r\\ m_2 & m_3 & m_1 & m_r & m_r & l_r\end{bmatrix}\begin{bmatrix} i_{sa}\\ i_{sb}\\ i_{sc}\\ i_{ra}\\ i_{rb}\\ i_{rc}\end{bmatrix} \tag{II.4}$$

Where:

l_s Is the self-inductance of a stator phase.

l_r Is the self-inductance of a rotor phase.

m_s Is the mutual inductance between two stator phases.

m_r Is the mutual inductance between two rotor phases.

m_{sr} Is the maximum mutual inductance between a stator phase and a rotor phase.

$$m_1 = m_{sr}\cos(\theta) \tag{II.5}$$

$$m_2 = m_{sr}\cos\left(\theta - \frac{2\pi}{3}\right) \tag{II.6}$$

$$m_3 = m_{sr}\cos\left(\theta + \frac{2\pi}{3}\right) \tag{II.7}$$

II.3.3.2 Three-Phase/Two-Phase Transformation (Concordia and Clarke Transformation)

The aim of using this transformation is to switch from a three-phase abc system to the stationary two-phase $\alpha\beta$ system [15] [16] [17]. There are mainly two transformations: Clarke and Concordia transformations. The magnitude of the converted quantities is saved by Clarke transformation, but neither the power nor the torque is (we must multiply by a coefficient of 3/2) [18]. While Concordia transformations keep the power but not the magnitude [19].

Table II. 1: Concordia and Clarke transformation.

Concordia Transformation	Clarke Transformation
$\begin{bmatrix}\boldsymbol{x_a}\\ \boldsymbol{x_b}\\ \boldsymbol{x_c}\end{bmatrix}\xrightarrow{\boldsymbol{F_{23}}}\begin{bmatrix}\boldsymbol{x_\alpha}\\ \boldsymbol{x_\beta}\end{bmatrix}$ i.e. $[\boldsymbol{x_{\alpha\beta}}]^{\boldsymbol{T}} = \boldsymbol{F_{23}}[\boldsymbol{x_{abc}}]^{\boldsymbol{T}}$ with : $\boldsymbol{F_{23}} = \sqrt{\frac{2}{3}}\begin{bmatrix}\boldsymbol{1} & -\frac{\boldsymbol{1}}{\boldsymbol{2}} & -\frac{\boldsymbol{1}}{\boldsymbol{2}}\\ \boldsymbol{0} & \frac{\sqrt{\boldsymbol{3}}}{\boldsymbol{2}} & -\frac{\sqrt{\boldsymbol{3}}}{\boldsymbol{2}}\end{bmatrix}$	$\begin{bmatrix}x_a\\ x_b\\ x_c\end{bmatrix}\xrightarrow{G_{23}}\begin{bmatrix}x_\alpha\\ x_\beta\end{bmatrix}$ **i.e.** $[x_{\alpha\beta}]^T = G_{23}[x_{abc}]^T$ with: $G_{23} = \frac{2}{3}\begin{bmatrix}1 & -\frac{1}{2} & -\frac{1}{2}\\ 0 & \frac{\sqrt{3}}{2} & -\frac{\sqrt{3}}{2}\end{bmatrix}$

Table II. 2: Transformation of a two-phase αβ system to a three-phase abc system.

Inverse Concordia transformation	Inverse Clarke transformation
$\begin{bmatrix} x_\alpha \\ x_\beta \end{bmatrix} \xrightarrow{F_{32}} \begin{bmatrix} x_a \\ x_b \\ x_c \end{bmatrix}$ i.e. $[x_{abc}]^T = F_{32}[x_{\alpha\beta}]^T$ with : $F_{32} = \sqrt{\frac{2}{3}} \begin{bmatrix} 1 & 0 \\ -\frac{1}{2} & \frac{\sqrt{3}}{2} \\ -\frac{1}{2} & -\frac{\sqrt{3}}{2} \end{bmatrix}$	$\begin{bmatrix} x_\alpha \\ x_\beta \end{bmatrix} \xrightarrow{G_{32}} \begin{bmatrix} x_a \\ x_b \\ x_c \end{bmatrix}$ i.e. $[x_{\alpha\beta}]^T = G_{32}[x_{abc}]^T$ with : $G_{32} = \begin{bmatrix} 1 & 0 \\ -\frac{1}{2} & \frac{\sqrt{3}}{2} \\ -\frac{1}{2} & -\frac{\sqrt{3}}{2} \end{bmatrix}$

II.3.3.3 Three-Phase/Two-Phase Transformation (Park Transformation)

Park transformation is a transformation of the fixed three-phase reference frame relative to the stator in a two-phase reference frame [20]. It allows moving from the abc reference to the (d, q) reference, where d refers to the direct axis and q to the quadrature axis. The (α, β) reference frame is always fixed according to the abc frame [21], where the (d, q) reference frame is mobile [22].

This transformation reduces the complexity of the system. The reference frame position can be fixed according to the three referential [23] [24]:

- Reference system linked to the rotating field.
- Referential linked to the stator.
- Reference system linked to the rotor.

The transformation matrix of Park and its inverse are given by:

$$\begin{cases} P(\theta) = k \begin{pmatrix} \cos(\theta) & \cos\left(\theta - \frac{2\pi}{3}\right) & \cos\left(\theta + \frac{2\pi}{3}\right) \\ -\sin(\theta) & -\sin\left(\theta - \frac{2\pi}{3}\right) & -\sin\left(\theta + \frac{2\pi}{3}\right) \\ \frac{1}{\sqrt{2}} & \frac{1}{\sqrt{2}} & \frac{1}{\sqrt{2}} \end{pmatrix} \\ P(\theta)^{-1} = P(\theta)^T = k \begin{pmatrix} \cos(\theta) & -\sin(\theta) & \frac{1}{\sqrt{2}} \\ \cos\left(\theta - \frac{2\pi}{3}\right) & -\sin\left(\theta - \frac{2\pi}{3}\right) & \frac{1}{\sqrt{2}} \\ \cos\left(\theta + \frac{2\pi}{3}\right) & -\sin\left(\theta + \frac{2\pi}{3}\right) & \frac{1}{\sqrt{2}} \end{pmatrix} \end{cases} \tag{II.8}$$

Where k is a constant that can take the value $2/3$ for the transformation with no power conservation or $\sqrt{2/3}$ for the transformation with power conservation [25].

II.3.4 Model of the induction machine in the Park referential

The Park transformation consists in applying to the currents, voltages, and flux a change of variables involving the angle between the windings axis and the axis of the Park (d, q) frame [26].

Equations (I.2), (I.3), and (I.4) give rise to the following system [27]:

$$\begin{cases} v_{sd} = R_s i_{sd} + \frac{d\phi_{sd}}{dt} - \omega_s \varphi_{sq} \\ v_{sq} = R_s i_{sq} + \frac{d\phi_{sq}}{dt} + \omega_s \varphi_{sd} \end{cases} \tag{II.9}$$

$$\begin{cases} v_{rd} = 0 = R_r i_{rd} + \frac{d\phi_{rd}}{dt} - \omega_r \varphi_{rq} \\ v_{rq} = 0 = R_r i_{rq} + \frac{d\phi_{rq}}{dt} + \omega_r \varphi_{rd} \end{cases} \tag{II.10}$$

With:

$$\begin{bmatrix} \varphi_{sdq} \\ \varphi_{rdq} \end{bmatrix} = \begin{bmatrix} L_s & 0 & L_m & 0 \\ 0 & L_s & 0 & L_m \\ L_m & 0 & L_r & 0 \\ 0 & L_m & 0 & L_r \end{bmatrix} \begin{bmatrix} i_{sdq} \\ i_{rdq} \end{bmatrix} \tag{II.11}$$

Indeed, the sub-matrices are now diagonal and no longer depend on θ (the electrical angle between the stator and the rotor).

The matrix system can also be written as [28]:

$$\begin{cases} \varphi_{sd} = L_s i_{sd} + L_m i_{rd} \\ \varphi_{sq} = L_s i_{sq} + L_m i_{rq} \end{cases} \tag{II.12}$$

$$\begin{cases} \varphi_{rd} = L_m i_{sd} + L_r i_{rd} \\ \varphi_{rq} = L_m i_{sq} + L_r i_{rq} \end{cases} \tag{II.13}$$

Where $L_s = l_s - m_s$, $L_r = l_r - m_r$, $L_m = \frac{2}{3} m_{sr}$

We have expressed the machine's equations, but there also remains the electromagnetic torque. The latter can be derived from the co-energy expression, or obtained using power balance.

The instantaneous power supplied to the stator and rotor windings is written as [29]:

$$P_e = [V_s]^T [I_s] + [V_r]^T [I_r] \tag{II.14}$$

By applying Park transformation, it is expressed in terms of the axes quantity dq

$$P_e = [v_{sd} \quad v_{sq}] \begin{bmatrix} i_{sd} \\ i_{sq} \end{bmatrix} + [v_{rd} \quad v_{rq}] \begin{bmatrix} i_{rd} \\ i_{rq} \end{bmatrix} = \underbrace{\frac{2}{3}\left[i_{sd} \frac{d\varphi_{sd}}{dt} + i_{sq} \frac{d\varphi_{sq}}{dt} + i_{rd} \frac{d\varphi_{rd}}{dt} + i_{rq} \frac{d\varphi_{rq}}{dt} \right]}_{first\ term}$$

$$+ \underbrace{\frac{2}{3}\left[(\varphi_{sd} i_{sq} - \varphi_{sq} i_{sd}) \omega_s + (\varphi_{rq} i_{rd} - \varphi_{rd} i_{rq}) \omega_r \right]}_{second\ term} \tag{II.15}$$

$$+\underbrace{\frac{2}{3}\left[R_s\left(i_{sd}^2+i_{sq}^2\right)+R_r\left(i_{rd}^2+i_{rq}^2\right)\right]}_{third\ term}$$

- The first term represents the magnetic energy stored in iron.
- The second term represents the electromechanical power P_{em} of the machine.
- The third term represents joule losses.

Taking into account the flux equations (II.12) and (II.13), several equal expressions result

$$\begin{cases} \Gamma_{em} = p(\varphi_{sd}i_{sq} - \varphi_{sq}i_{sd}) \\ \Gamma_{em} = p(\varphi_{rq}i_{rd} - \varphi_{rd}\, i_{rq}) \\ \Gamma_{em} = pL_m(i_{sq}i_{rd} - i_{sd}i_{rq}) \\ \Gamma_{em} = p\frac{L_m}{L_r}(\varphi_{rd}i_{sq} - \varphi_{rq}i_{sd}) \end{cases} \tag{II.16}$$

Where p is the number of pole pairs. The power P_{em} is also equal to $\Gamma_{em}\omega_r/p$, and the movement equation is [30]:

$$\Gamma_{em} - \Gamma_r = f\Omega_m + J\frac{d\Omega_m}{dt} \tag{II.17}$$

II.3.5 Selecting the dq Frame

The machine's equations and electrical quantities have been expressed thus far in a reference dq, which makes an electrical angle θ_s and θ_r with the stator and with the rotor respectively, but which is not defined elsewhere, i.e., it is free [31][32].

According to the application purpose, there are three main choices for the axis (d, q) frame orientation: a frame linked to the stator, rotor, or linked to the rotating field [33] [34]. In each of these referential, the equations of the machine become simpler than in any other referential [35]. Generally, the operating conditions will typically determine the most convenient reference for analysis and/or simulation purposes.

II.3.5.1 Reference linked to the stator

Regarding the stator, this referential is immobile. It is carried out to investigate machine braking and starting (i.e., this reference frame is better adapted to work with instantaneous quantities) [36]. In addition, this choice is used for direct torque control design [37].
It is characterized by:
$\omega = \omega_s = 0$ and therefore $\omega_r = -\omega_m$ (where ω is the arbitrary frame rate).
The system of equations in this reference frame is [38][39][40]:

$$\begin{cases} v_{sd} = R_s i_{sd} + \frac{d\varphi_{sd}}{dt} \\ v_{sq} = R_s i_{sq} + \frac{d\varphi_{sq}}{dt} \\ v_{rd} = 0 = R_r i_{rd} + \frac{d\varphi_{rd}}{dt} - \omega_r\varphi_{rq} \\ v_{rq} = 0 = R_r i_{rq} + \frac{d\varphi_{rq}}{dt} + \omega_r\varphi_{rd} \end{cases} \tag{II.18}$$

II.3.5.2 Reference linked to the rotor

In the case where the (d, q) reference frame is synchronized with the rotor $\omega = \omega_s = \omega_m$ and $\omega_r = 0$. This reference frame is used for the simulation of the dynamic state of machines where the speed is assumed constant [41]. In this case, the system of equations is [42]:

$$\begin{cases} v_{sd} = R_s i_{sd} + \frac{d\varphi_{sd}}{dt} - \omega_s \varphi_{sq} \\ v_{sq} = R_s i_{sq} + \frac{d\varphi_{sq}}{dt} + \omega_s \varphi_{sd} \\ v_{rd} = 0 = R_r i_{rd} + \frac{d\varphi_{rd}}{dt} \\ v_{rq} = 0 = R_r i_{rq} + \frac{d\varphi_{rq}}{dt} \end{cases} \quad \text{(II.19)}$$

II.3.5.3 Reference linked to the rotating magnetic field

This choice allows obtaining a sliding pulsation and properly adapts vector control through rotor flux orientation [43]. The reference frame linked to the synchronism (or rotating field), is fixed relative to the rotating field. It is used for the machine vector control and it is characterized by $\omega = \omega_s$, which implies that the adjustment variables are continuous [44]. The advantage of using this reference frame is to have constant quantities in a steady state; then it is easier to carry out the regulation. [45]. Then we can write [46]:

$$\begin{cases} v_{sd} = R_s i_{sd} + \frac{d\varphi_{sd}}{dt} - \omega_s \varphi_{sq} \\ v_{sq} = R_s i_{sq} + \frac{d\varphi_{sq}}{dt} + \omega_s \varphi_{sd} \\ v_{rd} = 0 = R_r i_{rd} + \frac{d\varphi_{rd}}{dt} - \omega_r \varphi_{rq} \\ v_{rq} = 0 = R_r i_{rq} + \frac{d\varphi_{rq}}{dt} + \omega_r \varphi_{rd} \end{cases} \quad \text{(II.20)}$$

These equations can be rewritten to have a different state vector (state variables system), i.e., instead of having the flux, we can write it in currents; we just need to make substitutions of equations (II.12) and (II.13) in equations (II.20).

II.3.6 Model of the induction machine in the (α, β) frame

The dynamic model of an induction motor can be developed from its basic electrical and mechanical equations [47]. In the stationary reference frame, the voltages are expressed as follows [48]:

$$\begin{cases} v_{s\alpha} = R_s i_{s\alpha} + s\varphi_{s\alpha} \\ v_{s\beta} = R_s i_{s\beta} + s\varphi_{s\beta} \\ v_{r\alpha} = 0 = R_r i_{r\alpha} + s\varphi_{r\alpha} + \omega_r \varphi_{r\beta} \\ v_{r\beta} = 0 = R_r i_{r\beta} + s\varphi_{r\beta} - \omega_r \varphi_{r\alpha} \end{cases} \quad \text{(II.21)}$$

Where s indicates the differential operator (d/dt).
The stator and rotor fluxes equations are [49]:

$$\begin{cases} \varphi_{s\alpha} = L_s i_{s\alpha} + L_m i_{r\alpha} \\ \varphi_{s\beta} = L_s i_{s\beta} + L_m i_{r\beta} \\ \varphi_{r\alpha} = L_r i_{r\alpha} + L_m i_{s\alpha} \\ \varphi_{r\beta} = L_r i_{r\beta} + L_m i_{s\beta} \end{cases} \tag{II.22}$$

In these equations, R_s, R_r, L_s, and L_r are respectively the resistors and the inductances of the stator windings and the rotor windings, L_m is the mutual inductance and $\omega_r = p.\Omega_r$ is the rotor speed (with p is the pairs poles number). Additionally, ω_s is the synchronous pulsation.

$v_{s\alpha}$, $v_{s\beta}$, $v_{r\alpha}$, $v_{r\beta}$, $i_{s\alpha}$, $i_{s\beta}$, $i_{r\alpha}$, $i_{r\beta}$, $\emptyset_{s\alpha}$, $\emptyset_{s\beta}$, $\emptyset_{r\alpha}$ and $\emptyset_{r\beta}$ are the direct and quadratic components, respectively of the voltages and currents as well as the fluxes of both the stator and the rotor.

The mechanical equation is [50]:

$$\Gamma_{em} - \Gamma_r = f\Omega_m + J\frac{d\Omega_m}{dt} \tag{II.23}$$

Where Γ_{em} is the electromagnetic torque [N.m] and Γ_r is the resistive torque imposed by the machine shaft [N. m].

The electromagnetic torque is [51]:

$$\Gamma_{em} = \frac{3}{2}p\left(\varphi_{s\alpha} i_{s\beta} - \varphi_{s\beta} i_{s\alpha}\right) \tag{II.24}$$

For the complete model of the induction machine, the flux expressions are replaced in the voltage equations. We obtain a mechanical equation and four electrical equations in terms of the stator currents, rotor fluxes components and the induction machine's electric speed as well [46].

$$\begin{cases} \frac{di_{s\alpha}}{dt} = -\frac{1}{\sigma L_s}\left(R_s + \frac{1}{T_r}\frac{L_m^2}{L_r}\right) i_{s\alpha} + \frac{1}{\sigma L_s}\left(\frac{L_m}{L_r}\frac{1}{T_r}\right)\varphi_{r\alpha} + \frac{1}{\sigma L_s}\left(\frac{L_m}{L_r}\right)\omega_r \varphi_{r\beta} \\ \frac{di_{s\beta}}{dt} = -\frac{1}{\sigma L_s}\left(R_s + \frac{1}{T_r}\frac{L_m^2}{L_r}\right) i_{s\beta} - \frac{1}{\sigma L_s}\left(\frac{L_m}{L_r}\right)\omega_r \varphi_{r\alpha} + \frac{1}{\sigma L_s}\left(\frac{L_m}{L_r}\frac{1}{T_r}\right)\varphi_{r\beta} \\ \frac{d\varphi_{r\alpha}}{dt} = \frac{L_m}{T_r} i_{s\alpha} - \frac{1}{T_r}\varphi_{r\alpha} - \omega_r \varphi_{r\beta} \\ \frac{d\varphi_{r\beta}}{dt} = \frac{L_m}{T_r} i_{s\alpha} + \omega_r \varphi_{r\alpha} - \frac{1}{T_r}\varphi_{r\beta} \end{cases} \tag{II.25}$$

Such as: $\omega_m = p\Omega_m ; \omega_r = \left[\omega_s - \omega_m\right] ; \sigma = 1 - \frac{L_m^2}{L_s L_r} ; T_r = \frac{L_r}{R_r} ; T_s = \frac{L_s}{R_s}$

Modeling the machine in this way reduces the number of quantities that we need to know, in order to simulate machine operation. In fact, only the instantaneous values of the stator voltages and the resistive torque must be determined to impose them on the machine. Therefore, we do not need to know the stator pulsation value, or the slip as in the case of the model whose equations are written in the reference frame rotating in synchronism [109].

II.3.7 Voltage Powered Machine State Space Representation

The state space representation of the induction machine depends on the selected frame and the selection of state variables for the electrical equations. We write the equations in the (α, β) frame because it is the most general and complete solution [52]. The objectives for either the control or observation determines the state variables to be used [53].

For a three-phase IM powered by voltage, the stator voltages $(v_{s\alpha}, v_{s\beta})$ are considered as control variables, and the load torque Γ_r as a disturbance [54]. In our case, we choose the state vector $x = [i_{s\alpha} \quad i_{s\beta} \quad \varphi_{r\alpha} \quad \varphi_{r\beta}]^T$, we obtain [40]:

$$\dot{x}(t) = A(t)x(t) + B(t)u(t) \tag{II.26}$$

with:

$$A(t) = \begin{bmatrix} -\frac{1}{\sigma L_s}\left(R_s + \frac{1}{T_r}\frac{L_m^2}{L_r}\right) & 0 & \frac{1}{\sigma L_s}\left(\frac{L_m}{L_r}\frac{1}{T_r}\right) & \frac{1}{\sigma L_s}\left(\frac{L_m}{L_r}\right)\omega_r \\ 0 & -\frac{1}{\sigma L_s}\left(R_s + \frac{1}{T_r}\frac{L_m^2}{L_r}\right) & -\frac{1}{\sigma L_s}\left(\frac{L_m}{L_r}\right)\omega_r & \frac{1}{\sigma L_s}\left(\frac{L_m}{L_r}\frac{1}{T_r}\right) \\ \frac{L_m}{T_r} & 0 & -\frac{1}{T_r} & -\omega_r \\ 0 & \frac{L_m}{T_r} & \omega_r & -\frac{1}{T_r} \end{bmatrix} \tag{II.27}$$

$$B(t) = \begin{bmatrix} \frac{1}{L_s\sigma} & 0 \\ 0 & \frac{1}{L_s\sigma} \\ 0 & 0 \\ 0 & 0 \end{bmatrix} \tag{II.28}$$

and: $$u(t) = \begin{bmatrix} v_{s\alpha} \\ v_{s\beta} \end{bmatrix} \tag{II.29}$$

II.3.8 Simulation Results

The purpose of this test is to validate our motor block before using it with space vector PWM (SVPWM) and with direct torque control. Our goal is to integrate it later in the simulations. To carry out the simulation, we translate the mathematical model of the machine using the SimPowerSystem blocks of the Matlab/Simulink software.

No-load test:

For an induction machine supplied directly by the 220/380V three-phase network and running off-load, we visualize the mechanical speed, the electromagnetic torque, the stator currents as well as the components of both the current and the stator flux.

The simulation results are represented in the figures (II.3 - II.7)

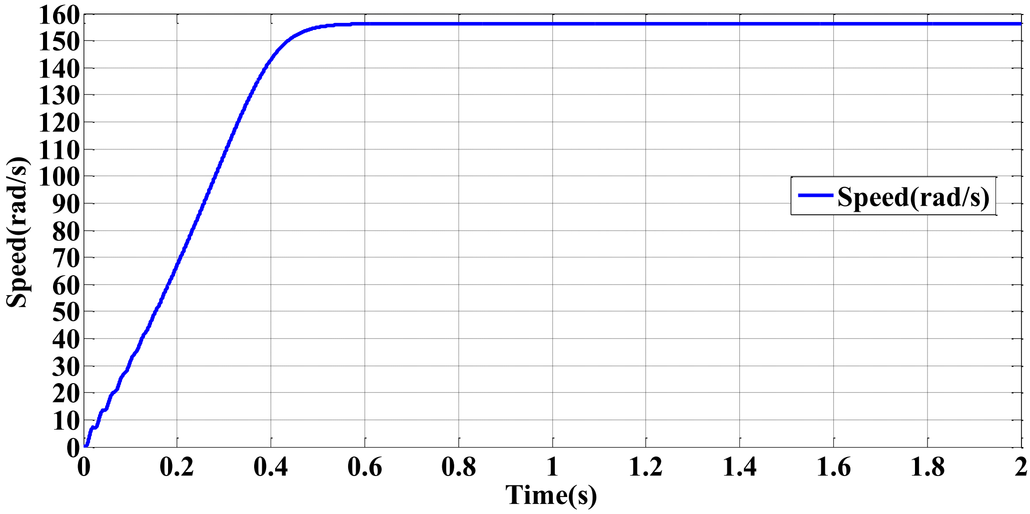

Figure II. 3: Rotor speed simulation result

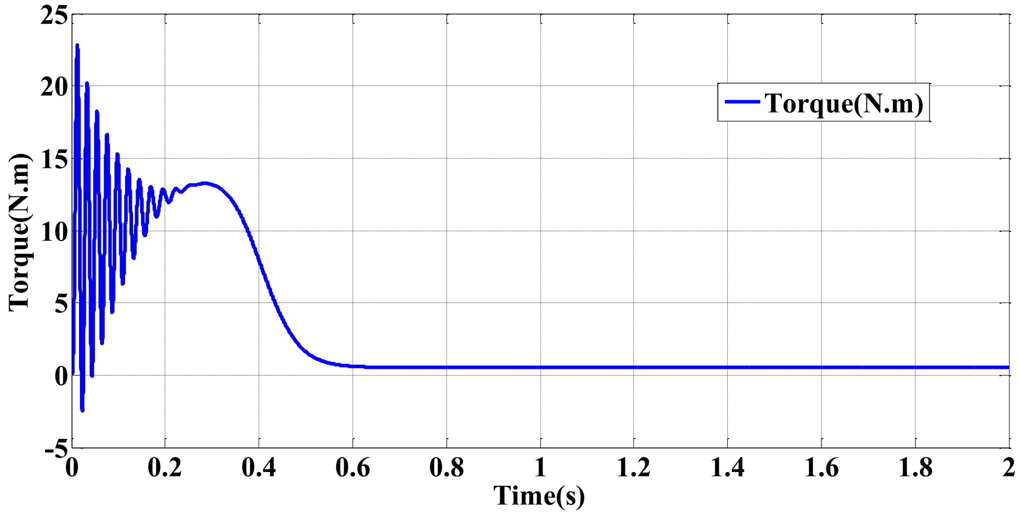

Figure II. 4: Magnetic torque simulation result.

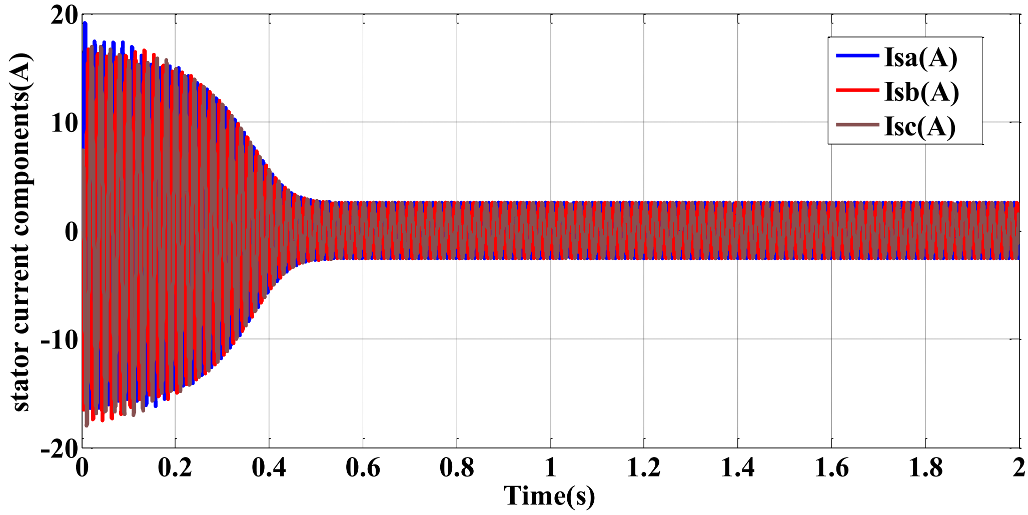

Figure II. 5: Stator currents simulation result.

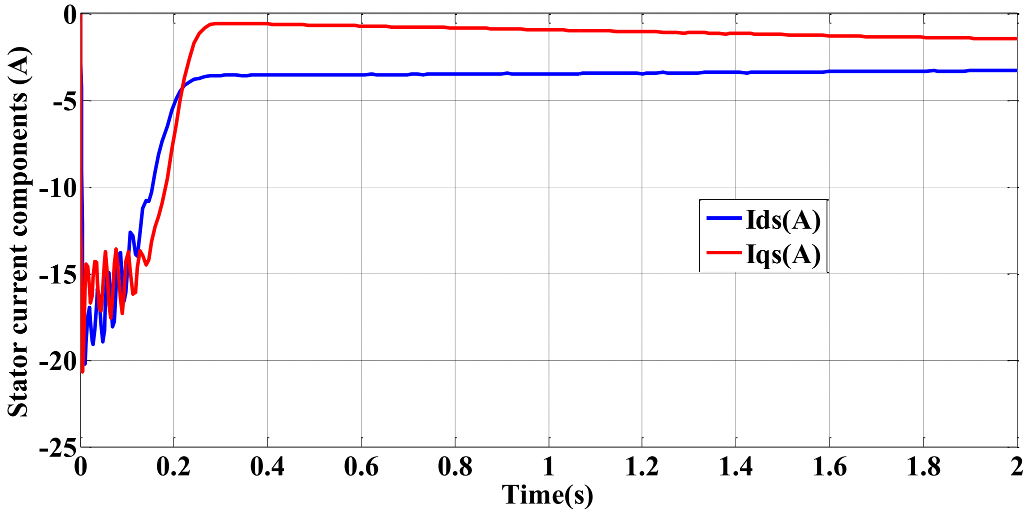

Figure II. 6: Stator currents components simulation result.

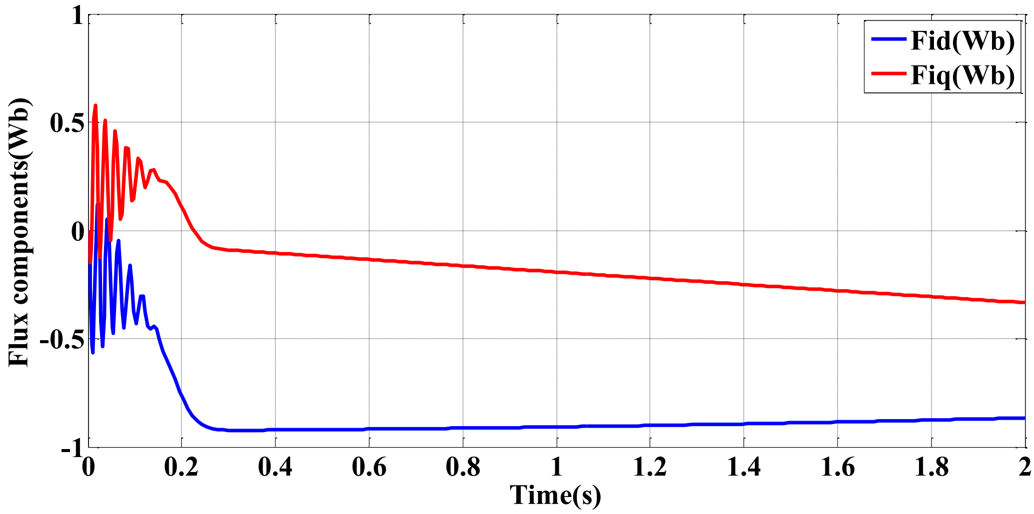

Figure II. 7: Stator flux components simulation result.

The steady-state speed stabilizes at a value close to the synchronism speed because the machine is not loaded. At no-load starting, the torque is strongly pulsating; it reaches a maximum value in the range of 3.2 times the nominal torque. This is due to the noises generated by the mechanical part, and after the disappearance of the transitory mode, it tends towards the value corresponding to the zero load. The absorbed current is high at start-up; it is about three times the rated. At a steady state, there remains the current corresponding to the inductive behavior of the no-loaded motor. The rotor current is significant during start-up and drops completely at a steady state.

Load variations after no-load starting:

Figures (II.8-II.12) represent the three-phase currents, the rotational speed, and the electromagnetic torque of the motor respectively. Two cases are carried out in this simulation with no load and with a loaded motor:

- When the motor run under no load condition, in the dynamic state, we observe an excessively absorbed current that stabilizes to produce a sinusoidal form with constant amplitude.

  When the motor is not loaded, we observe at the beginning of the start-up running that the increase in speed is virtually linear, and the total inertia around the rotating shaft determines the speed-up time (about $0.5\ s$), where the obtained speed is close to $157\ rad/s$
- Under load: a load torque ($\Gamma_r = 7\ N.m$) is applied to the machine shaft (at time $t = 1.5\ s$). When the electromagnetic torque reaches the load torque, obviously there is a reduction in rotating speed. Additionally, we notice an increase in the stator currents' magnitude and a slight decrease in the flux.

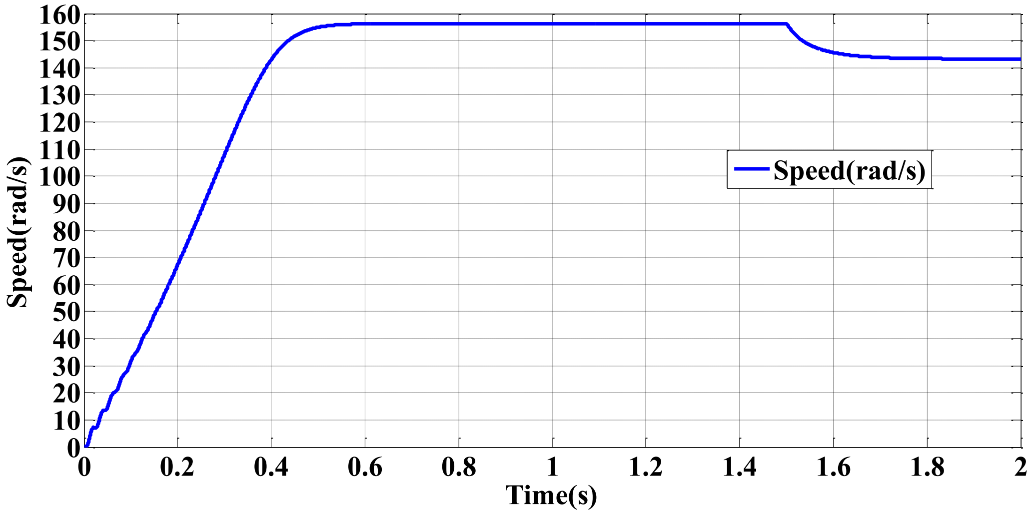

Figure II. 8: Rotor speed simulation result.

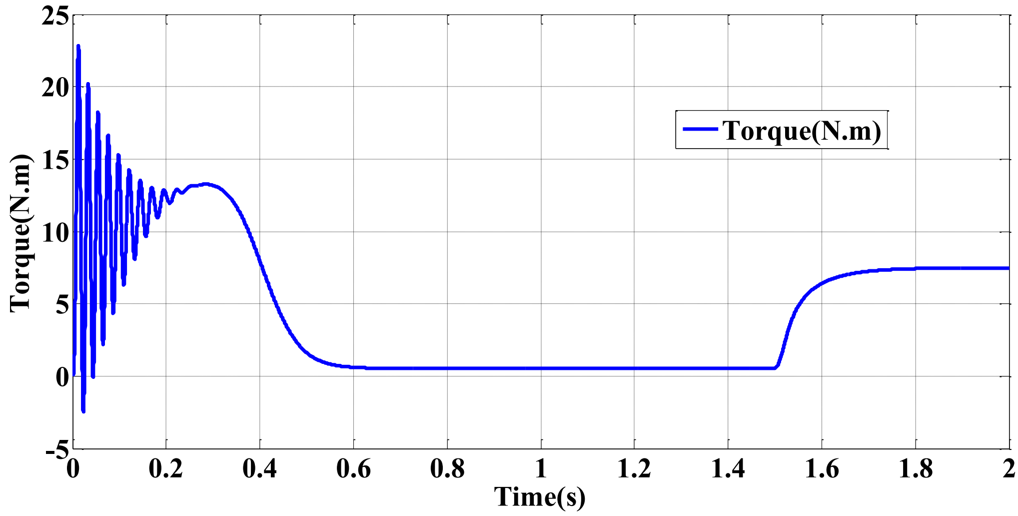

Figure II. 9: Magnetic torque simulation result.

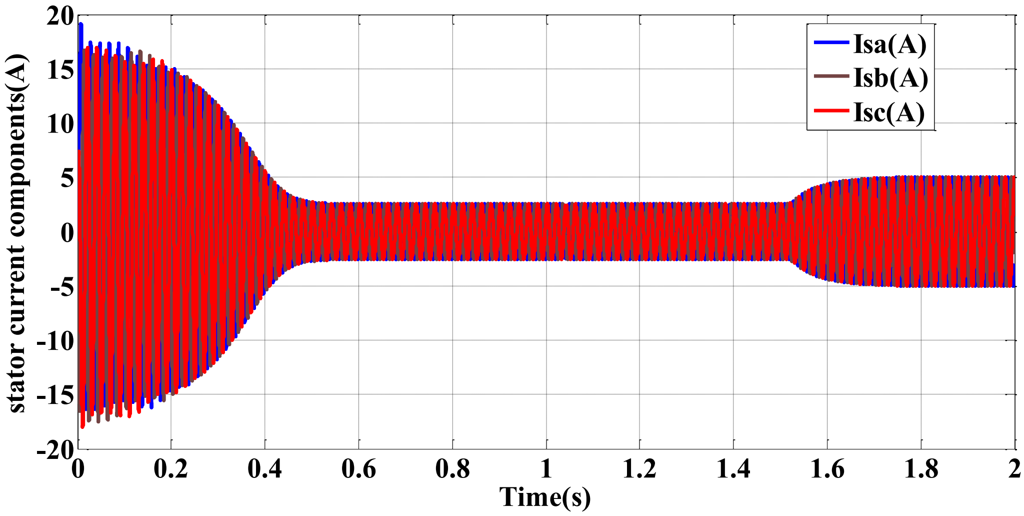

Figure II. 10: Simulation result stator currents.

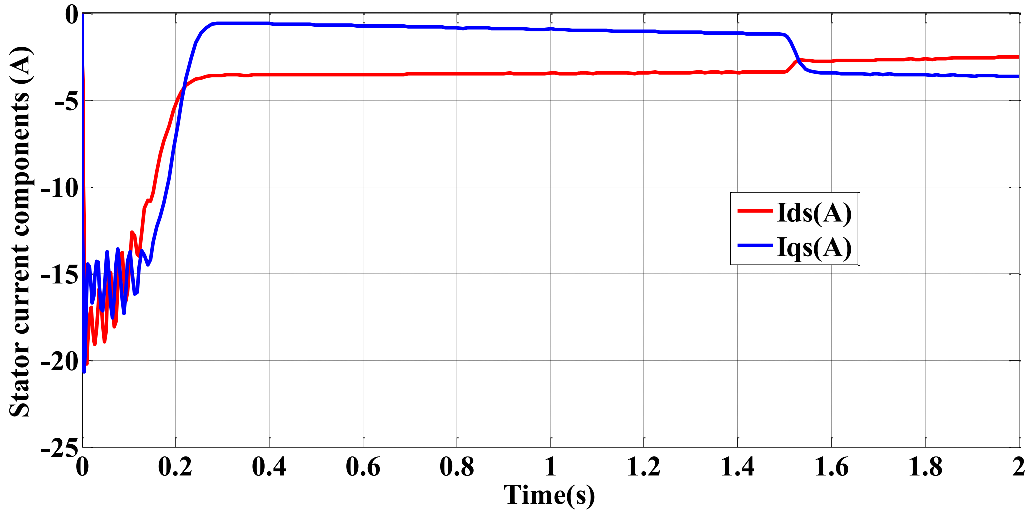

Figure II. 11: Stator currents components simulation result.

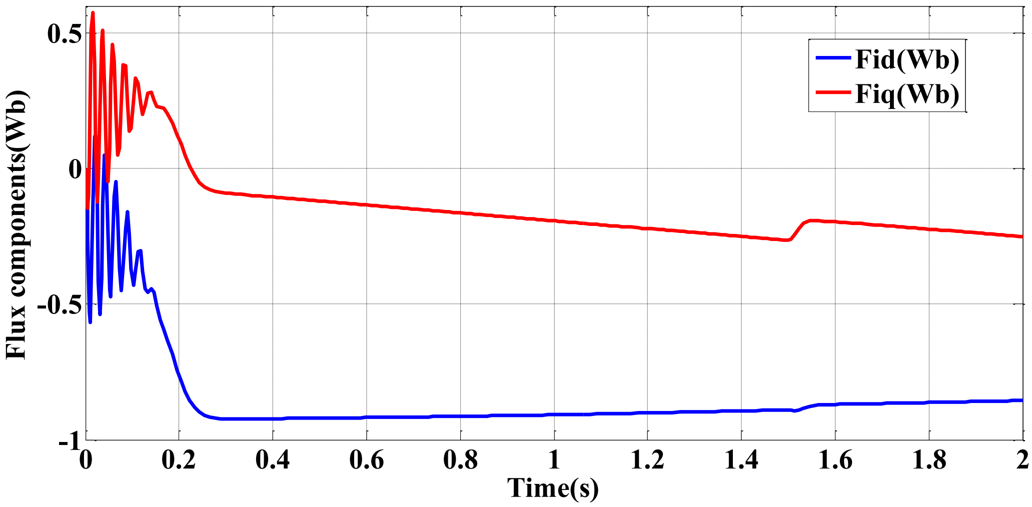

Figure II. 12: Stator flux components simulation result.

Starting under load:

While starting under load Figures (II.13-II.17), the electromagnetic torque responds instantly (because Γ_{em} is greater than Γ_r) and the asynchronous motor accelerates, where the speed is slightly disturbed. Without control, a high overshoot response for electromagnetic torque is obtained. Therefore, it is not recommended to be used in an open loop system for stability reasons.

In steady state operation, for the motor to operate correctly, the electromagnetic torque Γ_{em} must be equal to the resistive torque Γ_r. All of these characteristics and the moment of the resistive torque define the operating point of the induction machine.

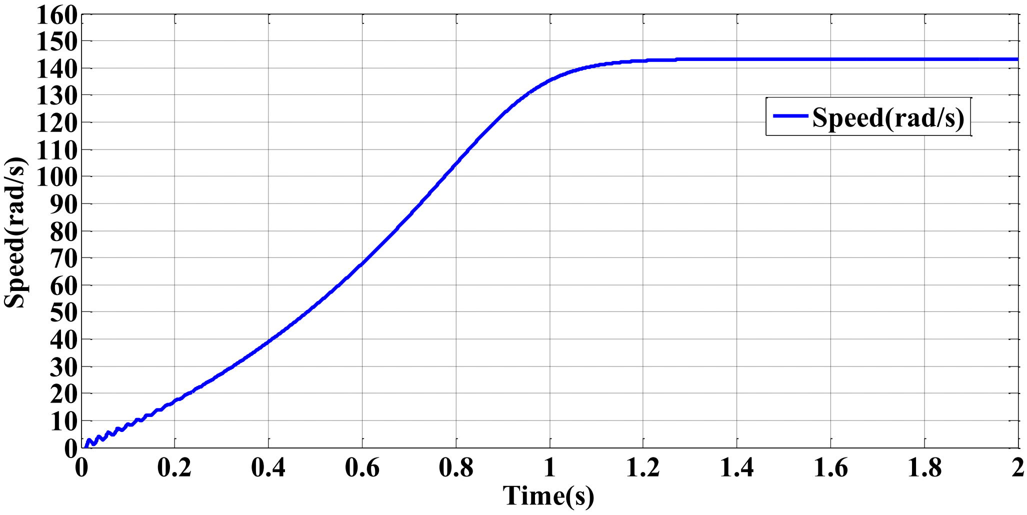

Figure II. 13: Rotor speed simulation result.

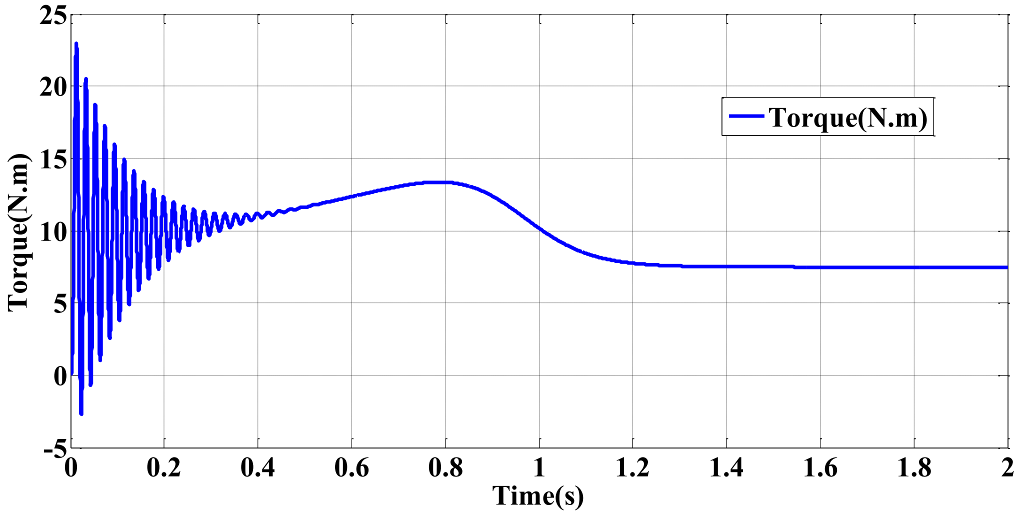

Figure II. 14: Magnetic torque simulation result.

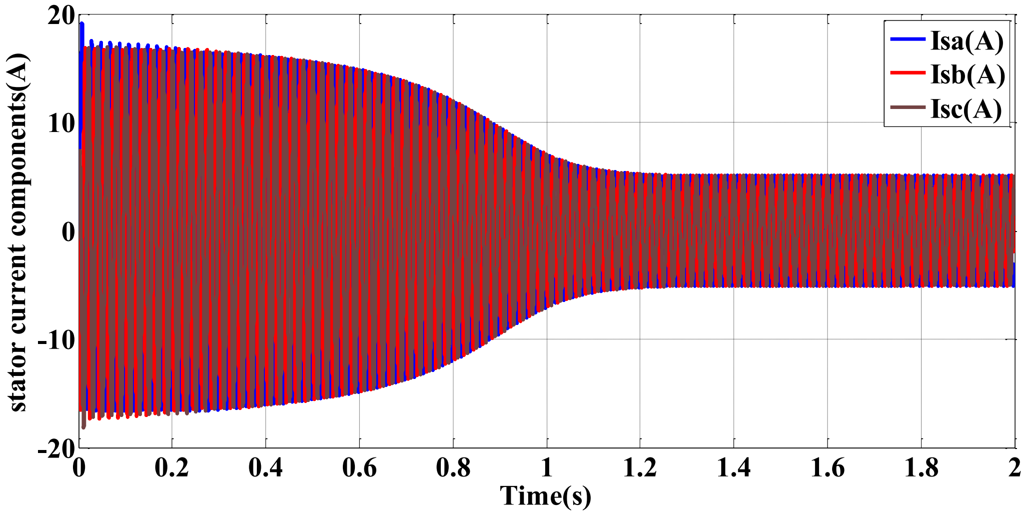

Figure II. 15: Simulation result stator currents.

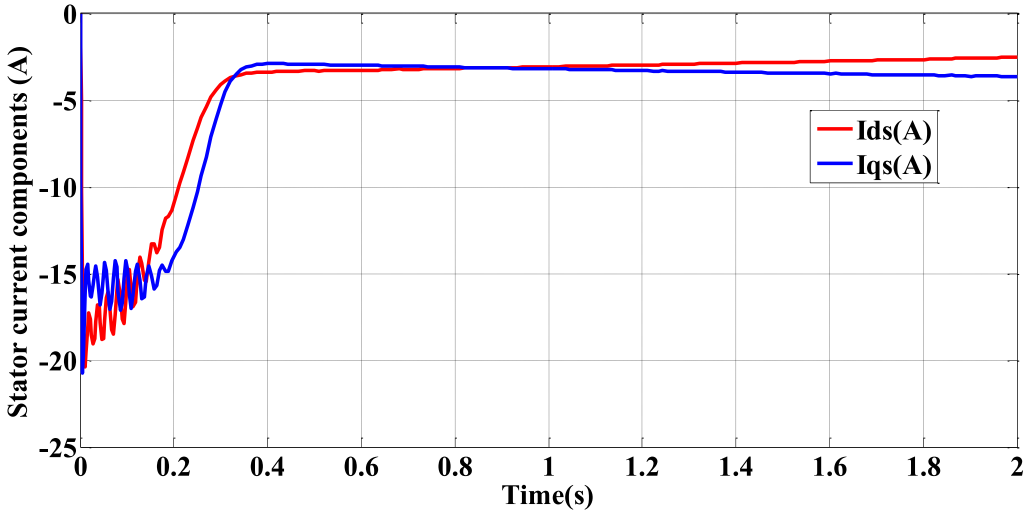

Figure II. 16: Stator currents components simulation result.

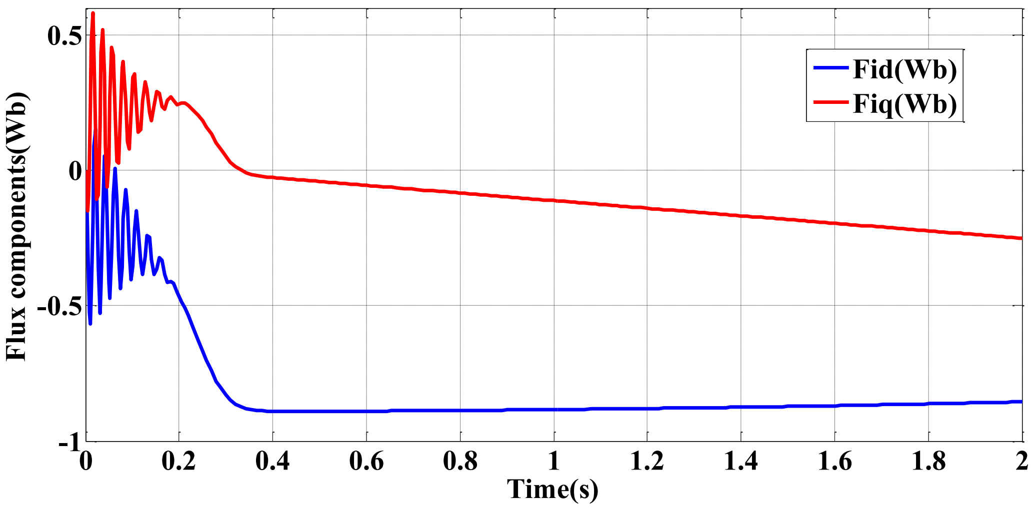

Figure II. 17: Simulation result stator flux components.

II.4 Study of different pulse width modulation techniques (PWM)

The extremely fast development of high-performance controls intended for alternating current machines requires similarly high-performance adjustment tools for voltage and frequency quantities [55] [56]. The PWM technique is a necessary step to make these adjustments from a fixed frequency and fixed voltage source (generally a DC voltage source) through a direct converter [57]. In fact, using switches, the converter creates electrical connections between the source and the load, and the only mode of operation accessible is temporal, i.e. the control of the switches' opening and closing times, and their order as well [58].

The inverter used consists of IGBT- transistor type controlled by the PWM technique [59]. The idea behind this is to supply chopped voltages at a fixed frequency across the induction machine's terminals, to make the fundamental voltage as close as feasible to the reference voltages acquired from the current regulators [10]. Several PWM techniques are used to control the switching times and the conduction time of each inverter switch (triangular sinusoidal, optimized, calculated, with homopolar harmonics injection, vector modulation…). The PWM function acts as an interface between the control part of a variable speed drive and the associated electrical machine [60]. This function acts on the voltage inverter's power part and serves an essential role with consequences on all system performance [61].

Certainly, Space Vector Pulse Width Modulation (SVPWM) is the most suitable modulation method for controlling asynchronous motors [62]. Unlike other methods, the SVPWM does not depend on individual modulation calculations for each of the inverter's arms [63]. A control voltage vector is globally calculated and approximated over a modulation period by an average voltage vector [63].

II.4.1 Pulse width modulation

The waves delivered by inverters with conduction mode 180°or conduction mode 120° are rich in harmonics [64][65]. To attenuate these harmonics, a filter can be placed at the inverter's output [66][67]. Filtering the output voltage or current of an inverter (that delivers only one voltage or current pulse per alternation) is difficult and expensive because the first harmonic to be eliminated (the 3rd or 5th order harmonic) is at a frequency extremely close to that of the fundamental [68]. PWM proves to be the most appropriate technique for controlling the inverter while having a good output wave [69].

II.4.1.1 Main objectives of a PWM

- Obtain currents in the electrical load whose variation is close to a sinusoid by controlling the duty cycle evolution due to the high switching frequency of the switches compared to the frequency of the output voltages [70].
- Allow adequate control of the fundamental magnitude of the output voltages generally over the widest possible range and for a widely varying output frequency [71].

II.4.1.2 Different PWM techniques

Several modulation techniques have been adopted to enhance the voltage quality at the inverter's output, among which we can mention:

II.4.1.2.1 Uniform Pulse with Modulation (UPWM)

In this technique, a triangular carrier is compared with a rectangular reference signal [72]. A pulse train with identical width crenellations makes up the output wave figure (II.18).

If the modulation index is equal to one, we obtain the singular modulation, in which the output signal is formed of a single pulse per half-period.

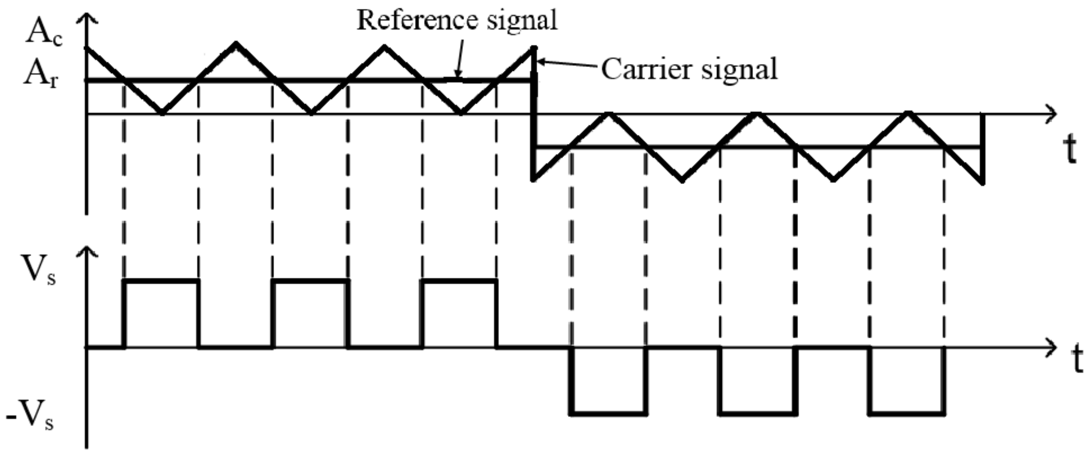

Figure II. 18: Multiple pulse width modulation.

II.4.1.2.2 Sinusoidal PWM (PWM by natural sampling)

In this case, the reference signal is sinusoidal; a wave formed by a pulse train of variable width is obtained at the inverter's output (figure II.19).

Points, where the modulating and the carrier intersect determine the switching instants.

The carrier fixes the switching frequency of the switches [73]. This type of PWM is the most used in industrial applications, as it has proven to be the most effective in harmonics neutralizing [74].

The essential PWM parameters are [75][76]:

- ✓ The modulation index: $m_f = \frac{f_p}{f_r}$

Where

f_p is the frequency modulation (carrier).

f_r is the fundamental frequency of the inverter's output quantities.

- ✓ The adjustment coefficient or the amplitude modulation index: $m_a = \frac{A_r}{A_p}$

With A_r is the peak fundamental voltage for the required load.

A_p: Magnitude of the output voltage pulses.

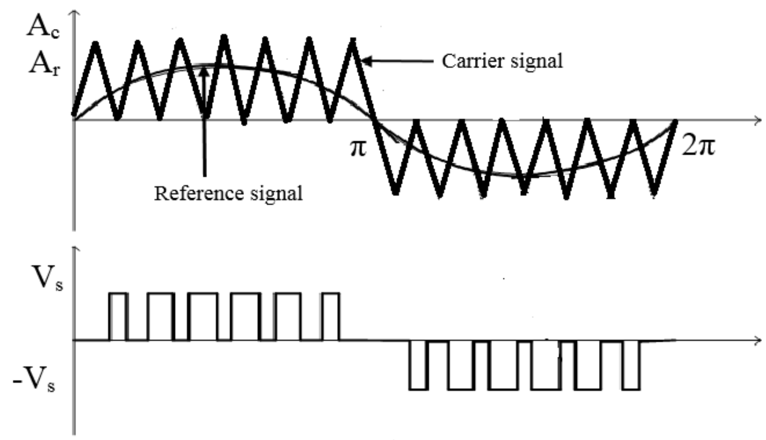

Figure II. 19: Unipolar triangular sinusoidal PWM.

Increasing m_f rejects first non-zero harmonics towards higher frequencies and makes filtering easier [77] [78]. However, m_f is limited by the switching times of the converter switches and therefore by the pulses' minimum width.

II.4.1.2.3 Symmetrical regular sampling PWM

Unlike the natural PWM, in this technique, the reference voltages sampling (the sinusoid) is done at periodically spaced instants [79]. This modulation technique is a version of the previous ones, where we try to make the signal symmetrical at time T_e, to reduce harmonics [80]. The modulating wave is sampled at each carrier positive peak. This value is kept constant for a chopping period T (period of the triangular signal) using a zero-order blocker [81].
The principle of this modulation is shown in figure (II.20)

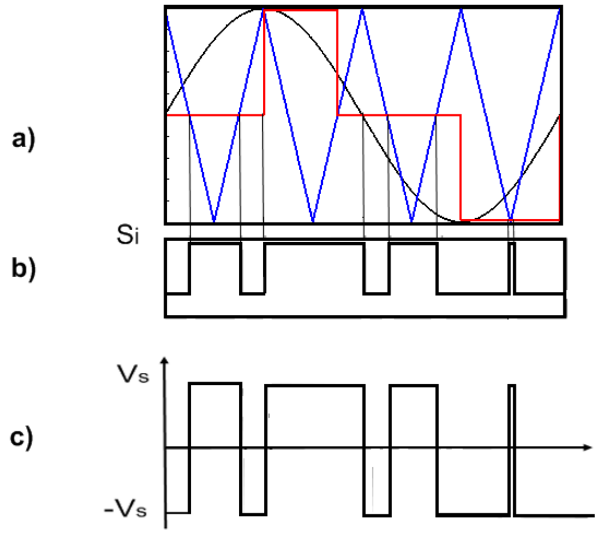

Figure II. 20: PWM with symmetric sampling.

a) Black color curve: sinusoidal reference of phase **i** ($\boldsymbol{V_{ref}(t) = V_m \sin(\omega t)}$)

Blue color curve: triangular carrier $\boldsymbol{V_t(t)}$.

Red color curve: sampled version of the modulating wave $\boldsymbol{V_{ref}(k)}$.

b) Control pulse for phase **i**.

c) Output voltage for phase **i**, $\boldsymbol{V_{out}(t)}$.

This process generates a step wave, which is the sine reference approximation. The step wave is then compared to the triangular carrier.

II.4.1.2.4 Asymmetrical regular sampling PWM

Harmonics distortion can be reduced by sampling the sine reference twice per triangle wave period [80].

Thus, while keeping the same frequency for switch switching, the sampling frequency can be doubled, and the response can be enhanced by reducing the distortion rate [81].

To do this, we sample the entire half-period of the PWM (or the sampling period is divided by two: ($T_e = T_h/2$)) and we calculate independently the passage instant to 1 and the return instant to 0 [82]. Figure (II.21) shows the principle of this modulation.

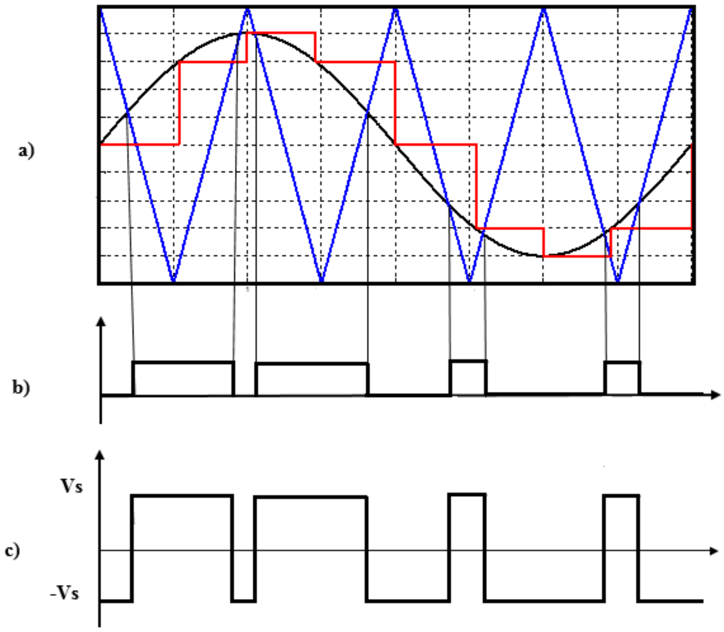

Figure II. 21: Asymmetric sampling PWM.

a) Blue color curve: triangular carrier $\boldsymbol{V_t\ (t)}$

Black color curve: sinusoidal reference of phase **i** ($\boldsymbol{V_{ref}(t)\ =\ V_m\ sin(\omega t)}$).

Red color curve: sampled version of the modulating wave $\boldsymbol{V_{ref}\ (k)}$.

b) Control pulse for phase **i**.

c) Output voltage for phase i, $\boldsymbol{V_{out}(t)}$.

II.4.1.2.5 Suboptimal PWM

In three-phase, it is possible to reduce harmonics without reducing the output voltages magnitude, since third harmonics or its multiples are eliminated from the output voltages [83] [84].

A third harmonic can be added to the sinusoid of frequency f to generate the reference wave [85] [86]. The third harmonic will be found in the fictional voltages V_{a0}, V_{b0}, V_{c0} relative to the fictitious midpoint 0 of the input, but it disappears in the ground-to-neutral voltages V_{an}, V_{bn}, V_{cn} and in $V_{ab},\ V_{bc}, V_{ca}$ at the output [87] [88].

The third harmonic addition allows the maximum fundamental magnitude to be increased in the output voltages [89] [90]. Figure (II.22) shows the principle of this modulation.

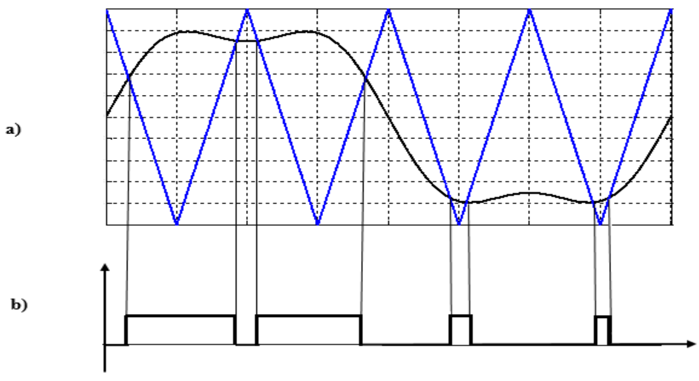

Figure II. 22: Suboptimal PWM.

a) Blue color curve: triangular carrier $V_t(t)$
Black color curve: reference signal V_{ref}
b) Control pulse for phase **i**.

II.4.1.2.6 Calculated PWM (SPWM)

With this PWM technique, the switches' switching times are calculated to satisfy a requirement set related to the frequency spectrum of the wave supplied by the inverter [91] [92].
The criteria usually used are [93] [94]:

- ✓ Removing a specified rank harmonics,
- ✓ Elimination of harmonics in a specified band,
- ✓ Reduction of global harmonic criteria.

Typically, we take a wave that has asymmetries about a quarter of the period and then use the symmetry to define the other angles [95] [96]. After Fourier series decomposition, figure (II.23) shows the presence of odd-order harmonics in a bipolar PWM signal that is symmetric with respect to the quarter period and ant-symmetric with respect to the half period [97] [98].
The switching angles α_1, α_2, α_3, α_4,... α_N allow us, by controlling them, to eliminate $(N-1)$ harmonics and to control the fundamental [99] [100].

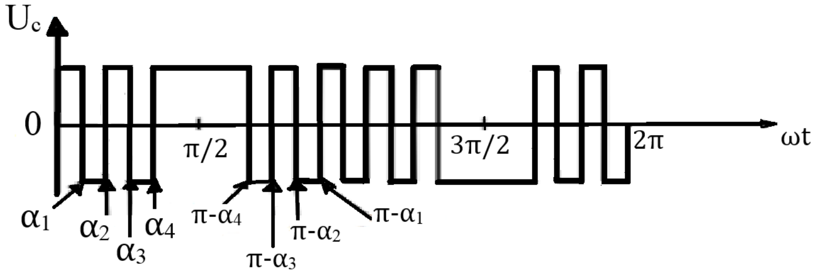

Figure II. 23: Bipolar PWM signal.

II.4.1.2.7 Space Vector PWM (SVPWM)

This method is highly desired in the control field, it has significant effects on current and torque ripples, which is why it is the most used by researchers and industrialists [101]. It makes it possible to determine the sequences of ignitions and extinctions of the converter's components, and thus reduces the harmonics of the voltages applied to the motor [102].
The SVPWM vector modulation technique differs from that of SPWM in that instead of using a separate modulator for each of the three phases, the reference voltages are given by a global control vector approximated over a modulation period T_z[103].
It is based on the spatial representation of the voltage vector in the stationary frame (α,β) [104]. The eight switching states (Figure II. 24) can be expressed in the (α,β) frame by eight voltage vectors, $\overrightarrow{V_0},\overrightarrow{V_1},\overrightarrow{V_2},\overrightarrow{V_3},\overrightarrow{V_4},\overrightarrow{V_5},\overrightarrow{V_6},\overrightarrow{V_7}$ among them, two are null $(\overrightarrow{V_0})$ and $(\overrightarrow{V_7})$ which correspond to $S(000)$ and $S(111)$ respectively, the others are called active states [105].
SVPWM is recently the most suitable method for controlling induction motors [106]. Unlike other methods, SVPWM does not rely on separate modulation calculations for each of the inverter arms [107].
This PWM technique follows the following principles [108]:

- A control voltage vector V_{sref} is calculated globally and approximated over a modulation period « T_z » by an average voltage vector.
- For each phase, the production of a pulse of width T with a period-centered average value equal to the reference voltage, at the sampling instant.
- All the switches of the same half-bridge have an identical state, at the center and both ends of the period.

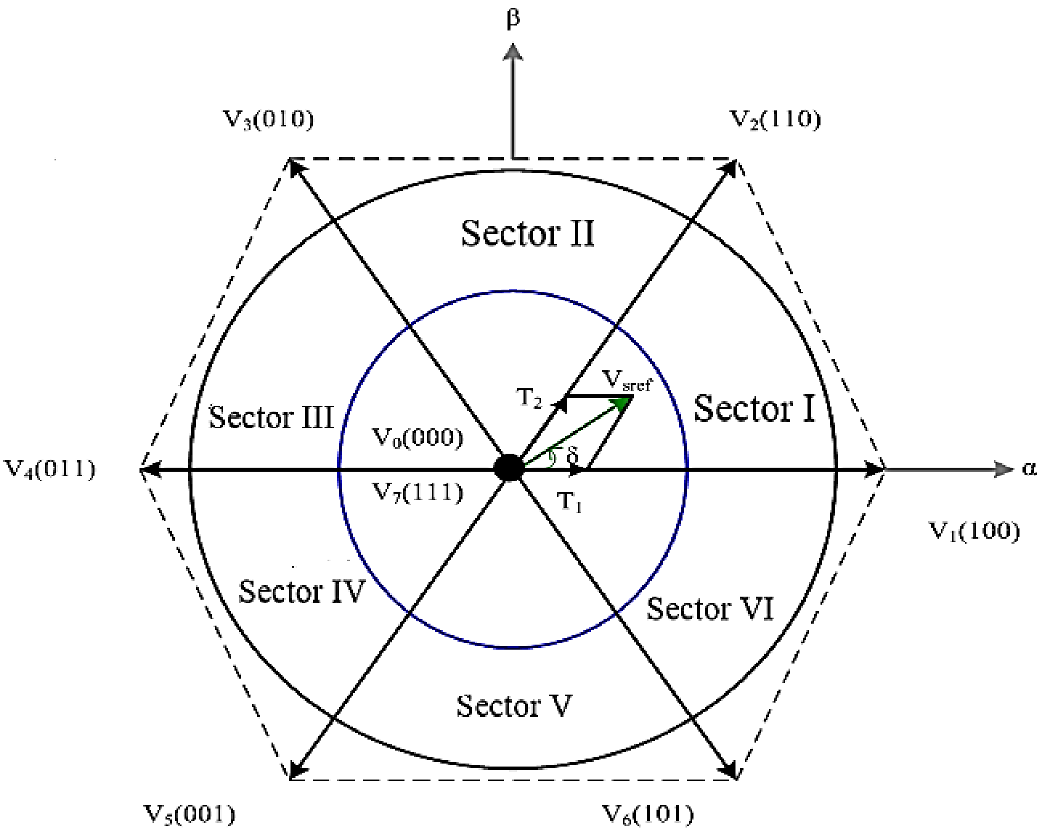

Figure II. 24: Voltage vectors representation in the (α,β) reference frame.

II.4.2 Simulation results

In our study, we used both PWM techniques (SPWM and SVPWM) which are the most used in the industry, to assess the signal quality generated by the induction motor's response. Using as continuous source $V_s = 330\ v$

The motor response after applying the output voltages of the inverter, controlled by both PWM techniques are given in figures (II. 25) to (II. 30) for SPWM, and in figures (II. 31) to (II. 36) for SVPWM, which are used to compare the results.

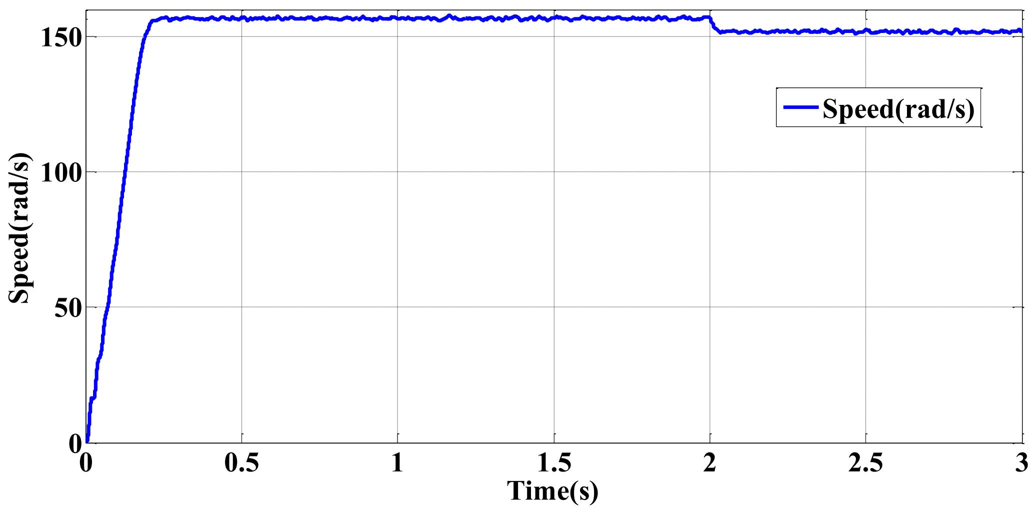

Figure II. 25: Rotor speed simulation result

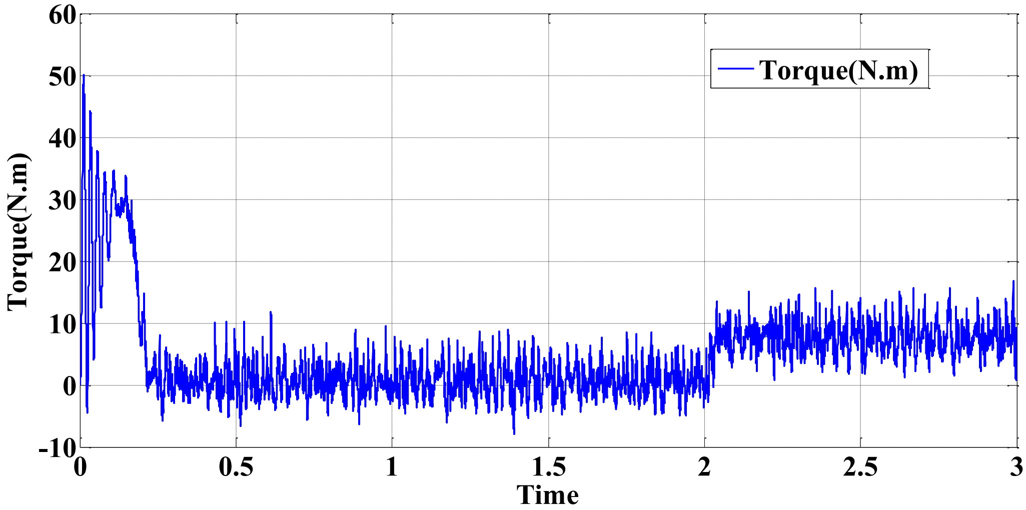

Figure II. 26: Electromagnetic torque simulation result.

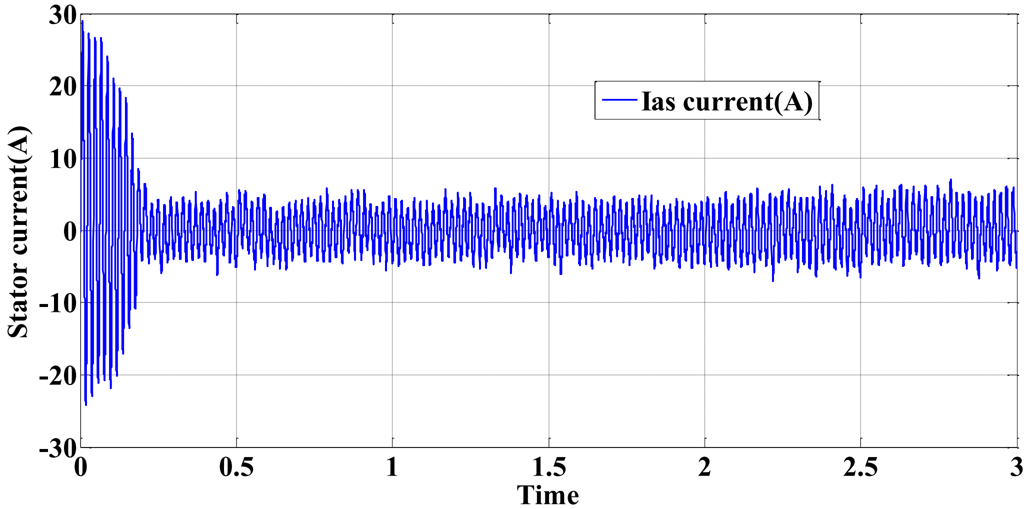

Figure II. 27: Stator current simulation result.

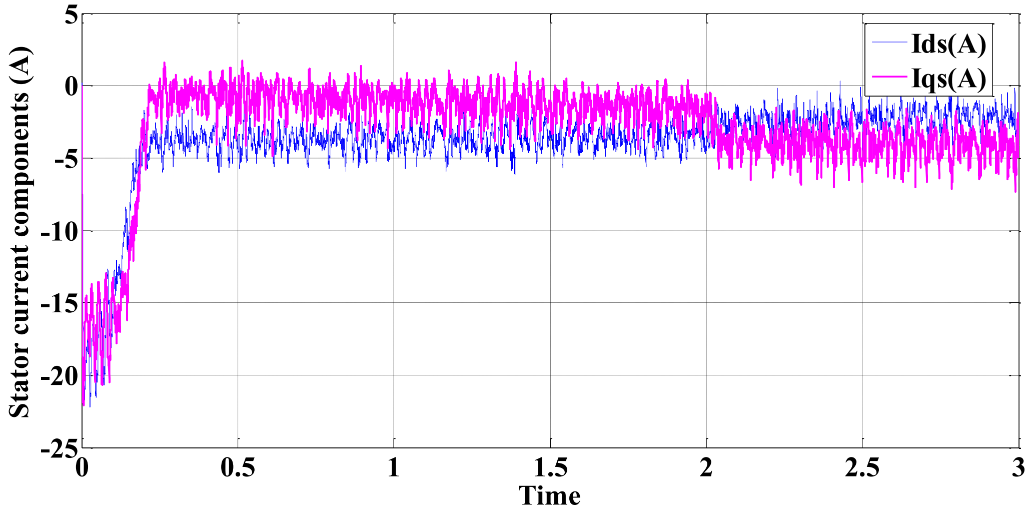

Figure II. 28: Stator currents component simulation result.

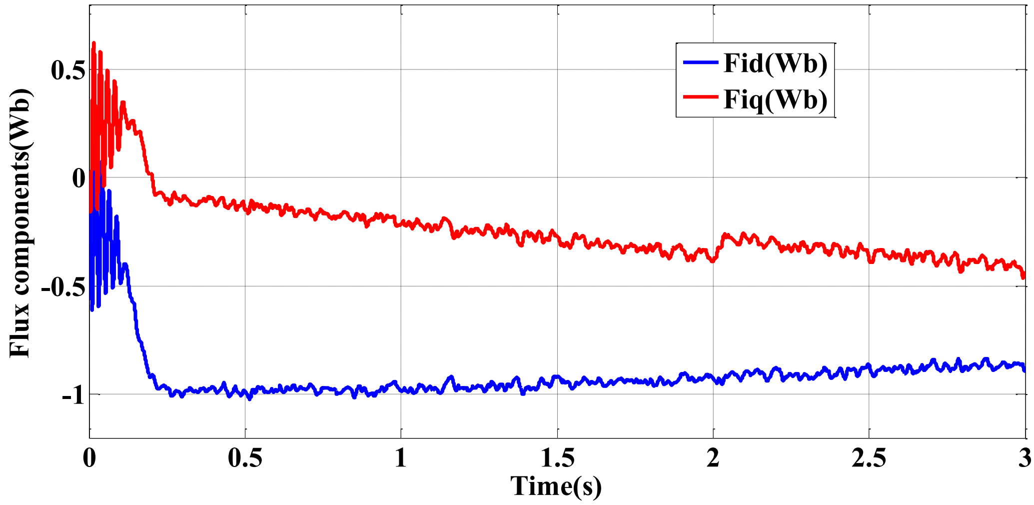

Figure II. 29: Simulation result of the stator flux components.

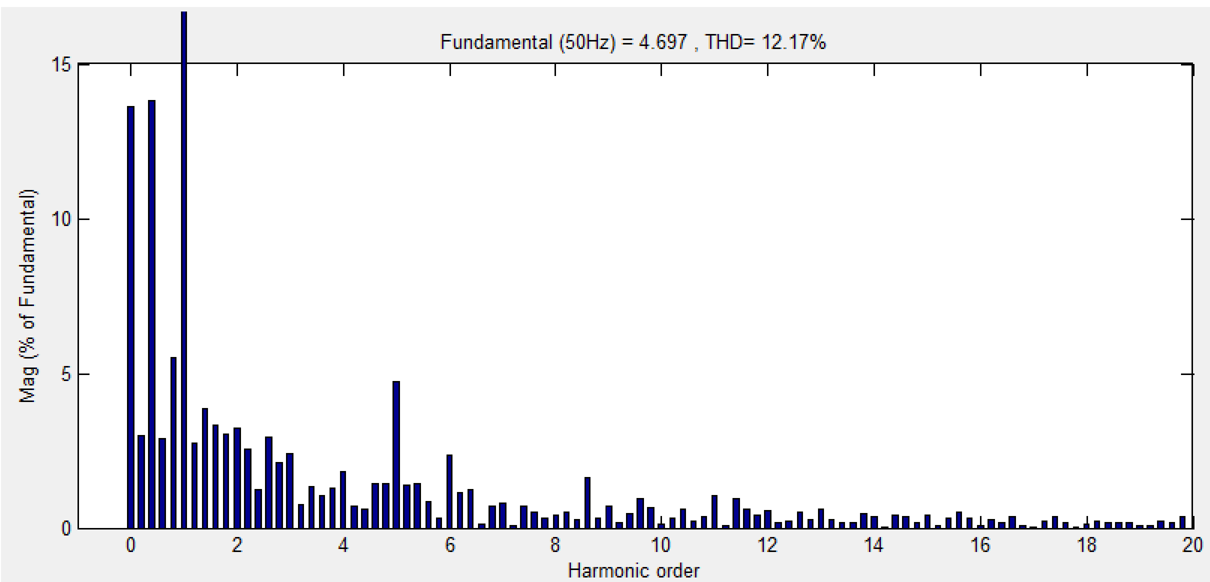

Figure II. 30: THD of Isa

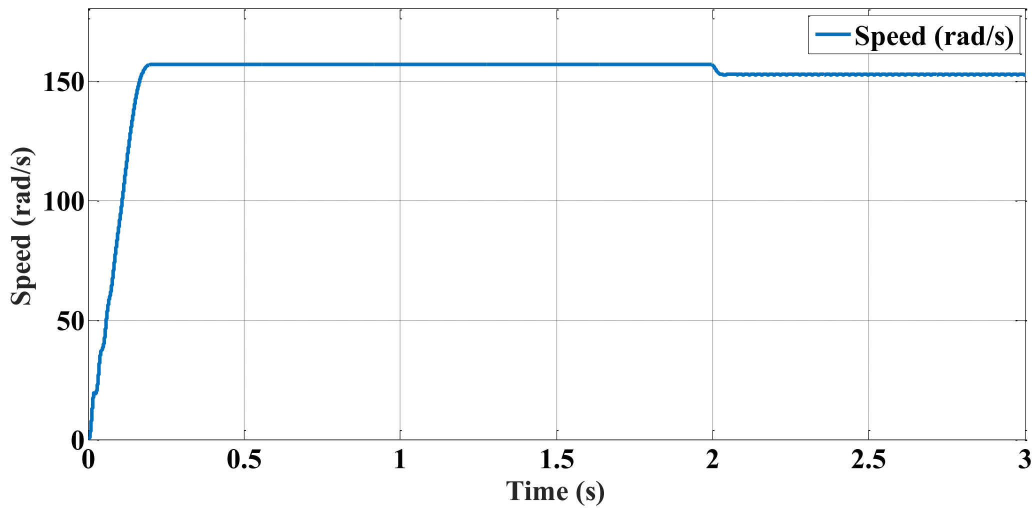

Figure II. 31: Rotor speed simulation result.

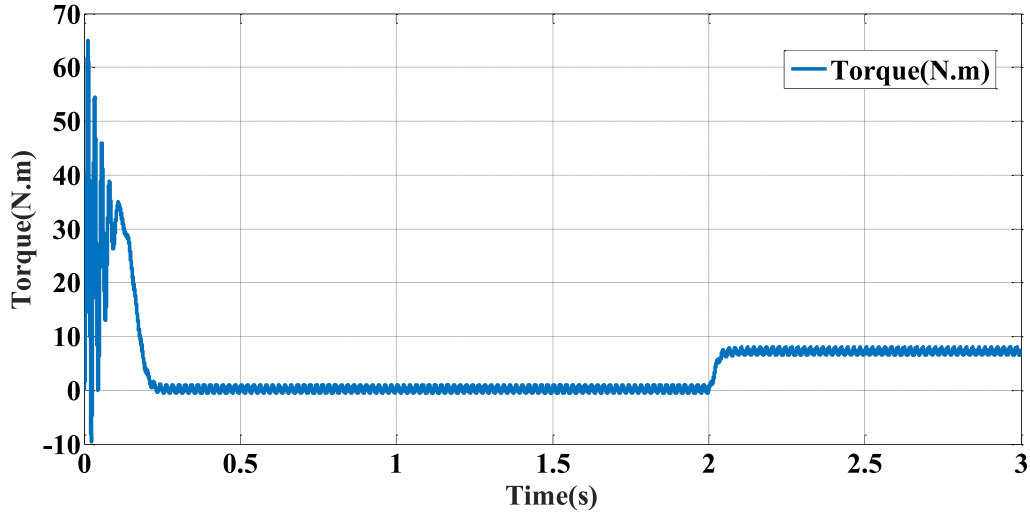

Figure II. 32: Electromagnetic torque simulation result.

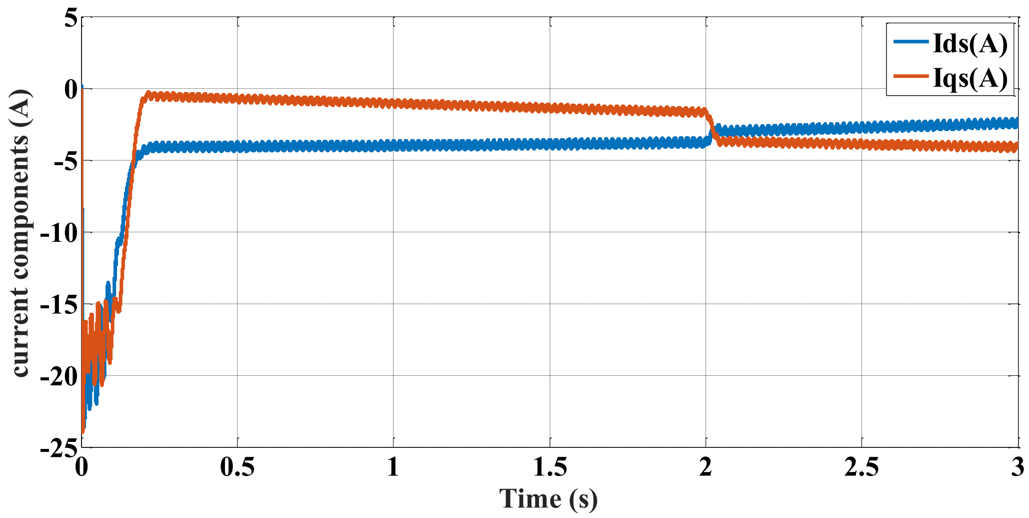

Figure II. 33: Stator current component simulation result.

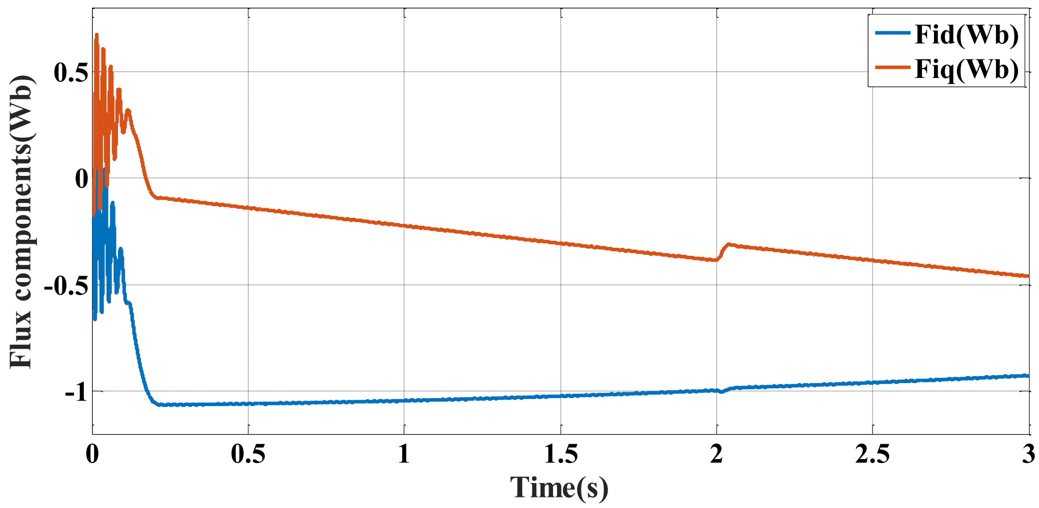

Figure II. 34: Simulation result of the stator flux components.

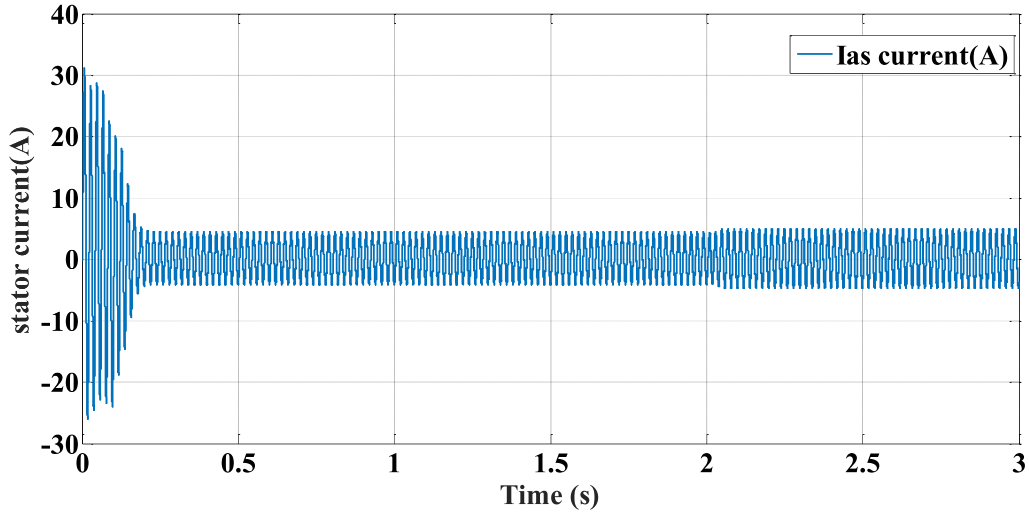

Figure II. 35: Stator current Isa simulation result.

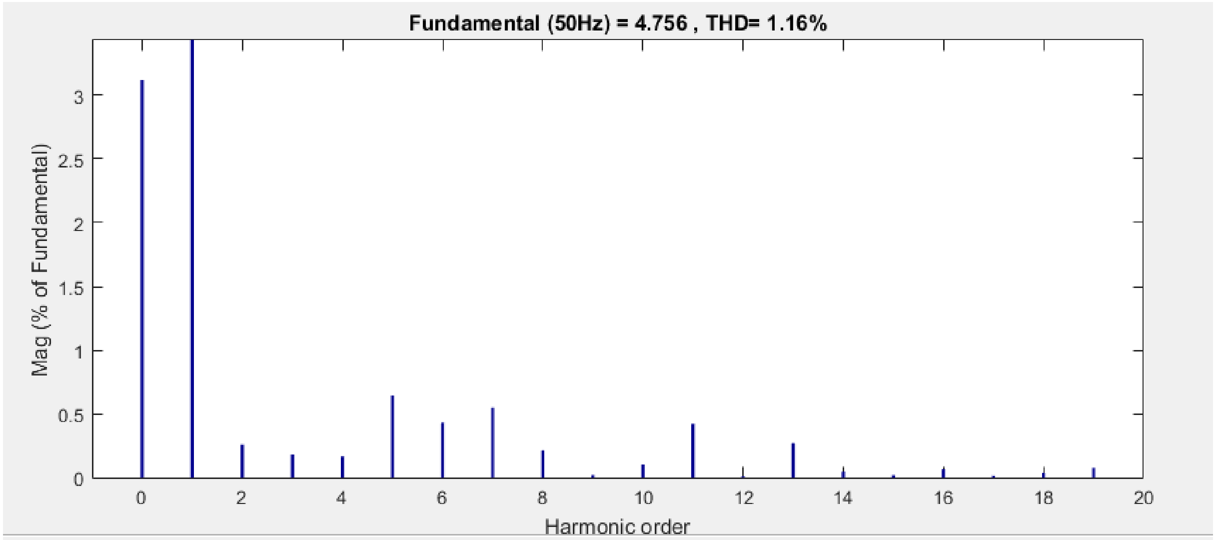

Figure II. 36: THD of current Isa

We notice that at start-up, the machine requires a high starter current that exceeds 27A, i.e. almost 5 times the nominal current for both PWM techniques.

We also noticed a poor quality of; current, speed, torque, as well as stator flux for the SPWM control, because the THD before and after applying a torque Γ_r =7 N.m (at =2s) is higher (THD=12,17 for SPWM control, and THD=1,16 for SVPWM control), compared to the quality of these quantities generated by the SVPWM control.

The simulation results show that the SVPWM technique is able to generate good quality sine wave, with low THD. This technique continues to be one of the most popular in the industry [110].

II.4.3. Conclusion

In this chapter, a modeling analysis of induction motor and PWM control structures of voltage inverters has been done. First, we studied the modeling and open loop simulation behavior of the squirrel cage induction motor. Its model is strongly nonlinear, however, by taking into account some simplification assumptions, the model becomes more simplified. The obtained simulation results show the validity of the model developed.

In a second step, we highlighted, by theoretical study the different PWM structures, while underlining the interest of PWM for voltage inverters that operate at high frequencies. The Pulse-width modulation was made to eliminate harmonics or push them back to higher frequencies to be easy to filter out. These harmonics can cause disturbances in the load voltage and generate current peaks and pulsating torques in a machine controlled by an inverter. Thus creating acoustic noise harmful to the immediate environment and consequently significant losses. They risk damaging the load if no precautions are taken for their disposal.

SVPWM is an advanced technique involving significant PWM calculations and is probably one of the most commonly used PWM techniques for variable speed drive applications. Combining DTC with SVPWM is a very effective technique against torque ripples, as we will see in Chapter III.

References

[1] Shultz, G. (2012). Transformers and motors. Elsevier.
[2] Farid TAZERART "Étude, Commande et Optimisation des Pertes d'Énergie d'une Machine à Induction Alimentée par un Convertisseur Matriciel" Ph.D. thesis, Bejaia University, Algeria, 2016.
[3] Shultz, G. (1989). Transformers and motors. Newnes.
[4] Ozpineci, B., & Tolbert, L. M. (2003, June). Simulink implementation of induction machine model-a modular approach. In IEEE International Electric Machines and Drives Conference, 2003. IEMDC'03. (Vol. 2, pp. 728-734). Ieee.
[5] Abdelkarim, A. M. M. A. R. (2017). *Amélioration des Performances de la Commande Directe de Couple (DTC) de La Machine Asynchrone par des Techniques Non-Linéaires* (Doctoral dissertation, Université Mohamed Khider-Biskra).
[6] https://automationforum.co/three-phase-induction-motor-basics/ (10/jun/2023).
[8] J.P. Caron, Hautier.J.P, "Modélisation et commande de la machine asynchrone", Edition Technip, 1995.
[9] J. Chatelain, "Machines électriques", Tome1, Editions Dunod, 1987.
[10] Mehazzem, F. (2010). Contribution à la Commande d'un Moteur Asynchrone destiné à la Traction électrique (Doctoral dissertation, Paris Est).
[11] G. Grellet, G. Clerc " Actionneurs électriques : Principes /Modèle/Commandes ", Collection Electrotechnique; Edition Eyrolles,1997.
[12] J. Lesenne, F. Notel " Introduction à l'électrotechnique approfondie ", Technique et documentation, Paris, France 1981.
[13] Duan, F., & Zivanovic, R. (2012, September). A model for induction motor with stator faults. In 2012 22nd Australasian Universities Power Engineering Conference (AUPEC) (pp. 1-5). IEEE.
[14] P. C. Krause, O. Wasynczuk, and S. D. Sudhoff, Analysis of Electric Machinery. New York: IEEE Press, 1996.
[15] Gandhi, A., Corrigan, T., & Parsa, L. (2010). Recent advances in modeling and online detection of stator interturn faults in electrical motors. IEEE Transactions on Industrial Electronics, 58(5), 1564-1575.
[16] AlShorman, O., Irfan, M., Saad, N., Zhen, D., Haider, N., Glowacz, A., & AlShorman, A. (2020). A review of artificial intelligence methods for condition monitoring and fault diagnosis of rolling element bearings for induction motor. Shock and vibration, 2020.
[17] Concordia, C., Crary, S. B., & Lyons, J. M. (1938). Stability characteristics of turbine generators. Electrical Engineering, 57(12), 732-744.
[18] Tan, G., Sun, X., Xu, W., Wang, H., & Li, S. (2019, August). Power Definition for Three-Phase Unbalanced Power System Based on Tan-Sun Coordinate Transformation System. In 2019 22nd International Conference on Electrical Machines and Systems (ICEMS) (pp. 1-6). IEEE.
[19] Nguyen, N. K., Kestelyn, X., & Dos Santos Moraes, T. J. (2015). Generalized Vectorial Formalism–based multiphase series-connected motors control.
[20] Athari, H., Niroomand, M., & Ataei, M. (2017). Review and classification of control systems in grid-tied inverters. Renewable and Sustainable Energy Reviews, 72, 1167-1176.
[21] Ali, Z., Christofides, N., Hadjidemetriou, L., Kyriakides, E., Yang, Y., & Blaabjerg, F. (2018). Three-phase phase-locked loop synchronization algorithms for grid-connected renewable energy systems: A review. Renewable and Sustainable Energy Reviews, 90, 434-452.
[22] Li, J., Konstantinou, G., Wickramasinghe, H. R., & Pou, J. (2018). Operation and control methods of modular multilevel converters in unbalanced AC grids: A review. IEEE Journal of Emerging and Selected Topics in Power Electronics, 7(2), 1258-1271.
[23] DissaAbdennour,"Contrôle direct du couple du moteur à induction sans capteur de vitesse associée à un observateur non linéaire ", thèse de magister ,Université de Batna.
[24] Yesma, B. E. N. D. A. H. A. (2013). Contribution à la commande avec et sans capteur mécanique d'un actionneur électrique (Doctoral dissertation, Université Mohamed Boudiaf des sciences et de la technologi).
[25] Zerbo, M. (2008). Identification des paramètres et commande vectorielle adaptative à orientation du flux rotorique de la machine asynchrone à cage (Doctoral dissertation, Université du Québec à Trois-Rivières).
[26] Jia, H., Djilali, N., Yu, X., Chiang, H. D., & Xie, G. (2015). Computational science in smart grids and energy systems. Journal of Applied Mathematics, 2015.

[27] P. Kundur, Power System Stability and Control, McGraw-Hill, New York, NY, USA, 1993.
[28] CHERIFI, D. (2014). Estimation de la vitesse et de la résistance rotorique pour la commande par orientation du flux rotorique d'un moteur asynchrone sans capteur mécanique. Université des Sciences et de la Technologie d'Oran Mohamed Boudiaf.
[29] LAKHDAR, D. (2017). CONTRIBUTION A LA COMMANDE PREDICTIVE DIRECTE DU COUPLE DE LA MACHINE À INDUCTION (Doctoral dissertation, Université Mustapha Ben Boulaid Batna 2, Département de l'éléctrotechnique).
[30] Aouragh, N. (2005). Implémentation d'une Identification En Temps Réel De La Machine Asynchrone A Cage Sur Le DSP TMS320 LF 2404 A (Doctoral dissertation, Université Mohamed Khider Biskra).
[31] Rezgui, S. E., & Benalla, H. (2009). Commande de machine électrique en environnement Matlab/Simulink et temps réel (Doctoral dissertation, Université Mentouri Constantine).
[32] Robyns, B., François, B., & Degobert, P. (2007). Commande Vectorielle de la Machine Asynchrone: Désensibilisation et optimisation par la logique floue (Vol. 14). Editions TECHNIP.
[33] J. Chatelain "Machine électriques", tome I, Edition Dunod 1983, ISBN 2-04-015620-8
[34] Rosendo Peña Eguiluz "Commande algorithmique d'un système mono-onduleur bimachine asynchrone destiné à la traction ferroviaire", These Doctorat De l'INPT Toulouse 2002
[35] Malatji, M. M. Derivation and implementation of a DQ model of an induction machine using MATLAB/SIMULINK.
[36] Rezgui, S. E. Techniques de commande avancées de la machine asynchrone.
[37] Yu, J., Zhang, T., & Qian, J. (2011). Electrical motor products: International energy-efficiency standards and testing methods. Elsevier.
[38] Thongam, J. S. (2006). Commande de haute performance sans capteur d'une machine asynchrone= High performance sensorless induction motor drive. Université du Québec à Chicoutimi.
[39] Khoury, G. (2018). Energy efficiency improvement of a squirrel-cage induction motor through the control strategy (Doctoral dissertation).
[40] Legrioui, S., & Benalla, H. Observation et commande non-linéaire de la machine asynchrone avec identification on line des paramètres (Doctoral dissertation, جامعة الإخوة منتوري قسنطينة).
[41] Bourbia, W.(2016) Etude Comparée des Estimateurs de Vitesse pour la Commande de la Machine Asynchrone(THESE Présentée en vue de l'obtention du diplôme de DOCTORAT en sciences)
[42] Koteich, M. (2016). Modélisation et observabilité des machines électriques en vue de la commande sans capteur mécanique (Doctoral dissertation, Université Paris-Saclay).
[43] Chaikhy, H. (2013). Contribution au développement et à l'implantation des stratégies de commandes évoluées des machines asynchrones.
[44] MEFTAH, L. (2014). simulation et commande de la machine asynchrone double étoile pour aerogeneration. Mémoire de Magister, promotion.
[45] Baghli, L. (1999). Contribution à la commande de la machine asynchrone, utilisation de la logique floue, des réseaux de neurones et des algorithmes génétiques (Doctoral dissertation, Université Henri Poincaré-Nancy I).
[46] Kouzi, K. (2008). Contribution des techniques de la logique floue pour la commande d'une machine à induction sans transducteur rotatif (Doctoral dissertation, Université de Batna 2).
[47] Duan, F. (2015). Induction motor parameters estimation and faults diagnosis using optimisation algorithms (Doctoral dissertation).
[48] Ghanes, M. (2005). Observation et commande de la machine asynchrone sans capteur mécanique (Doctoral dissertation, Ecole Centrale de Nantes (ECN); Université de Nantes).
[49] Moussaoui, L. (2007). Etude de la commande de l'ensemble machine asynchrone-Onduleur à source de courant (Doctoral dissertation, Batna, Université El Hadj Lakhdar. Faculté des sciences de l'ingénieur).
[50] Aouragh, N. (2005). Implémentation d'une Identification En Temps Réel De La Machine Asynchrone A Cage Sur Le DSP TMS320 LF 2404 A (Doctoral dissertation, Université Mohamed Khider Biskra).
[51] Martins, C. D. A. (2000). Contrôle direct du couple d'une machine asynchrone alimentée par convertisseur multiniveaux à fréquence imposée.
[52] JAMOUSSI, Kaïs, OUALI, Mohamed, et CHARRADI, Hassen. Reconstructeur d'état d'un moteur asynchrone par DSP. In : The seventh International Conference on Science and Techniques of Automatic control STA'2006. 2006. p. 1-11.
[53] Tarek, B. E. N. M. I. L. O. U. D. (2012). Commande du moteur asynchrone avec compensation des effets des

variations paramétriques (Doctoral dissertation, Université Mohamed Boudiaf des sciences et de la technologi).
[54] BOUHAFNA, S. (2013). Commande par DTC d'un moteur asynchrone apport des réseaux de neurones (Doctoral dissertation, Université de Batna 2).
[55] Bimal K. Bose, "Modern Power Electronics and AC Drives", Pearson Education, 2003.
[56] Muhammad H. Rashid, "Power Electronics, Circuits, Derives and applications". Pearson Education Inc. 2004.
[57] Saxena, A., Singh, B., & Rai, J. N. (2020, June). Comparative Analysis of PWM Techniques and SVPWM operated V/f control of Induction Motor having different power ratings. In 2020 5th International Conference on Communication and Electronics Systems (ICCES) (pp. 6-11). IEEE.
[58] Singh, S. K., Kumar, H., Singh, K., & Patel, A. (2014). A survey and study of different types of PWM techniques used in induction motor drive. International journal of engineering science & advanced technology, 4(1), 108-122.
[59] Mishra, I., Singh, M., & Roy, D. (2018, February). Comparative evaluation of different pulse width modulation techniques on VSI fed three phase induction motor. In 2018 Recent Advances on Engineering, Technology and Computational Sciences (RAETCS) (pp. 1-5). IEEE.
[60] Deb Barman, S., & Roy, T. (2014). Different Types of PWM Techniques analysis for Z-Source Inverter. IOSR Journal of Electrical and Electronics engineering, 9(3), 09-17.
[61] Chen, H., & Zhao, H. (2016). Review on pulse□width modulation strategies for common□mode voltage reduction in three□phase voltage□source inverters. IET Power Electronics, 9(14), 2611-2620.
[62] Kumar, A., & Chatterjee, D. (2017, December). A survey on space vector pulse width modulation technique for a two-level inverter. In 2017 National Power Electronics Conference (NPEC) (pp. 78-83). IEEE.
[63] Mohammed, G. H. O. U. I. S. S. E. M. (2016). Commande par logique floue d'un moteur asynchrone alimenté par un onduleur sous défaut (Doctoral dissertation, Université Mohamed Boudiaf des Sciences et de la Technologie d'Oran).
[64] Sandulescu, P. (2013). Modélisation et commande d'un système à trois phases indépendantes à double fonctionnalité: Traction Électrique et Chargeur Forte Puissance pour application automobile (Doctoral dissertation, Ecole nationale supérieure d'arts et métiers-ENSAM).
[65] Sediki, H. (2010). Contribution à la synthèse d'observateurs des systèmes non linéaires. Application à la commande des machines électroniques et réalisation d'un banc d'essai (Doctoral dissertation, Université Mouloud Mammeri).
[66] Klingshirn, E. A. (1985). Harmonic filters for six-phase and other multiphase motors on voltage source inverters. IEEE Transactions on Industry applications, (3), 588-594.
[67] Klingshirn, E. A. (1983). High phase order induction motors-part I-description and theoretical considerations. IEEE Transactions on power Apparatus and Systems, (1), 47-53.
[68] Shirabe, K., Swamy, M., Kang, J. K., Hisatsune, M., Wu, Y., Kebort, D., & Honea, J. (2012, September). Advantages of high frequency PWM in AC motor drive applications. In 2012 IEEE Energy Conversion Congress and Exposition (ECCE) (pp. 2977-2984). IEEE.
[69] Singh, S. K., Kumar, H., Singh, K., & Patel, A. (2014). A survey and study of different types of PWM techniques used in induction motor drive. International journal of engineering science & advanced technology, 4(1), 108-122.
[70] Kumar, K. V., Michael, P. A., John, J. P., & Kumar, S. S. (2010). Simulation and comparison of SPWM and SVPWM control for three phase inverter. ARPN journal of engineering and applied sciences, 5(7), 61-74.
[71] Patel, M. A., Patel, A. R., Vyas, D. R., & Patel, K. M. (2009). Use of PWM techniques for power quality improvement. International Journal of Recent Trends in Engineering, 1(4), 99.
[72] Sahajwani, M., & Patel, S. (2016). A review on modern pulse width modulation techniques based inverters. Int J Adv Res Electr Electron Instrum Eng, 5(9), 7233-7237.
[73] Dekka, A., Yaramasu, V., Fuentes, R. L., & Ronanki, D. (2021). Modular multilevel converters. In Multilevel Inverters (pp. 147-179). Academic Press.
[74] ALFEU. SGUAREZI. (2022). MODEL PREDICTIVE CONTROL FOR DOUBLY-FED INDUCTION GENERATORS AND THREE-PHASE POWER CONVERTERS. Elsevier.
[75] A.M. Hava, "Carrier Based PWM-VSI Drives in the Overmodulation Region", PhD thesis, University of Winconsin, Madison, USA, 1998
[76] D. Grahame Holmes, Thomas A. Lipo, "Pulse Width Modulation for Power Converters: Principles and Practice", Wiley-IEEE Press, 2003

[77] Joseph Vithyathil, Power Electronics , McGraw Hill Publication, 2010
[78] A. Cataliotti, F. Genduso, G. RiccoGalluzzo ,A Space Vector Modulation Control Algorithm for VSI Multilevel Converters
[79] F. Labrique, G. Séguier, R. Bausier e « Les convertisseurs statiques de l'électronique de puissance», Vol.N°4. Edition Technique et documentation-Lavoisier.1995.
[80] B. Bourahla, A. Bouabnani « Commande par différentes MLI d'un moteur asynchrone»,PFE Université des Sciences et de la Technologie d'Oran Mohamed Boudiaf juin 2004.
[81] Brahim, R. (2014). Étude du déséquilibre de l'alimentation d'un onduleur multi niveaux. Université Mohamed Boudiaf des sciences et de la technologie d'Oran.
[82] M. Chergui, H. Mezrai «Etude d'une commande d'un ensemble onduleur- machine asynchrone en utilisant les réseaux de neurones sous Matlab», PFE Université des Sciences et de la Technologie d'Oran Mohamed Boudiaf juin 2004.
[83] Quinn, C. A., Mohan, N., & Mehta, H. (1993, March). A four-wire, current-controlled converter provides harmonic neutralization in three-phase, four-wire systems. In Proceedings Eighth Annual Applied Power Electronics Conference and Exposition, (pp. 841-846). IEEE.
[84] Blasko, V. (1997). Analysis of a hybrid PWM based on modified space-vector and triangle-comparison methods. IEEE Transactions on industry applications, 33(3), 756-764.
[85] https://www.electricalindia.in/analysis-and-elimination-of-third-harmonics/
[86] ASKER, M. E., & KİLİC, H. (2017). Modulation Index and Switching Frequency Effect on Symmetric Regular Sampled SPWM. European Journal of Technique (EJT), 7(2), 102-109.
[87] Zhang, Z. C., He, W. D., & Fang, Q. (1999). Phase-shifted SPWM technique-A new concept. JOURNAL-ZHEJIANG UNIVERSITY ENGINEERING SCIENCE, 33(4), 343-348.
[88] Bowes, S. R., & Midoun, A. (1985, May). Suboptimal switching strategies for microprocessor-controlled PWM inverter drives. In IEE Proceedings B (Electric Power Applications) (Vol. 132, No. 3, pp. 133-148). IET Digital Library.
[89] Benali, F. H., Bachir, G., & Azzouz, F. (2015). The Operating improvement of the Supply Source and the Optimization of PWM Control. International Journal of Power Electronics and Drive System (IJPEDS), 03-14.
[90] Fu, Q. (2014). The Method of Design Sine Grating based on Suboptimal PWM. The Open Cybernetics & Systemics Journal, 8(1).
[91] Bin, Z. Simulation Investigation of SPWM, THIPWM and SVPWM Techniques for Three Phase Voltage Source Inverter. International Journal of Power Electronics and Drive Systems (IJPEDS) pp, 223-240.
[92] CHEN M X, SHI B, CHEN Y G. A novel sampling method of SPWM Based on DSP [J]. Electrical Automation, 2011, 33 (5): 45-47 (in Chinese).
[93] Hren, A., & Mihalič, F. (2018). An improved SPWM-based control with over-modulation strategy of the third harmonic elimination for a single-phase inverter. Energies, 11(4), 881.
[94] Mohan, N.; Undeland, T.M.; Robbins, W.P. Power Electronics, Devices, Converter, Application and Design, 2nd ed.; John Wiley & Sons: New York, NY, USA, 1995.
[95] Ericson, R.W.; Maksimovic, D. Fundamentals of Power Electronics; Kluwer Academic Publishers: Dordrecht, The Netherlands, 2001.
[96] Holmes, D.G.; Lipo, T.A. Pulse Width Modulation for Power Converters: Principles and Practice; IEEE Press: Piscataway, NJ, USA; John Wiley & Sons, Inc.: New York, NY, USA, 2003.
[97] Manias, S. (2016). Power electronics and motor drive systems. Academic Press.
[98] Akram, S., & Ann, Q. U. (2015). Newton raphson method. International Journal of Scientific & Engineering Research, 6(7), 1748-1752.
[99] Meyrand, L. (2019). Modes Non Linéaires: Approches réduites par PGD/HBM et applications aux réponses forcées (Doctoral dissertation, Aix-Marseile Université).
[100] Saifizi, M., Kasdi, N. S., Rahim, H. A., Mashagba, H. A., Mustafa, W. A., Aihsan, M. Z., & Syahmi, M. S. (2021, July). Selective harmonic elimination of five level cascaded H-bridge inverter using the Newton-Raphson technique. In Journal of Physics: Conference Series (Vol. 1962, No. 1, p. 012023). IOP Publishing.
[101] Muduli, U. R., Chikondra, B., & Behera, R. K. (2020, December). Continuous and discontinuous svpwm with switching loss control for five-phase two-level vsi fed induction motor drive. In 2020 IEEE International Conference on Power Electronics, Drives and Energy Systems (PEDES) (pp. 1-6). IEEE.
[102] Elkholi, O. A., Enany, M. A., Abdo, A. F., & Eid, M. (2020). Novel approach for SVPWM of two-level

inverter fed induction motor drive. International Journal of Power Electronics and Drive System (IJPEDS), 11(4), 1750-1758.
[103] Ting, N. S., Yasa, Y., Aksoy, I., & Sahin, Y. (2015, September). Comparison of SVPWM, SPWM and HCC control techniques in power control of PMSG used in wind turbine systems. In 2015 Intl Aegean Conference on Electrical Machines & Power Electronics (ACEMP), 2015 Intl Conference on Optimization of Electrical & Electronic Equipment (OPTIM) & 2015 Intl Symposium on Advanced Electromechanical Motion Systems (ELECTROMOTION) (pp. 69-74). IEEE.
[104] M. Ranjit, “Space Vector Pulse Width Modulation Based Indirect Vector Control of Induction Motor Drive,” Journal of Electrical & Electronic Systems, vol. 1, issue 4, pp. 1-6, Sept. 2015
[105] Pinto, J. O., Bose, B. K., Da Silva, L. B., & Kazmierkowski, M. P. (2000). A neural-network-based space-vector PWM controller for voltage-fed inverter induction motor drive. IEEE Transactions on Industry Applications, 36(6), 1628-1636.
[106] Zhai, L., & Li, H. (2008, September). Modeling and simulating of SVPWM control system of induction motor in electric vehicle. In 2008 IEEE International Conference on Automation and Logistics (pp. 2026-2030). IEEE.
[107] Bouyakoub, I., Taleb, R., Mellah, H., & Zerglaine, A. (2020). Implementation of space vector modulation for two level Three-phase inverter using dSPACE DS1104. Available at SSRN 3918716.
[108] Giyantara, A., & Rameli, M. (2017, January). Comparison between SVPWM two level in internal and external circle of hexagon. In AIP Conference Proceedings (Vol. 1788, No. 1, p. 030007). AIP Publishing LLC.
[109] H. Camblong, "Minimisation de l’impact des perturbations d’origine éolienne dans la génération d’électricité par des aérogénérateurs à vitesse variable", thèse de Doctorat, centre de Bordeaux, 2003.
[110] Agrawal, K., Gandhi, A., Shah, M. T., & Gojiya, M. V.. Design, analysis and realization of SVPWM using embedded code generation technique for a three phase, two level inverter. In 2016 International Conference on Electrical Power and Energy Systems (ICEPES) (pp. 377-382). IEEE, (2016, December).

Chapter III
Mechanical Sensorless Control

III.1 Introduction

Currently, asynchronous machines are the most used electrical machines in industrial applications because of their simplicity of construction and their robustness. The non-measurable or inaccessible electrical and mechanical quantities in this machine lead to the use of sensors placed suitably in the air gap of the machine. However, the use of these sensors alters the stability of the machine, and the advantages of the asynchronous motor are then lost. In addition, the additional cost brought by their use, their fragility or the problems of reliability limit their implementation in industrial applications [1]

To solve the difficulties related to the use of sensors, we will see in this chapter:

- Observers used in a closed loop.
- Estimators used in open loop.
- Proposing an open-loop estimator.

At the end of this chapter, we will present the simulation results of the proposed estimator.

III.2 Overview of different mechanical sensorless control methods

The main quantity that should be known in controlling induction motor in some applications is the stator flux. This can be estimated or measured. Direct flux measurement imposes high-cost probes and a need for a machine design modification. Thus, estimating the flux overcomes all these issues. In general, the flux is calculated using the motor's measured currents and voltages. In algorithms based on the current model, the motor flux is estimated by solving a collection of equations including currents, rotor speed, and rotor position [2]. On the other hand, algorithms based on the voltage model, just require voltages and currents, and they are considered more convenient due to their simplicity [3]. Due to model uncertainties and stator resistance error, the voltage model is typically employed in the high-speed range. In terms of experimental implementation, providing acceptable real-time performance is a difficulty due to the pure integrator, especially at low speed.

Several works have been done to overcome the problems of the pure integrator used by the voltage model method to estimate stator flux at low speed [15–32].

Many researchers have used observers (closed-loop estimators) instead of open-loop estimators, such as sliding mode observer used in [4] and [5], interfacing multiple models of extended Kalman filter proposed in [6]; it consists of mixing two models of extended Kalman filter together, the first one optimizes the motor’s parameters, where the second eliminates the noise. Reference [7] proposed a neural network flux observers. To increase speed estimation performance, a nonlinear adaptation approach based on sliding mode theory is suggested in [8]. In [9] the authors proposed a sliding mode control based observer that presented a behavior similar to a second-order low pass filter (LPF). These techniques require only the machine’s voltages and currents. However, they have problems, such as complex algorithms, using the motor’s parameters, and requiring a calculation time in experimental implementation, more than the estimators require [10].

Other techniques were used to improve the speed control in low and zero regions. In [11], the authors used a model reference adaptive system (MRAS). This method was used also in [12] to enhance the torque at low-speed. The authors in [13] proposed to compensate for the inverter nonlinearity by an accurate voltage error model. In [14], predictive control was employed to estimate the speed and rotor flux of an induction motor. Nevertheless, those techniques also have some complexity in their algorithm and require knowledge of the motor’s parameters.

To avoid the problems of using the motor’s parameters, and due to the advantages of the voltage model, many researchers prefer using this model with a modified integrator to estimate stator flux. The authors in [15] used three-cascaded low pass filters (LPFs) with the same time constants. A fixed cutoff frequency for the LPF was proposed in [16]. The LPF is paired with the integrator's closed-loop dc offset compensation to build the estimator. Speed reversal issues are addressed by performing the compensation before low-pass filtering.

The authors in [17] proposed a sensorless vector control of induction motors using a configurable LPF. The cutoff frequency varied with the excitation frequency, this latter was estimated with a phase-locked- loop (PLL). In [18], Instead of using a pure integrator, two LPFs with one stage each are used, which has a phase angle that is the same as the phase angle of the pure integration. This method introduces a problem at zero speed; it sets the estimator at zero due to multiplication by operating frequency. In [19], LPF with cut-off frequency selection is proposed. A phase and magnitude compensation has been added to the LPF's output to compensate for the error. The authors in [20] proposed a method to solve the problem of the pure integrator. A high pass filter (HPF), fifth-order LPF and a logical calculation part has been used in that work. In [21], the authors used two simple coordinate transformation modules, as well as a third-order LPF and an HPF. These methods can definitely filter out high-frequency harmonics and the dc drift in the back electromotive force (EMF). However, the amplitude error compensation requires the multiplication by the operating frequency. In [22], the pure integrators of the traditional direct torque control (DTC) method are substituted by a PID controller with an LPF and a HPF. In [23], the pure integrator of the conventional DTC method has been replaced by a bandpass filter (BPF). The compensation mechanism would be introduced before the BPF, according to this reference.

To improve the DTC's implementation, a process for estimating stator flux is proposed in [24], an integrator and a second-order HPF are used in the suggested method. A resonating frequency of the second-order HPF can make the motor out of control.

Because of the effectiveness of the LPF integrator in eliminating the problem of the pure integrator, many recent researches focus on introducing some modifications to the LPF to solve the problem of error in the magnitude and phase of the predicted stator flux generated by the LPF.

In [25] the authors proposed to compensate for the phase and magnitude error before the LPF. In [26] and [27] the LPF has been used with adaptive control, in [28] with a compensation and a PI controller, and in [29] with a complex gain included before the LPF. In [30], the authors estimated the stator flux using LPF and compensation after the LPF to implement a direct power control (DPC) for a doubly fed induction generator. In [31], in order to eliminate the dc offset, a LPF with real-time-varying equivalent resistance was used to estimate the stator flux of an aero flywheel motor. However, by using the classical LPF the estimated stator flux is still affected by undesirable high frequency.

The pure integrator, as aforementioned, cannot always achieve the intended performances due to the complexity of the process automation and dynamic variations. To solve this problem, a different design method known as fractional order layout has been employed [32], so a fractional order integrator will replace the pure integrator.

In this chapter, we propose a modified stator flux estimator of the induction motor, a fractional-order LPF estimator has been used for this aim. We are focusing in this chapter on the elimination of noise not the elimination of phase error. The phase error can be eliminated by using a phase-locked-loop (PLL). The proposed estimator has been compared with the classical LPF estimator used in [25]. This modified estimator has the advantages of the classical LPF (elimination of dc offset and overcoming the problem of saturation of the pure integrator) moreover, a good results in the elimination of the undesirable high-frequency noise and simple implementation.

III.3. Description of the most commonly used observers (Closed loop estimator)

III.3.1. Principle of an observer

Foremost, a deterministic state observer is an estimator operating in a closed loop, with a specific dynamic set. Using the gains matrix L, it possible to impose the specific dynamic on this observer [37]. However, its structure is still more complex than the open loop estimator.

Figure (III.1) shows the block diagram of an observer. The different quantities mentioned in this figure represent respectively:

- An input vector u of the real system and the observer, the latter vector is compared to the equivalent vector $\hat{y}$ given by the observer to ensure closed-loop operation. Thus, we define a new variable, the observation error ε_y. This latter is multiplied by a gains matrix L and sent to the observer input to affect the estimated states $\hat{x}$. Thus, by a judicious choice of the gain matrix L, it is possible to modify the observer dynamics, and consequently, make the error's convergence speed evolve toward zero [38] [1].

They require greater computing resources. Their robustness is high against parametric variations with high static accuracy [39].

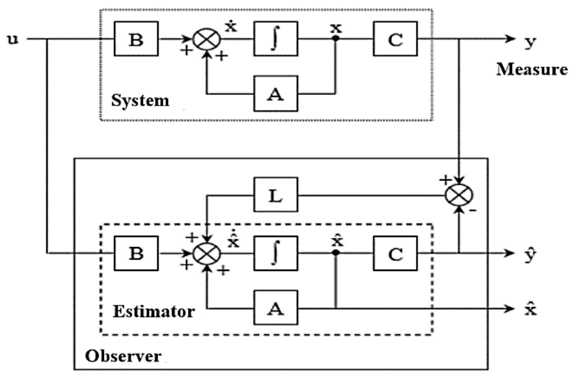

Figure III. 1: Block diagram of an observer.

III.3. 1.2 LUENBERGER OBSERVER

This observer allows the state of the observable system to be reconstructed from the measurement of the inputs and outputs [40]. It is used when the entire or a portion of the state vector cannot be measured [41]. It allows the estimation of variable or unknown parameters of a system [42].

The Luenberger observer equation can be expressed as [43], [44]:

$$\dot{\hat{X}} = A\hat{X} + BU + \varepsilon_y \tag{III.1}$$

$$\hat{Y} = C\hat{X} \tag{III.2}$$

Such as: $\varepsilon_y = Y - \hat{Y}$

Where:

$$[A] = \begin{bmatrix} -a_1 & 0 & \frac{K}{T_r} & K\omega_r \\ 0 & -a_1 & K\omega_r & \frac{K}{T_r} \\ \frac{L_m}{T_r} & 0 & \frac{-1}{T_r} & -\omega_r \\ 0 & \frac{L_m}{T_r} & -\omega_r & \frac{-1}{T_r} \end{bmatrix} \quad [B] = \begin{bmatrix} \frac{1}{\sigma L_s} & 0 \\ 0 & \frac{1}{\sigma L_s} \\ 0 & 0 \\ 0 & 0 \end{bmatrix} \quad [C] = \begin{bmatrix} 1 & 0 & 0 & 0 \\ 0 & 1 & 0 & 0 \end{bmatrix}$$

In addition:

$$a_1 = -\left(\frac{1}{T_s\sigma} + \frac{1-\sigma}{T_r\sigma}\right) \; ; a_2 = K = \frac{L_m}{T_r L_s L_r \sigma} \; ; a_3 = \frac{L_m}{T_r} \; ; a_4 = \frac{1}{T_r}$$

III.3. 1.2.1 Determination of the gain matrix L

The determination of the matrix L uses the conventional pole placement procedure [45][46]. We proceed by imposing the observer's polarities and, its dynamics as a result. The coefficients of L are determined by comparing the characteristic equation of the observer "$Det\ (PI - A + LC) = 0$" with the one that we want to impose. By developing, the different matrices A, L and C we obtain the following equation [43]:

$$P^2 + \left(\frac{1}{\sigma T_s} + \frac{1}{\sigma T_r} - j\hat{\Omega}_r + K'\right)P + \left(\frac{1}{T_r} - j\hat{\Omega}_r\right)\left\{\left(\frac{1}{\sigma T_s} + \frac{1}{\sigma T_r}\right) + K'\right\} + \left(\frac{L_m}{T_r} - k''\right)\left(\frac{L_m}{\sigma L_s L_r}\right)\left(\frac{1}{T_r} - j\hat{\Omega}_r\right) = 0 \tag{III.3}$$

Such as:

$$K' = K_1 + j\,K_2 \tag{III.4}$$

$$K'' = K_3 + j\,K_4 \tag{III.5}$$

Where K_1, K_2, K_3 and K_4 are complex gains.

The observer dynamics is defined by the following equation [47]:

$$P^2 + \left(\frac{1}{\sigma T_s} + \frac{1}{\sigma T_r} - j\hat{\Omega}_r\right)P + K^2\left(\frac{1}{T_r} - j\hat{\Omega}_r\right)\left\{\left(\frac{1}{\sigma T_s} + \frac{1}{\sigma T_r}\right)\right\} + \left(\frac{L_m}{T_r}\right)\left(\frac{L_m}{\sigma L_s L_r}\right)\left(\frac{1}{T_r} - j\hat{\Omega}_r\right) \tag{III.6}$$

Whose roots are proportional to the induction motor poles.

The proportionality constant k is at least equal to ≥ 1.

According to the identification:

$$K' = (k-1)\left(\frac{1}{\sigma T_s} + \frac{1}{\sigma T_r} - j\hat{\Omega}_r + K'\right) \tag{III.7}$$

$$K'' = (k-1)\left[\left\{\left[\frac{1}{\sigma T_s} + \frac{1}{\sigma T_r}\right]\frac{\sigma L_s L_m}{L_r} - \frac{L_m}{T_r}\right\}(k+1) - \frac{\sigma L_s L_m}{L_r}\left[\frac{1}{\sigma T_s} + \frac{1}{\sigma T_r}\right] + j\hat{\Omega}_r\frac{\sigma L_s L_m}{L_r}\right] \tag{III.8}$$

To obtain the coefficients of the observer's gain matrix, we obtain (after identification):

$$L = \begin{bmatrix} K_1 & -K_2 \\ K_2 & K_1 \\ K_3 & -K_4 \\ K_4 & K_3 \end{bmatrix}$$

Where:

$$\begin{cases} K_1 = (k-1)\left(\frac{1}{\sigma T_s} + \frac{1}{\sigma T_r}\right) \\ K_2 = (k-1)\hat{\Omega}_r \\ K_3 = (k^2-1)\left\{\left[\frac{1}{\sigma T_s} + \frac{1}{\sigma T_r}\right]\frac{\sigma L_s L_m}{L_r} - \frac{L_m}{T_r}\right\} + \frac{\sigma L_s L_m}{L_r}\left[\frac{1}{\sigma T_s} + \frac{1}{\sigma T_r}\right](k-1) \\ K_4 = -(k-1)\frac{\sigma L_s L_m}{L_r}\widehat{\Omega}_r \end{cases} \tag{III.9}$$

The observer poles are chosen to accelerate its convergence with respect to the open-loop system dynamics [48] [49]. In general, the poles are 5 to 6 times faster, but they must remain slow compared to the measurement noises, which means that we choose the constant k usually small [50].

III. 3. 1.2.2 Luenberger Observer State Representation

In general, the state is not accessible; the objective of an observer consists in carrying out a control with state feedback and estimating this state by a variable that we will denote $\hat{X}$ [51].

Such as:

$$\hat{X} = [\hat{I}_{s\alpha}\ \hat{I}_{s\beta}\ \widehat{\varphi}_{r\alpha}\ \widehat{\varphi}_{r\beta}] \tag{III.10}$$

The observer can be represented by the following equations system:

$$\frac{d}{dt}\begin{bmatrix} I_{s\alpha} \\ I_{s\beta} \\ \varphi_{r\alpha} \\ \varphi_{r\beta} \end{bmatrix} = \begin{bmatrix} a_1 & 0 & a_2 & a_2 P\Omega \\ 0 & a_1 & -a_2 P\Omega & a_2 \\ a_3 & 0 & a_1 & -P\Omega \\ 0 & a_3 & -P\Omega & a_4 \end{bmatrix}\begin{bmatrix} I_{s\alpha} \\ I_{s\beta} \\ \varphi_{r\alpha} \\ \varphi_{r\beta} \\ \omega_r \end{bmatrix} + \begin{bmatrix} \frac{1}{\sigma L_s} & 0 \\ 0 & \frac{1}{\sigma L_s} \\ 0 & 0 \\ 0 & 0 \end{bmatrix}\begin{bmatrix} v_{s\alpha} \\ v_{s\beta} \end{bmatrix} + \begin{bmatrix} K_1 & -K_2 \\ K_2 & K_1 \\ K_3 & -K_4 \\ K_4 & K_3 \end{bmatrix}\begin{bmatrix} I_{s\alpha} - \widehat{I_{s\alpha}} \\ I_{s\beta} - \widehat{I_{s\beta}} \end{bmatrix}$$

III.3.2 Model Reference Adaptive System

Currently, the Model Reference Adaptive System (MRAS) is among the most popular new control methods used mainly in sensorless electrical machine control applications [52][53]. Figure (III.2) depicts the technique's basic working, which includes a reference model and an adjustable (adaptive) model with an adaptation mechanism. The reference model does not rely on the information to be estimated, whereas the adaptive model does [54].

In order to estimate the adaptation parameters, the error introduced by comparing the outputs of the two models is added to an adaptation mechanism, which is frequently a PI regulator [55][56].

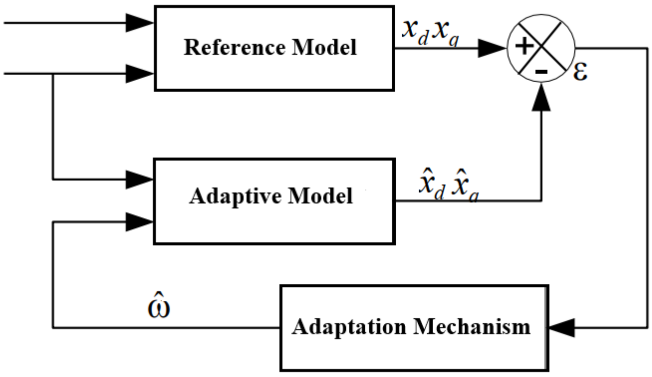

Figure III. 2: Principle of the MRAS observer.

III.3.2.1 MRAS Speed Estimator based on reactive power

The voltage equations of the induction machine can be expressed in the dq reference frame by [57][58]:

$$\begin{cases} V_{ds} = R_s I_{ds} + \sigma L_s \frac{di_{sd}}{dt} - \sigma L_s \omega_s i_{qs} + \frac{L_m}{L_r}\frac{d\varphi_{dr}}{dt} - \frac{L_m}{L_r}\omega_s \varphi_{qr} \\ V_{qs} = R_s I_{qs} + \sigma L_s \frac{di_{sq}}{dt} + \sigma L_s \omega_s i_{ds} + \frac{L_m}{L_r}\frac{d\varphi_{qr}}{dt} + \frac{L_m}{L_r}\omega_s \varphi_{dr} \end{cases} \tag{III.11}$$

The expression of the reactive power is given by:

$$Q_{es} = v_{sq} i_{sd} - v_{sd} i_{sq} \tag{III.12}$$

By replacing v_{sd} and v_{sq} in (III.12) we will have the reactive power expression as follow:

$$Q_{es} = \sigma L_s i_{ds} \frac{di_{sq}}{dt} + \sigma L_s \omega_s i_{ds}{}^2 + \frac{L_m}{L_r} i_{ds} \frac{d\varphi_{qr}}{dt} + \frac{L_m}{L_r}\omega_s i_{ds}\varphi_{dr} - \sigma L_s i_{sq}\frac{di_{sd}}{dt} + \sigma L_s \omega_s i_{qs}{}^2 - \frac{L_m}{L_r} i_{sq}\frac{d\varphi_{dr}}{dt} + \frac{L_m}{L_r}\omega_s i_{sq}\varphi_{qr} \tag{III.13}$$

taking into consideration that in the vector control $\varphi_{rq} = 0$, and that in steady state, the terms of the time derivatives disappear, knowing that, $\varphi_{rd} = L_m i_{sd}$, the equation (III.13) then becomes:

$$Q_{es} = \sigma L_s \omega_s \left(i_{sd}{}^2 + i_{sq}{}^2\right) + \frac{(L_m i_{sd})^2}{L_r}\omega_s \varphi_{rd}) \tag{III.14}$$

We express the reference reactive power in terms of the vector control reference voltages:

$$Q_{es} = \tilde{v}_{qs} i_{sd} - \tilde{v}_{sd} i_{sq} \tag{III.15}$$

In Figure (III.3), we give the block diagram of an MRAS speed estimator based on reactive power. The output of the reference model (equation III.14) is compared with that of the adaptive model (equation III.15). The adaptation mechanism based on the estimated value m_s fits the adaptive model [59].

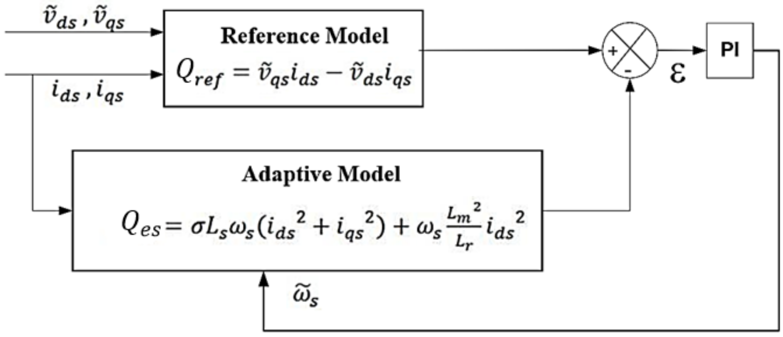

Figure III. 3: Reactive Power MRAS Speed Estimator Schematic.

III.3.2.2 MRAS estimator based on back electromotive force (emf)

By using the back emf based MRAS estimator scheme, we avoid the problem caused by calculating pure integrals [60]. Thus for the reference model, we express the components of the emf. These components will be obtained by simple currents and voltages measurements at the stator [61]. The same components are expressed for the adaptive model, which will be based on the current model [62]. The reference model will be based on the machine's voltage model.

$$e_{rd} = \frac{L_m}{L_r} \frac{d\varphi_{dr}}{dt} = V_{ds} - R_s I_{ds} - L_s \frac{di_{sd}}{dt} \tag{III.16}$$

$$e_{rq} = \frac{L_m}{L_r} \frac{d\varphi_{qr}}{dt} = V_{qs} - R_s I_{qs} - L_s \frac{di_{sq}}{dt} \tag{III.17}$$

$$\hat{e}_{ad} = \frac{L_m}{L_r} \frac{d\hat{\varphi}_{dr}}{dt} = \frac{L_m}{L_r} \frac{L_m i_{ds} - \varphi_{dr} - \omega_r T_r \varphi_{qr}}{T_r} \tag{III.18}$$

$$\hat{e}_{aq} = \frac{L_m}{L_r} \frac{d\hat{\varphi}_{qr}}{dt} = \frac{L_m}{L_r} \frac{L_m i_{qs} - \varphi_{qr} - \omega_r T_r \varphi_{dr}}{T_r} \tag{III.19}$$

The speed adaptation mechanism is the error expressed by the equation (III.20) and which is proportional to the angle between the back emf vector of the reference model $\overrightarrow{e_r}$ and that of the adaptive model $\overrightarrow{e_a}$ [63][64]. Figure (III.4), is illustrated an MRAS speed estimator based on the back emf:

$$\varepsilon_{fcem} = (\vec{e}_r \times \vec{e}_a) = e_{rq} \hat{e}_{ad} - e_{rd} \hat{e}_{aq} \tag{III.20}$$

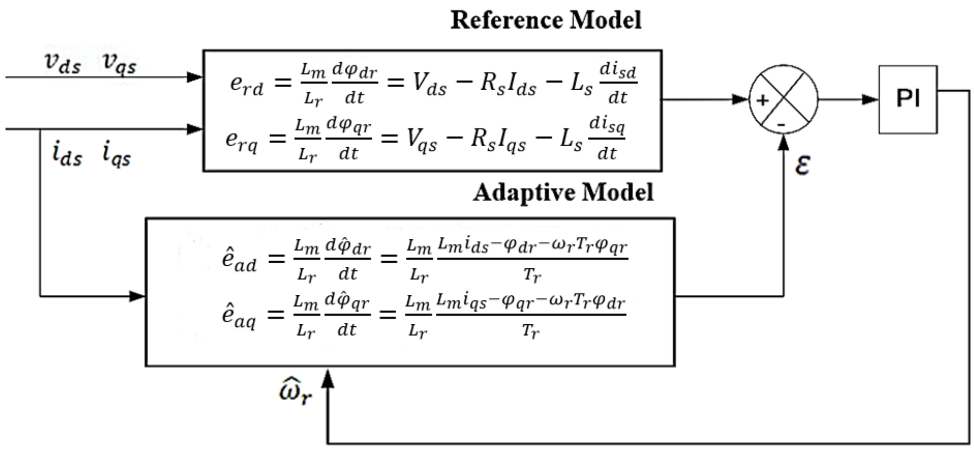

Figure III. 4: Back emf MRAS Speed Estimator Schematic.

III.3.3 Extended Kalman filter for IM

The extended Kalman filter estimates the state of a nonlinear process. In particular, it makes it possible to add, to the state vector, another variable that we wish to estimate. In the case of the IM, this filter is widely used to estimate various quantities such as rotor speed, load torque and electrical parameters.

The steps used for state vector estimation are as follows [82], [83]:

- Machine model selection.
- Discretization of the system model.
- Determination of the covariance matrices of the noises Q, R and state matrix P.
- Implementation of the Kalman filter algorithm.

This system must be discretized and linearized around a current operating point (estimated state vector) [84].

$$\begin{cases} \frac{d}{dt}x = f(x, u, t) + w(t) \\ y = h(x) + v(t) \end{cases} \tag{III.21}$$

$f(x)$, $h(x)$: Nonlinear functions.

The discrete model of equation (III.21) can be written as follows:

$$\begin{cases} x(k+1) = f(x(k), u(k)) + w(k) \\ y(k+1) = h(x(k)) + v(k) \end{cases} \tag{III.22}$$

Where: k is the temporal instant, $x(k)$ is the state vector, $y(k)$ is the output vector, and $u(k)$ is the command vector.

The discretization of the nonlinear model is done by applying the mean value theorem.

$$x(k+1) = x(k) + \int_{kte}^{(k+1)te} f(x(t), u(t), t)dt \tag{III.23}$$

Where: te is the discretization period.

The extended Kalman filter implementation in the case of the nonlinear system given by equation (III.22) consists of the execution of the following steps [84]:

Step 1: Initialization of the state vector and the covariance matrices: $X(0)$, Q_0, P_0, R_0

Step 2: State prediction

$\hat{x}(k+1)\cdot\hat{y}(k+1)$

$$\hat{x}(k+1/k) = f(x(k), u(k)) \tag{III.24}$$

$$y(k+1/k) = h(x(k+1))$$

Step3: Prediction of the covariance matrix

$$(k+1/k) = F(k)\cdot P(k)\cdot F(k)^T + Q \tag{III.25}$$

With: $F(x) = \frac{\partial(f(x(k),u(k)))}{\partial x} \mid x = \hat{x}(k+1/k)$ (III.26)

Step4: Calculation of the Kalman gain

$$K(k+1) = P(k+1/k)\cdot H^T(k+1)[h(k+1)\cdot P(k+1/k)H^T(k+1) + R]^{-1}$$

The gradient matrix defined as follows:

$$H(k+1) = \frac{\partial(h(x(k),u(k)))}{\partial x} \mid x = \hat{x}(k+1/k)$$

Step 5: Estimation of the state vector

$$\hat{x}(k+1) = \hat{x}(k+1/k) + K(k+1)[y_m(k+1) - y(k+1/k)]$$

With: $y_m(k+1)$ is the vector of the measured states.

Step 6: Estimation of the covariance matrix

$$P(k+1) = P(k+1/k) - K(k+1)H(k+1)P(k+1/k)$$

The estimation process continues by returning to step (2) and so on.

III.3.3.1 Application of the extended Kalman Filter to the induction machine

For this implementation, we focus on the state model of the IM. The aim of this model is to estimate the flux at the rotor as well as the rotation speed [65] [66]. In the following, we take the general state representation:

$$\dot{X}(t) = AX(t) + BU(t) \tag{III.27}$$

$$Y(t) = CX(t) \tag{III.28}$$

The stochastic model is similar to the deterministic one apart from the noises, which translate into ignorance of the system [67]. To the state equation, we add state noises $v(t)$ to the output equation, and $w(t)$ measurement noise vector, which translates the sensor errors as shown in equations (III.29) and (III.30) [81].

$$\dot{X}(t) = AX(t) + BU(t) + v(t) \tag{III.29}$$

$$Y(t) = CX(t) + w(t) \tag{III.30}$$

The deterministic state space model of the IM is given by:

$$\frac{d}{dt}\begin{bmatrix} I_{s\alpha} \\ I_{s\beta} \\ \varphi_{r\alpha} \\ \varphi_{r\beta} \\ \omega_r \end{bmatrix} = \begin{bmatrix} a & 0 & b & c\omega_r & 0 \\ 0 & a & -c\omega_r & b & 0 \\ d & 0 & e & -\omega_r & 0 \\ 0 & d & \omega_r & -e & 0 \\ 0 & 0 & 0 & 0 & 0 \end{bmatrix} \begin{bmatrix} I_{s\alpha} \\ I_{s\beta} \\ \varphi_{r\alpha} \\ \varphi_{r\beta} \\ \omega_r \end{bmatrix} + \begin{bmatrix} \frac{1}{\sigma L_s} & 0 \\ 0 & \frac{1}{\sigma L_s} \\ 0 & 0 \\ 0 & 0 \\ 0 & 0 \end{bmatrix} \begin{bmatrix} v_{s\alpha} \\ v_{s\beta} \end{bmatrix}$$

$$\begin{bmatrix} I_{s\alpha} \\ I_{s\beta} \end{bmatrix} = \begin{bmatrix} 1 & 0 & 0 & 0 & 0 \\ 0 & 1 & 0 & 0 & 0 \end{bmatrix} \begin{bmatrix} I_{s\alpha} \\ I_{s\beta} \\ \varphi_{r\alpha} \\ \varphi_{r\beta} \\ \omega_r \end{bmatrix}$$

Where :

$$a = -\left(\frac{1}{\sigma T_s} + \frac{1-\sigma}{\sigma T_s}\right); b = \frac{1}{MT_r} \times \frac{1-\sigma}{\sigma}; c = \frac{1}{M} \times \frac{1-\sigma}{\sigma};\ d = \frac{M}{T_r}\ ; e = -\frac{1}{T_r}$$

We consider from this state representation, that the stator voltages expressed in the fixed frame $(\alpha\beta)$ are the input vector, and the stator current is the output vector. Therefore, the state vector is composed of the current vector stator, the rotor flux components in the fixed reference $(\alpha\beta)$ and the rotation speed as well as shown below [69] [70].

$$X = \begin{bmatrix} I_{s\alpha} \\ I_{s\beta} \\ \varphi_{r\alpha} \\ \varphi_{r\beta} \\ \omega_r \end{bmatrix}, \qquad Y = \begin{bmatrix} I_{s\alpha} \\ I_{s\beta} \end{bmatrix}, \qquad U = \begin{bmatrix} v_{s\alpha} \\ v_{s\beta} \end{bmatrix}$$

Therefore, the state system's matrices are:

$$A = \begin{bmatrix} a & 0 & b & c\omega_r & 0 \\ 0 & a & -c\omega_r & b & 0 \\ d & 0 & e & -\omega_r & 0 \\ 0 & d & \omega_r & e & 0 \\ 0 & 0 & 0 & 0 & 0 \end{bmatrix}, \qquad B = \begin{bmatrix} \frac{1}{\sigma L_s} & 0 \\ 0 & \frac{1}{\sigma L_s} \\ 0 & 0 \\ 0 & 0 \\ 0 & 0 \end{bmatrix}, \qquad C = \begin{bmatrix} 1 & 0 & 0 & 0 & 0 \\ 0 & 1 & 0 & 0 & 0 \end{bmatrix}$$

The Extended Kalman filter (EKF) recursive aspect imposes digitization of all the quantities used [71][72]. Thus, the system’s matrices should be discretized by the application of the passage's equation:

$$A_d = I + T_s A \qquad \text{(III.31)}$$

$$B_d = T_s B \tag{III.32}$$
$$C_d = C \tag{III.33}$$

With: I the identity matrix, and T_s the sampling period.

We obtain the discretized matrices of the system as follows:

$$\frac{d}{dt}\begin{bmatrix} I_{s\alpha} \\ I_{s\beta} \\ \varphi_{r\alpha} \\ \varphi_{r\beta} \\ \omega_r \end{bmatrix} = \begin{bmatrix} 1+aT_s & 0 & bT_s & cT_s\omega_r & 0 \\ 0 & 1+aT_s & -cT_s\omega_r & bT_s & 0 \\ dT_s & 0 & 1+eT_s & -T_s\omega_r & 0 \\ 0 & dT_s & \omega_r T_s & 1+eT_s & 0 \\ 0 & 0 & 0 & 0 & 1 \end{bmatrix}\begin{bmatrix} I_{s\alpha} \\ I_{s\beta} \\ \varphi_{r\alpha} \\ \varphi_{r\beta} \\ \omega_r \end{bmatrix} + \begin{bmatrix} \frac{T_s}{\sigma L_s} & 0 \\ 0 & \frac{T_s}{\sigma L_s} \\ 0 & 0 \\ 0 & 0 \\ 0 & 0 \end{bmatrix}\begin{bmatrix} v_{s\alpha} \\ v_{s\beta} \end{bmatrix}$$

$$\begin{bmatrix} I_{s\alpha} \\ I_{s\beta} \end{bmatrix} = \begin{bmatrix} 1 & 0 & 0 & 0 & 0 \\ 0 & 1 & 0 & 0 & 0 \end{bmatrix}\begin{bmatrix} I_{s\alpha} \\ I_{s\beta} \\ \varphi_{r\alpha} \\ \varphi_{r\beta} \\ \omega_r \end{bmatrix}$$

The expressions of the matrices F and H are:

$$F = \frac{d(A_d X(t) + B_d U(t))}{dx} = \begin{bmatrix} 1+aT_s & 0 & bT_s & cT_s\omega_r & cT_s\varphi_{r\beta} \\ 0 & 1+aT_s & -cT_s\omega_r & bT_s & -cT_s\varphi_{r\alpha} \\ dT_s & 0 & 1+eT_s & -T_s\omega_r & T_s\varphi_{r\beta} \\ 0 & dT_s & \omega_r T_s & 1+eT_s & T_s\varphi_{r\alpha} \\ 0 & 0 & 0 & 0 & 1 \end{bmatrix}$$

$$H = \frac{\partial(C_d X(t))}{\partial x} = \begin{bmatrix} 1 & 0 & 0 & 0 \\ 0 & 1 & 0 & 0 \end{bmatrix}$$

III.3.3.2 Choice of the R and Q covariance matrix:

An important step in the Kalman filter's implementation is the selection and adjustment of R and Q matrices [73][74].

In fact, both the dynamic regime's duration and the operation of the filter's steady state are affected by changes in the covariance matrices of state noise Q and measurement noise R [75]. Several adjustments of the Q and R matrices are to be carried out to find a suitable adjustment to improve the performance of the filter [76].

In general, for a high value of R, the gain K is small and the dynamics are faster. Whereas for a high value of Q, the gain K is large and the dynamic performance is slower [77][78]. However, consideration must be given to the risk of the observation becoming unstable too high value of Q or too low value of R [79][80].

The covariance matrices are chosen through a process highlighting state noise and errors for a better compromise between filter stability and convergence time. We retained the matrices Q and R as follows:

$$Q=\begin{bmatrix}1e-9 & 0 & 0 & 0 & 0\\ 0 & 1e-9 & 0 & 0 & 0\\ 0 & 0 & 1e-9 & 0 & 0\\ 0 & 0 & 0 & 1e-9 & 0\\ 0 & 0 & 0 & 0 & 0.01\end{bmatrix},\ R=\begin{bmatrix}1e-3 & 0\\ 0 & 1e-3\end{bmatrix}$$

III.3.4 Estimator-based methods (open loop estimation)

These estimators rely on the use of a machine representation in the form of Park's equation defined in steady state (static estimator) or transient (estimator dynamic). They are obtained by a direct resolution of the equations associated with this model. Such an approach leads to the implementation of simple and fast algorithms. However, as mentioned in section (III.2) that the direct flux measurement requires expensive probes and the need to modify the machine design, hence the necessity of estimating the flux. In general, its estimation is based on the measured currents and voltages of the motor. In current model-based algorithms, motor flux is estimated by solving a set of equations in which currents, speed, or rotor position are required. Differently, voltage model based algorithms require only voltages and currents, therefore they are considered more convenient due to their simplicity.

In this chapter, we will present types of stator flux estimators based on using a fractional order integrator instead of a classical integrator with the necessary improvements at low-speed operation, starting with the presentation of the fractional order integrator.

III.3.1 Approximation of the Fractional order integrator

In the frequency domain, the fractional-order integrator's transfer function is represented by the irrational transfer function below [33]:

$$G(s)=\frac{1}{s^n} \tag{III.34}$$

Where: $s=j\omega$ and $0<n<1$.

In a frequency range (ω_L,ω_H), where ω_L is the lower limit of the frequency equal to 0.001 (rad/s), and ω_H is the higher limit of the frequency equal to 1000 (rad/s), (III.28) can be written as follows [33]:

$$G(s)=\frac{K_I}{(1+(s/\omega_b))^n} \tag{III.35}$$

where ω_b is the Cutoff frequency and K_I is the parameter of the rational function approximation, they are respectively given by [34]:

$$\omega_b=\omega_L\sqrt{10^{\varepsilon/(10m)}-1} \tag{III.36}$$

$$K_I=\frac{1}{\omega_b^n} \tag{III.37}$$

where ε is the allowable maximum error when substituting equation (III.34) by equation (III.35) in the desired frequency range (ω_L,ω_H).

In that range, the irrational transfer function can be approximated with a rational transfer function as follows [34]:

$$G(s)=\frac{K_I}{\left(1+\frac{s}{\omega_b}\right)^n}\cong K_I\frac{\prod_{i=0}^{N-1}\left(1+\frac{s}{z_i}\right)}{\prod_{i=0}^{N}\left(1+\frac{s}{p_i}\right)} \tag{III.38}$$

$$N=Integer\left[\frac{\log(\omega_H/P_0)}{\log(ab)}\right]+1 \tag{III.39}$$

The poles p_i and zeros z_i of equation (III.38) are given by [33]:

$$p_i=p_0(ab)^i, i=0,1\ldots N \tag{III.40}$$

$$z_i=z_0(ab)^i, i=0,1\ldots N-1 \tag{III.41}$$

The values of a, b, p_0 and z_i can be determined as follows[33]:

$$a=10^{[y/(10(1-m))]} \tag{III.42}$$

$$b=10^{[y/(10m)]} \tag{III.43}$$

$$p_0=\omega_b 10^{[y/(20m)]} \tag{III.44}$$

$$z_0=ap_0 \tag{III.45}$$

As a result, a rational function in a specific frequency selected area can approximate the fractional-order integrator as follows [34]:

$$G(s)=\frac{1}{s^n}=\frac{K_I}{\left(1+\frac{s}{\omega_b}\right)^n}\cong K_I.\frac{\prod_{i=0}^{N-1}\left[1+\left(\frac{s}{z_0(ab)^i}\right)\right]}{\prod_{i=0}^{N}\left[1+\left(\frac{s}{p_0(ab)^i}\right)\right]} \tag{III.46}$$

To improve the effectiveness of the integrator, its degree has to be increased. Thus, the function G is rewritten as follows [33]:

$$G(s)=\frac{1}{s}\frac{1}{s^\alpha}=\frac{1}{s}\frac{K_I}{\left(1+\frac{s}{\omega_b}\right)^n}\cong\frac{1}{s}K_I.\frac{\prod_{i=0}^{N-1}\left[1+\left(\frac{s}{z_0(ab)^i}\right)\right]}{\prod_{i=0}^{N}\left[1+\left(\frac{s}{p_0(ab)^i}\right)\right]} \tag{III.47}$$

Thus, the parameter α is defined as follows: $\alpha=n+1$ and $0<\alpha<1$.

III.3.2 Construction of the proposed integrator

The basic stator flux estimator is given by:

$$\phi_s=\frac{1}{s}e_s \tag{III.48}$$

where e_s is the feedback EMF, it is given by:

$$e_s=V_s-R_s i_s \tag{III.49}$$

and V_s is the stator voltage, it is given by:

$$V_s=\sqrt{V_{s\alpha}^2+V_{s\beta}^2} \tag{III.50}$$

The stator voltage components in (α,β) frame $V_{\alpha s}$ and $V_{\beta s}$ are estimated using the following equations:

$$V_{s\alpha}=\frac{2}{3}V_{dc}(D_1-0.5(D_2+D_3)) \tag{III.51}$$

$$V_{s\beta}=\frac{\sqrt{3}}{3}V_{dc}(D_2-D_3) \tag{III.52}$$

where D_1, D_2 and D_3 are duty cycles, V_{dc} is the dc bus voltage.

i_s in equation (III.49) is the stator current given by:

$$i_s = \sqrt{i_{s\alpha}^2 + i_{s\beta}^2} \quad \text{(III.53)}$$

$i_{s\alpha}$ and $i_{s\beta}$ are the components of i_s in the (α,β) frame, they are obtained from the three-phase stator currents using Clarke transformation.

For $s = j\omega_s$ where ω_s is the stator frequency, equation (III.49) can be expressed as follow:

$$\omega_s \cdot \phi_s = \frac{1}{j} e_s \quad \text{(III.54)}$$

An undesirable signal ε rises with the feedback EMF e_s, so equation (III.54) became:

$$\omega_s \cdot \phi_s = \frac{1}{j}(e_s + \varepsilon) \quad \text{(III.55)}$$

Let $\varepsilon_s = -j\varepsilon$, so we obtain [25]:

$$\varepsilon_s = \omega_s \cdot \phi_s + j \cdot e_s \quad \text{(III.56)}$$

where ε_s characterize both the undesirable offset and the noise generated by the voltage and current sensors.

In order to control the undesirable signals, [25] proposed to introduce a gain C in series with ε_s.

According to [25] to operate the motor in the two directions, the estimator scheme needs to be expanded by the factors $sign(\omega_s)$ and $|\omega_s|$.

The proposed integrator is shown in figure (III.5)

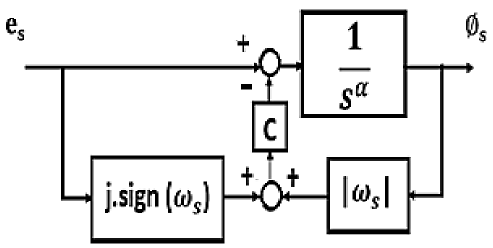

Figure III. 5: Proposed integrator.

From figure (III.5), the transfer function can be expressed as follow:

$$\frac{\phi_s}{e_s} = \frac{1 - j \cdot C \cdot sign(\omega_s)}{s^\alpha + C|\omega_s|} \quad \text{(III.57)}$$

$$\phi_s = j\frac{j + C \cdot sign(\omega_s)}{s^\alpha + C|\omega_s|}(e_{\alpha s} + j \cdot e_{\beta s}) \quad \text{(III.58)}$$

$$\phi_{\alpha s} = \frac{e_{\alpha s} + e_{\beta s} \cdot C \cdot sign(\omega_s)}{s^\alpha + C|\omega_s|} \quad \text{(III.59)}$$

$$\phi_{\beta s} = \frac{e_{\beta s} - e_{\alpha s} \cdot C \cdot sign(\omega_s)}{s^\alpha + C|\omega_s|} \quad \text{(III.60)}$$

The Bode plot of the function in equation (III.59) is performed using the Fomcon toolbox of MATLAB software using three different values of α (1.25, 1.5 and 1.75) with $\omega_s = 20$ and 0 (rad/s).

The obtained results are shown in figure (III.6) and figure (III.7).

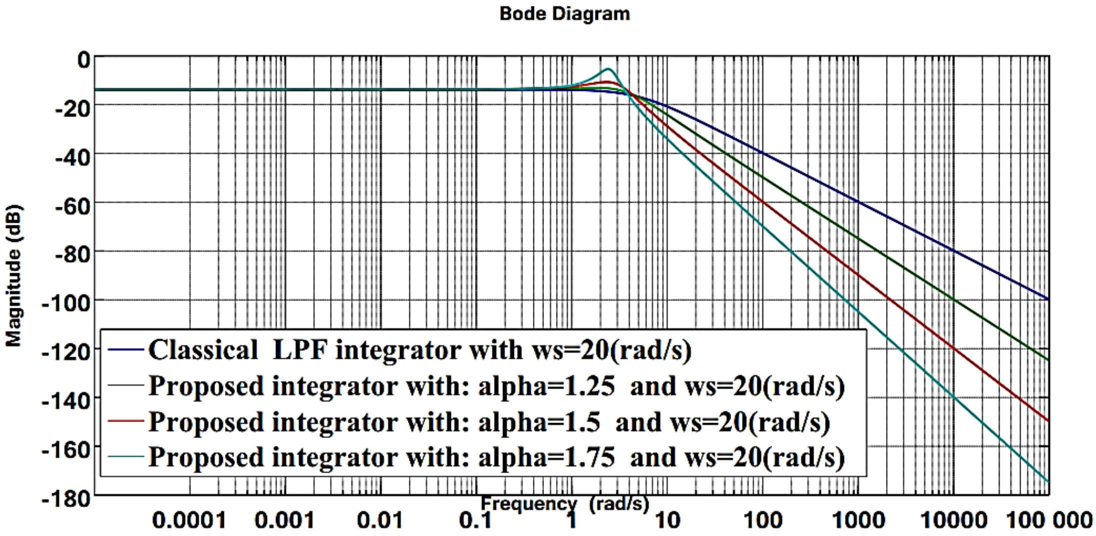

Figure III. 6: The effect of α on the proposed integrator at cutoff frequency=5 (rad/s).

From figure (III.6) when $\alpha > 1.25$ the resonance phenomenon appears at the cutoff frequency which disturbs the system. Therefore, our work has been done with $\alpha = 1.25$.

Figure (III.6) shows that the undesirable high-frequency signals are more attenuated by the proposed integrator than the classical LPF integrator, thus a good estimation for stator flux is achieved.

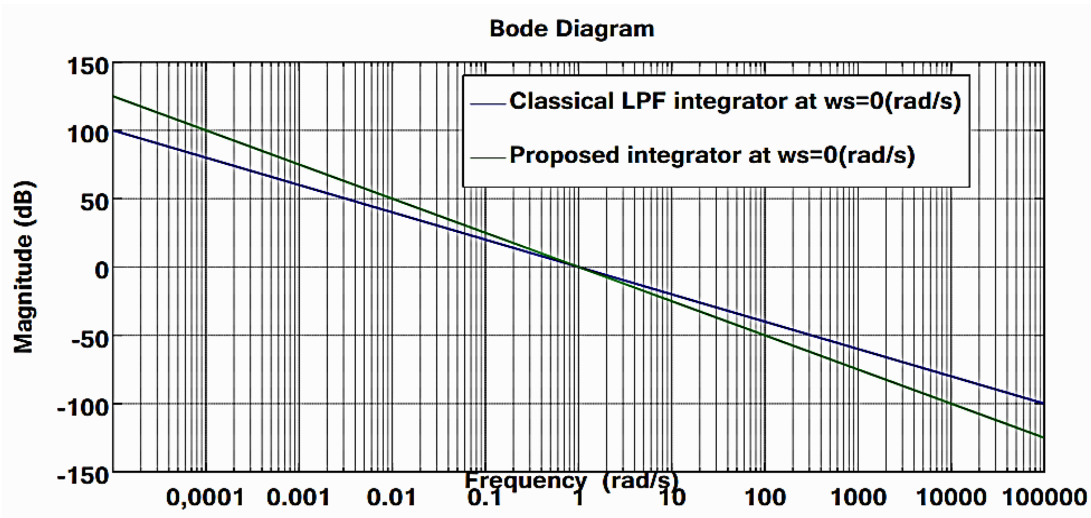

Figure III. 7: The classical and the proposed integrators at $\omega_s = 0$ (rad/s).

From figure (III.7) the problem of multiplication by ω_s, which makes the integrator act like a zero gain at $\omega_s = 0$ (rad/s), is eliminated.

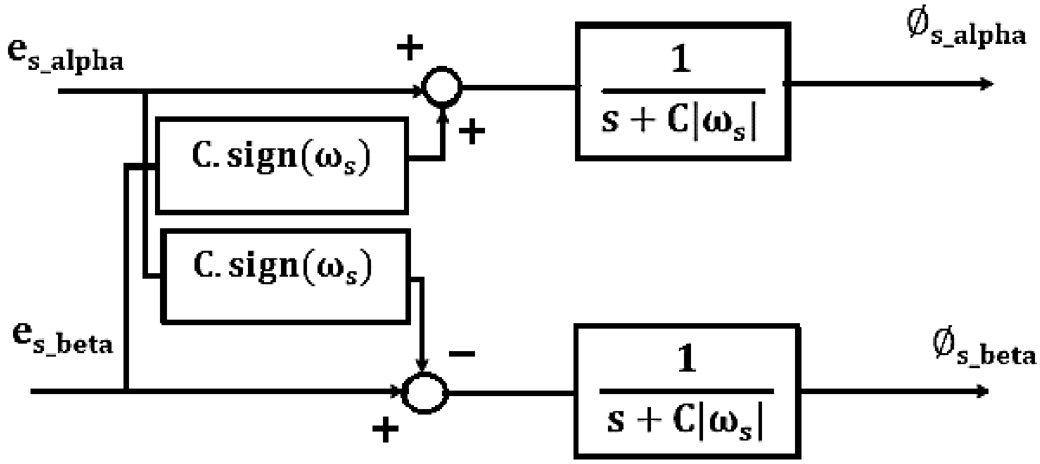

Figure III. 8: Classical LPF integrator.

Figure (III.8) shows the classical LPF integrator proposed in [25]. It has been compared with the proposed integrator shown in figure (III.9) in order to validate its effectiveness.

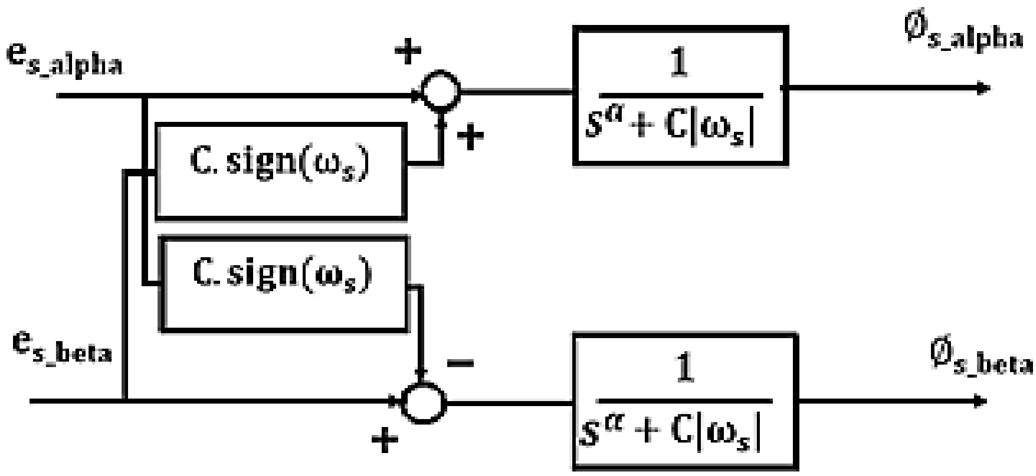

Figure III. 9: The proposed integrator.

The expression of the cutoff frequency is given by:

$$\omega_c = C\,|\,\omega_s\,| \tag{III.61}$$

where ω_s is the operating frequency.

From [35] and [8] the operating frequency is calculated by:

$$\omega_s = \frac{e_{s\alpha}\phi_{s\beta} - e_{s\beta}\cdot\phi_{s\alpha}}{|\,\phi_s\,|^2} \tag{III.62}$$

where $e_{s\alpha}$ and $e_{s\beta}$ are the composites of EMF in the (α,β) frame.

$\phi_{s\alpha}$ and $\phi_{s\beta}$ are the composites of stator flux in the (α,β) frame.

To introduce the cutoff frequency with the classical and fraction order LPF using the estimation of operating frequency, the two LPF block schematics illustrated in figure (III.6) and figure (III.7) should be modified from schematic shown in figure (III.8) and figure (III.9):

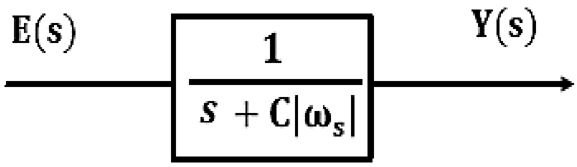

Figure III. 10: Classical LPF block.

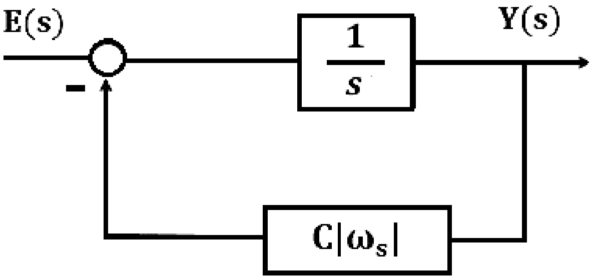

Figure III. 11: Modified classical LPF block.

Now we can easily introduce the estimated operating frequency into the LPF shown in Figure (III.11).

The same modification is carried out in Figure (III.10) and Figure (III.13) for the proposed integrator.

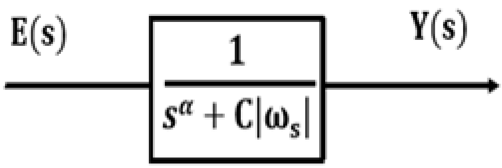

Figure III. 12: Fractional order LPF block.

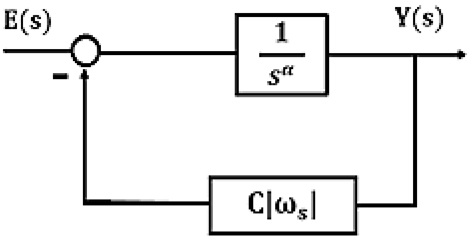

Figure III. 13: Modified fractional order LPF block.

The final proposed integrator and the classical integrator are presented in Figure (III.14) and Figure (III.15) respectively.

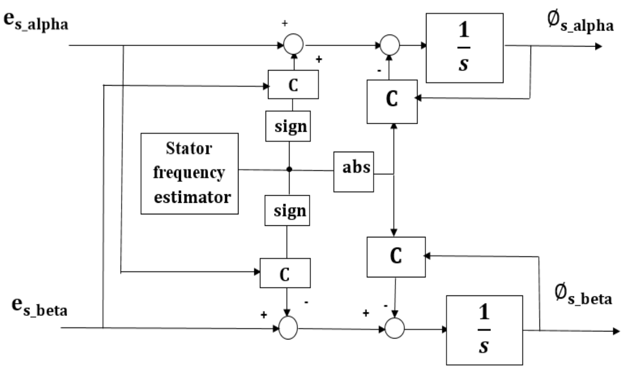

Figure III. 14: Final scheme of the classical LPF estimator.

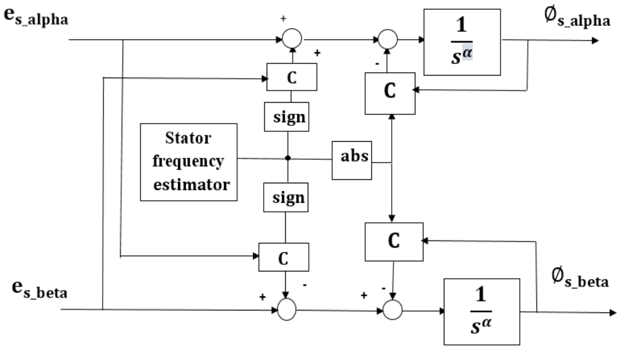

Figure III. 15: Final scheme of the proposed estimator.

Figure (III.14) and Figure (III.15) have been used in the block "Torque and flux estimation" shown in Figure (III.16) for comparison.

Using the stator flux estimation, the electromagnetic torque can be estimated as follow:

$$\Gamma_{em} = \frac{3}{2} p(\phi_{s\alpha} i_{s\beta} - \phi_{s\beta} i_{s\alpha}) \quad \text{(III.63)}$$

where p is the number of pole pairs of the induction motor.

The estimation of the stator flux phase angle is given by:

$$\delta = atan2(\phi_{s\beta}, \phi_{s\alpha}) \quad \text{(III.64)}$$

where the function $atan2$ is the four-quadrant arctangent of the elements of $\phi_{s\alpha}$ and $\phi_{s\beta}$.

III.3.3 Experimental results

To show the proposed method's validity, the DTC of an induction motor scheme shown in figure (III.16) has been implemented in the experimental test bench that is illustrated in the appendix.

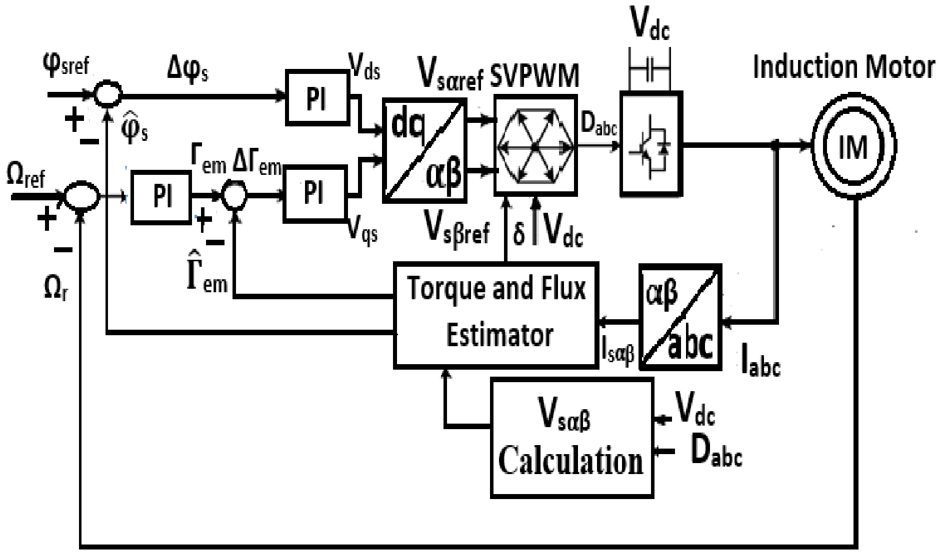

Figure III. 16: DTC scheme of induction motor.

The induction motor's parameters are given in "Table I". These parameters have been found using classical identification. The stator resistance is the only parameter used in the DTC drive shown in Figure (III.16). It was measured using a multimeter with a precision of 1.2%.

At rotor speed $\omega_r = 10$ (rad/s), the stator flux is estimated using both the LPF estimator proposed in the [25] and our proposed estimator, for comparison.

If the cutoff frequency is so lower than the operating frequency, the ability of the estimator to eliminate the dc offset is reduced. In addition, if it is chosen closer than the operating frequency, the error in phase and magnitude will be raised. Therefore, for optimal steady-state operation, selecting an adequate cutoff frequency for the estimator is necessary [36]. The value of C in equation (III.61) has been taken as 0.2 in this work [24].

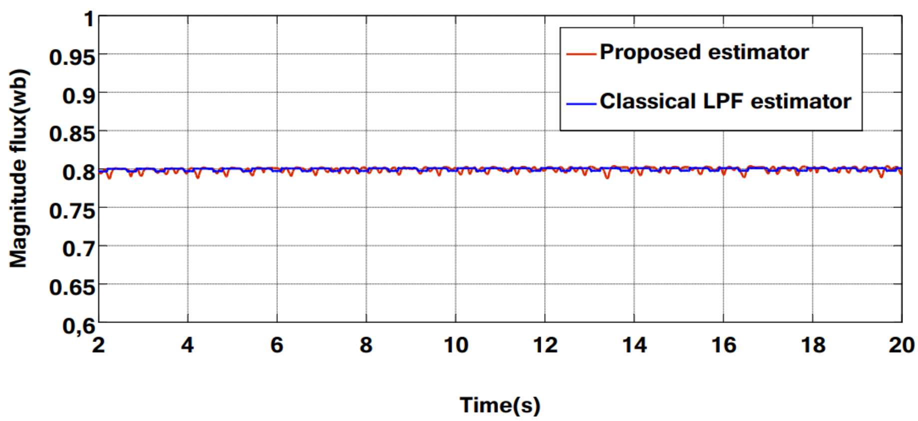

Figure III. 17: Experimental result of magnitude stator flux.

The stator flux magnitude reference is set to 0.8 (Wb). It is controlled with the PI regulator in the two cases (with the classical LPF estimator and with the proposed estimator), thus the magnitude error between the reference and the estimated flux is practically eliminated as it is shown in Figure (III.17). Therefore, we are interested to analyze only the estimated flux component waveforms and phase angle. It must be noticed that the real value of the stator flux is still unknown without using a sensor to measure it but anyway it can be controlled and estimated.

The reference speed of the induction motor is set at 10 (rad/s). The speed is reduced in the experiment because noise appears at a low speed. In each Figure below (Figure III.18 to Figure III.25), the proposed integration procedure is compared to the classical LPF integrator's performance.

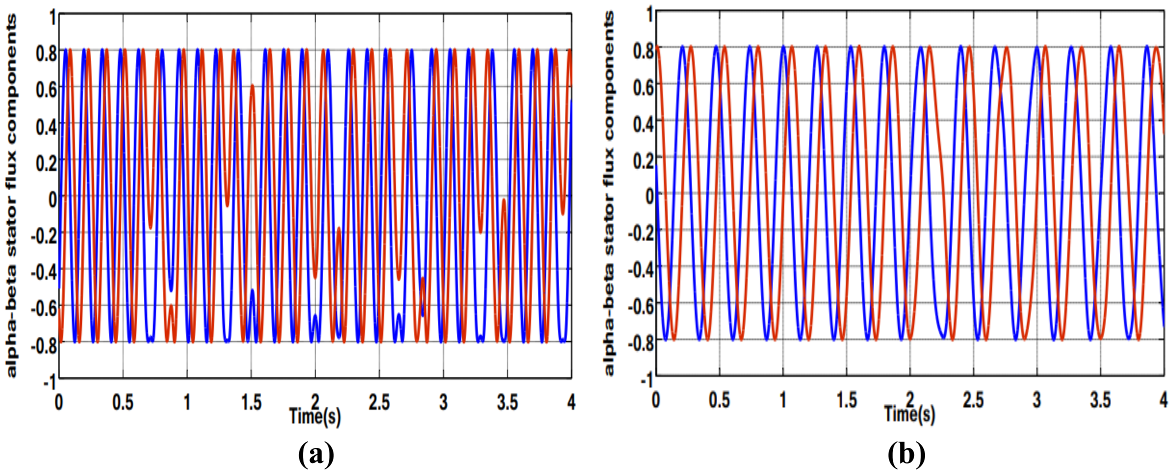

Figure III. 18 : Experimental result of alpha-beta stator flux components: (a) classical LPF estimator, (b) with the proposed estimator.

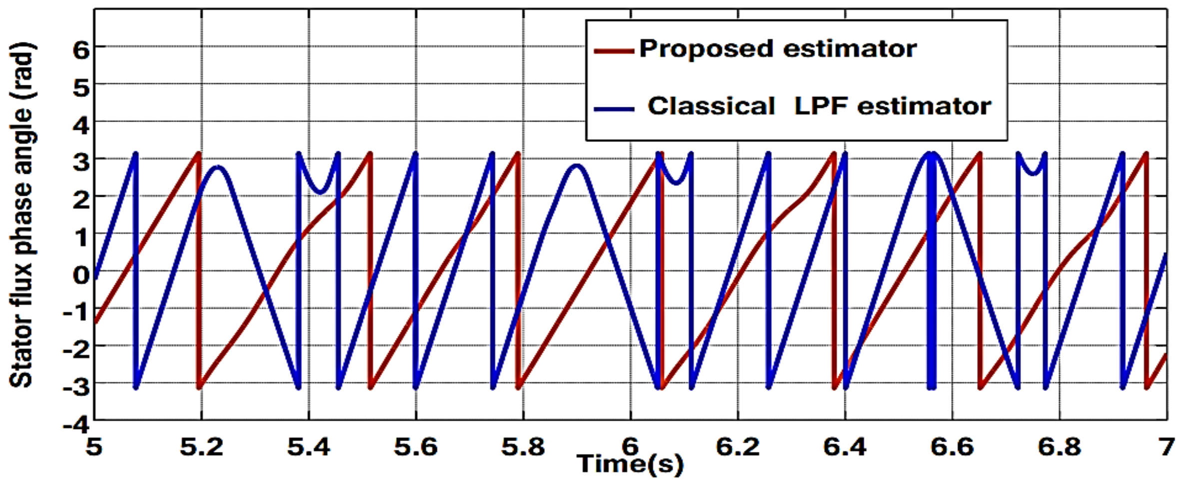

Figure III. 19: Experimental result of stator flux phase angle with the proposed estimator and the classical LPF estimator.

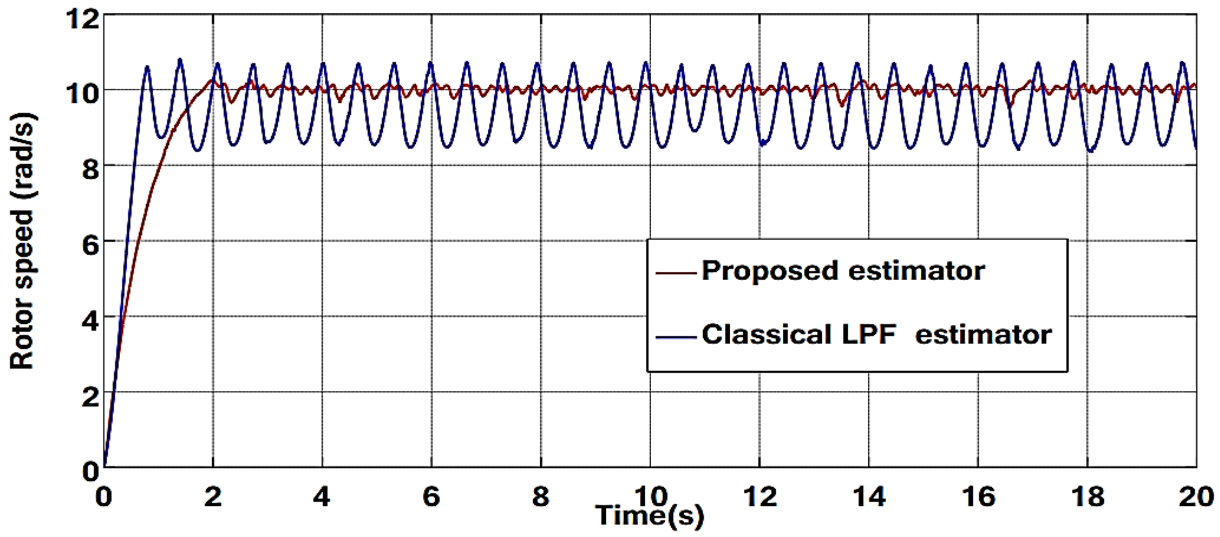

Figure III. 20: Experimental result of rotor speed with the proposed estimator and the classical LPF estimator.

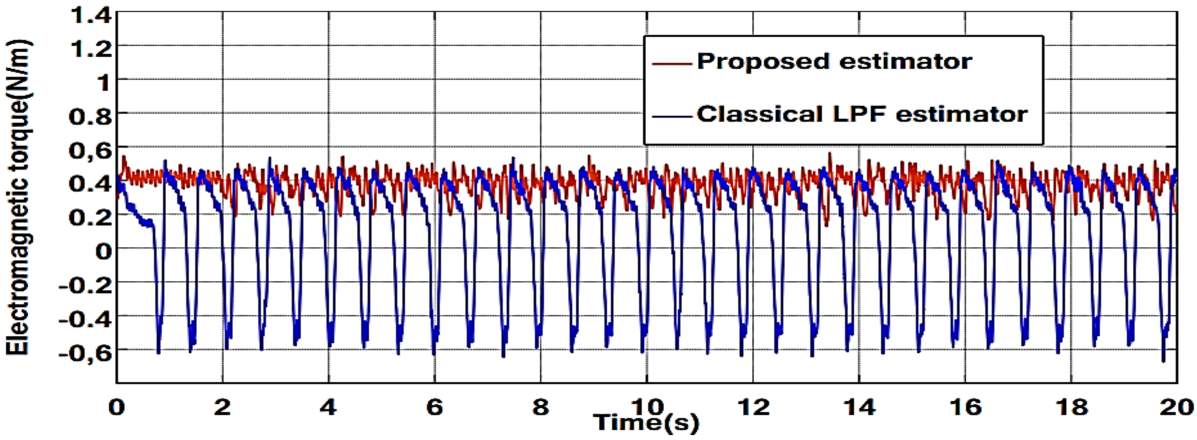

Figure III. 21: Experimental result of electromagnetic torque with the proposed estimator and the classical LPF estimator.

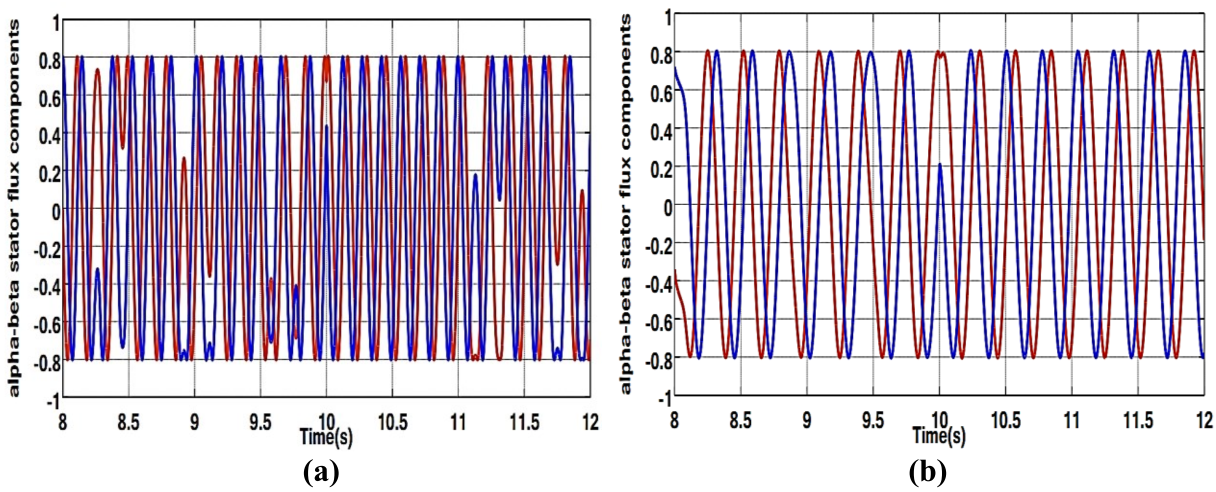

Figure III. 22: Experimental result of alpha-beta stator flux components in the case of inverting speed: (a) with the classical LPF estimator and (b) with the proposed estimator.

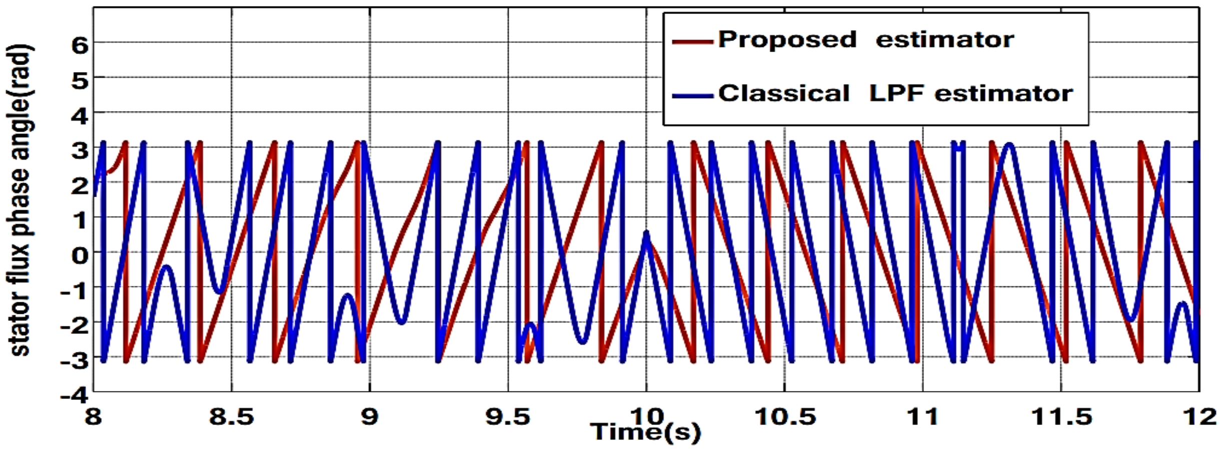

Figure III. 23: Experimental result of stator flux phase angle in the case of inverting speed.

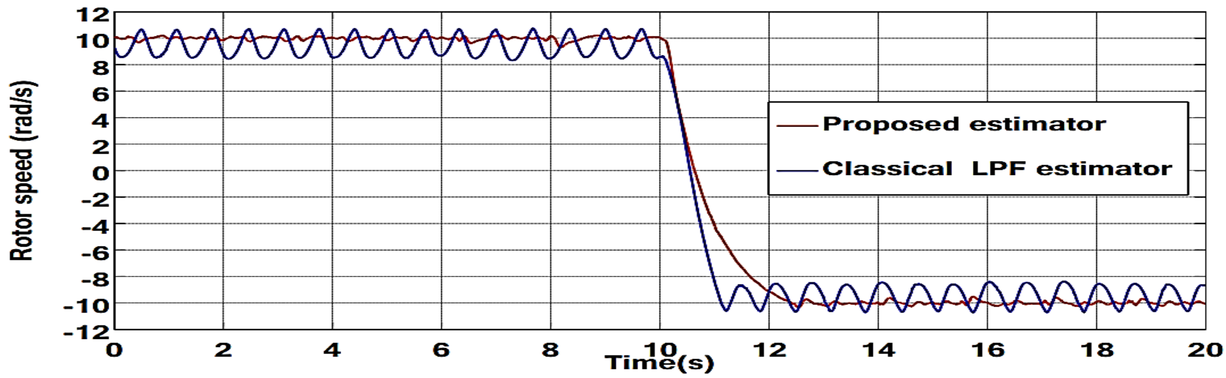

Figure III. 24: Experimental result of rotor speed in the case of inverting speed.

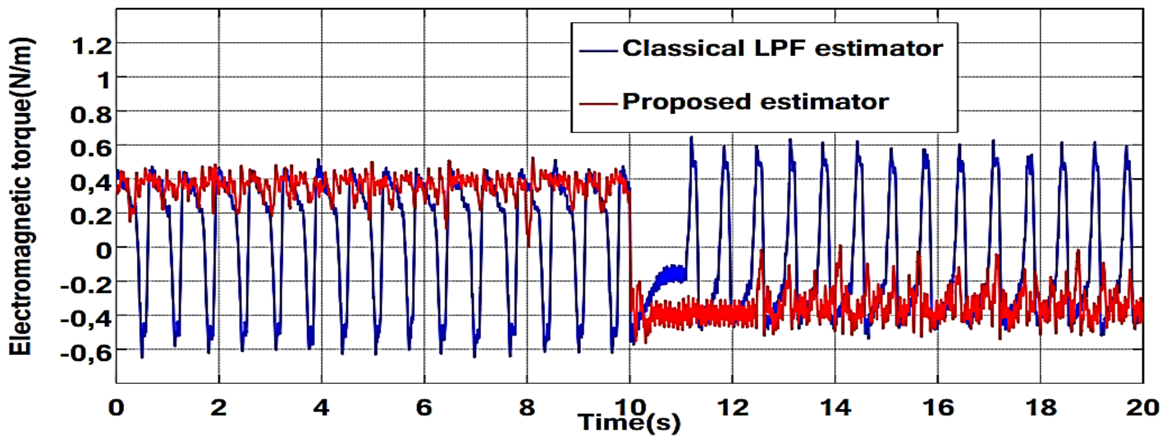

Figure III. 25: Experimental result of electromagnetic torque in the case of inverting speed.

The effect of the undesirable signal noise on the estimation stator flux is clearly observed from the above experimental results of DTC with the classical LPF estimator.

An accurate waveform of the alpha-beta stator flux components can be observed in Figure (III.18.b) obtained by the proposed estimator flux compared with the waveforms obtained by the classical LPF estimator in Figure (III.18.a).

Furthermore, from Figure.19 we can observe that the stator flux phase angle is distorted in the case of classical LPF. Moreover, speed and torque are also affected by undesirable high-frequency noise. Under no-load conditions, the motor generates a low torque to overcome the friction of both the rotor of the induction motor and the rotor of the DC machine, which is positive when the motor turns in the positive direction and negative when the motor turns in the negative direction. The induction motor respects this rule in the case of fractional order LPF estimator with reduced ripple. However, in the case of the classical LPF estimator, the torque and the speed are completely deformed as shown in figure (III.20) and figure (III.21).

When the induction motor's speed changes from 10 (rad/s) to -10 (rad/s), the component of the stator flux in figure (III.22.a), are deteriorated, on the other hand, this error is eliminated with the proposed integration method as shown in figure (III.22.b).

Figure (III.23) shows the stator flux phase angle. In the case of the proposed method, it is clear that this phase angle is quite smooth during the motor rotation change. In addition, the speed is accurate and stable and the torque ripple is reduced as shown in figure (III.24) and figure (III.25) respectively.

III.4. Conclusion

The problem of noise encountered, at low speeds, with stator flux, estimation in direct torque control of induction motors has been examined in this chapter. The modified integrator described in this chapter makes the estimated stator flux far less sensitive to the noise at low speed. The experimental results show clearly that the proposed integrator decreases the sensitivity of the voltage model against noise. Hence, good performance of induction motor direct torque control has been achieved.

REFERENCES

[1] BENAMOR Messaoud, « Etude et Simulation d'estimateurs et observateurs robustes de flux et de vitesse pour la machine asynchrone », thèse de MAGISTER -Université de BATNA (2012).

[2] K. Wang, et al., "Online updating of rotor time constant based on combined voltage and current mode flux observer for speed-sensorless AC drives." IEEE Transactions on Industrial Electronics, Vol. 61, pp.4583-4593, 2014.

[3] C. Lascu, I. Boldea, F. Blaabjerg, "A modified direct torque control for induction motor sensorless drive," IEEE Transactions on industry applications Vol. 36, pp.122-130, 2000.

[4] S. Krim, S. Gdaim, A. Mtibaa, M. F. Mimouni, "Hardware Implementation of a Predictive DTC-SVM with a Sliding Mode Observer of an Induction Motor on the FPGA," WSEAS Transactions on Systems and Control, Vol. 10, pp.2224-2856, 2015.

[5] C. Lascu, G.-D. Andreescu, "Sliding-mode observer and improved integrator with DC-offset compensation for flux estimation in sensorless-controlled induction motors," IEEE Transactions on Industrial Electronics, Vol. 53, pp.785-794, 2006.

[6] Z. G. Yin, C. Zhao, Y. R. Zhong, and J. Liu, "Research on robust performance of speed-sensorless vector control for the induction motor using an interfacing multiple-model extended Kalman filter," IEEE Transactions on Power Electronics, Vol. 29, pp.3011-3019, 2013.

[7] S. M. Gadoue, D. Giaouris, and J. W. Finch, "Sensorless control of induction motor drives at very low and zero speeds using neural network flux observers," IEEE Transactions on Industrial Electronics, Vol. 56, pp.3029-3039, 2009.

[8] S. M. Gadoue, D. Giaouris, and J. W. Finch, "MRAS sensorless vector control of an induction motor using new sliding-mode and fuzzy-logic adaptation mechanisms," IEEE Transactions on Energy conversion, Vol. 25, pp.394-402, 2009.

[9] W. Xu, S. Qu, J. Zhao, H. Zhang, X. Du, "An Improved Full-Order Sliding-Mode Observer for Rotor Position and Speed Estimation of SPMSM," IEEE Access, Vol. 9, pp.15099-15109, 2021.

[10] X. Xu, D.W. Novotny, "Implementation of direct stator flux orientation control on a versatile DSP based system," IEEE Transactions on Industry Applications, Vol. 27, pp.694-700, 1991.

[11] I. Benlaloui, S. Drid, L. Chrifi-Alaoui, and M. Ouriagli, "Implementation of a new MRAS speed sensorless vector control of induction machine," IEEE Transactions on Energy conversion, Vol. 30, pp. 588-595, 2014.

[12] A. N. Smith, S. M. Gadoue, J. W. Finch "Improved rotor flux estimation at low speeds for torque MRAS-based sensorless induction motor drives," IEEE Transactions on Energy Conversion, Vol. 31, pp. 270-282, 2015.

[13] G. Shen, W. Yao, B. Chen, K. Wang, K. Lee, and Z. Lu, "Automeasurement of the inverter output voltage delay curve to compensate for inverter nonlinearity in sensorless motor drives," IEEE Transactions on Power Electronics, Vol. 29, pp.5542-5553, 2013.

[14] P. Alkorta, O. Barambones, J.A Cortajarena, and A. Zubizarrreta, "Efficient multivariable generalized predictive control for sensorless induction motor drives," IEEE Transactions on Industrial Electronics, Vol. 61, pp.5126-5134, 2013.

[15] B. Karanayil, M.F. Rahman, C. Grantham, "An a of a programmable cascaded low-pass filter for a rotor flux synthesizer for an induction motor drive," IEEE Transactions on Power Electronics, Vol.19, pp. 257-263, 2004.

[16] M. Hinkkanen, J. Luomi, "Modified integrator for voltage model flux estimation of induction motors," IEEE Transactions on Industrial Electronics, Vol. 50, pp. 818-820, 2003.

[17] M. Comanescu, L. Xu, "An improved flux observer based on PLL frequency estimator for sensorless vector control of induction motors," IEEE Transactions on Industrial Electronics, Vol. 53, pp.50-56, 2006.

[18] G. Tan, X. Wu, Z. Ye, Y. Han, & P. Guo, "Dual three-level double-fed induction motor control based on novel stator flux observer," in Conf. Electrical and Control Engineering, Wuhan, China, 2010, pp.3668- 3671.

[19] A. Choudhury, P. Pillay, and S. S. Williamson. "Modified stator flux estimation based direct torque controlled PMSM drive for hybrid electric vehicle," in Conf. IEEE Industrial Electronics Society, Montreal, QC, Canada, 2012, pp. 2965-2970.

[20] Y. Wang, and Z. Deng, "An integration algorithm for stator flux estimation of a direct-torque-controlled electrical excitation flux-switching generator." IEEE Trans. Energy Conversion, Vol. 27, No. 2, pp.411-420, June

2012.
[21] Y. Wang, and Z. Deng, "Improved stator flux estimation method for direct torque linear control of parallel hybrid excitation switched-flux generator." IEEE Trans. Energy Conversion, Vol. 27, pp.747-756, Sep 2012.
[22] A. G. Khandekar, and J. G. Chaudhari. "Modified integration method to estimate stator flux in induction motor with offset error," in Conf. Advances in Electrical, Electronics, Information, Communication and Bio-Informatics (AEEICB), Chennai, India, 2017, pp. 450-453.
[23] Y. Zhang, X. Zhang, S. Yang, and P. Cao, "An Improved Voltage Model for Closed-loop Torque Control in Induction Motor Drives." in Conf. IEEE International Power Electronics and Application, Shenzhen, China, 2018, pp.1-4 .
[24] Belbali, A., & Makhloufi, S.. Direct Torque Control of Induction Motor with Stator Flux Estimation Based on an Improved Voltage Model. Electronics/Elektronika, Vol. 26(1) (1450-5843), (2022).
[25] D. Stojić, M. Milinković, S. Veinović, I. Klasnić, "Improved stator flux estimator for speed sensorless induction motor drives," IEEE Trans. Power Electronics, Vol. 30, pp.2363-2371, April 2015.
[26] T Sharma, A Bhattacharya, H Ahmed, "Transient and steady-state study of a speed sensorless IPMSM drive with an advanced integrator-based stator flux estimator," IET Power Electronics, Vol. 14, pp.1157-1172, 2021.
[27] T Sharma, A Bhattacharya, "Performance analysis of encoderless DTC of IPMSM for wide operating range," Arabian Journal for Science and Engineering Vol.45, pp.6501-6515, 2020.
[28] A Shukla, R Sharma, "Modified DTC with Adaptive Compensator for Low-Speed Region of Induction Motor in Electric Vehicle Applications," Smart Science, Vol. 8, pp.101-116, 2020.
[29] O. Chandra Sekhar, S. Lakhimsetty, and A. Bhat. "A comparative experimental analysis of fractional order PI controller based direct torque control scheme for induction motor drive," International Transactions on Electrical Energy Systems, Vol. 31, pp. e12705, 2021.
[30] A Kadri, H Marzougui, F Bacha, "Implementation of direct power control based on stator flux estimation using low-pass filter estimator for doubly fed induction generator–wind energy conversion system," Proceedings of the Institution of Mechanical Engineers, Part I: Journal of Systems and Control Engineering, Vol. 233, pp.764-778, 2019.
[31] K. Lv, Z. Xie, M. Zhou, J. Bu, "A comparative study of three starting strategies for an aero flywheel motor using the modified DTC method," IEEE Access, Vol.7, pp.59548-59558, 2019.
[32] ML. Wardi, M. Amairi, and M. N. Abdelkrim. "Fractional PID controller design for nonlinear systems based on singular perturbation technique," International Journal of Digital Signals and Smart Systems, Vol.2, pp. 95-120, 2018.
[33] A. Charef, "Analogue realisation of fractionalorder integrator, differentiator and fractional PIλDμ controller," IEE Proc.-Control Theory Appl, Vol.153, pp.714-720, 2006.

[34] H. Walid, R. Djamel, M. Sami, and D. A. Elbaki, "Fractional order direct torque control of permanent magnet synchronous machine," European Journal of Electrical Engineering, Vol.21, pp.431-438, 2019.
[35] M. H. Shin, D. S. Hyun, S. B. Cho, and S.Y. Choe, "An improved stator flux estimation for speed sensorless stator flux orientation control of induction motors," in conf. 29th Annual IEEE Power Electronics Specialists, Fukuoka, Japan , 1998, pp. 1581-1586.
[36] N.R.N. Idris, A.H.M. Yatim, "An improved stator flux estimation in steady-state operation for direct torque control of induction machines," IEEE Transactions on Industry Applications, Vol. 38, pp.110-116, 2002.
[37] Jansen, P. L., & Lorenz, R. D. (1994). A physically insightful approach to the design and accuracy assessment of flux observers for field oriented induction machine drives. IEEE Transactions on Industry Applications, 30(1), 101-110.
[38] BAGHLI Lotfi, « Etude et Simulation d'estimateurs et observateurs robustes de flux et de vitesse pour la machine asynchrone », thèse de doctorat -Université HENRI POINCARE NANCY1 (1999).
[39] Jansen, P. L., & Lorenz, R. D. (1994). A physically insightful approach to the design and accuracy assessment of flux observers for field oriented induction machine drives. IEEE Transactions on Industry Applications, 30(1), 101-110.
[40] Shoukry, Y., & Tabuada, P. (2014, December). Event-triggered projected Luenberger observer for linear systems under sparse sensor attacks. In 53rd IEEE Conference on Decision and Control (pp. 3548-3553). IEEE.
[41] Quintero-Marmol, E., Luyben, W. L., & Georgakis, C. (1991). Application of an extended Luenberger

observer to the control of multicomponent batch distillation. Industrial & engineering chemistry research, 30(8), 1870-1880.
[42] Tornambè, A. (1989, December). Use of asymptotic observers having-high-gains in the state and parameter estimation. In Proceedings of the 28th IEEE Conference on Decision and Control, (pp. 1791-1794). IEEE.
[43] U.D.L Sidi Bel-Abbès «Commande vectorielle indirecte de la MAS sans capteur mécanique », Support de cours.
[44] Merzoug Med salah, « Etude comparative des performances d'un DTC et d'un FOC d'une Machine synchrone à aimants permanents (MSAP) », thèse de MAGISTER, Université de Batna
[45] Griva, G., Profumo, F., Rosell, L., & Bojoi, R. (2000, October). Optimization of fuzzy-like Luenberger observer for high speed sensorless induction motor drives using genetic algorithms. In Conference Record of the 2000 IEEE Industry Applications Conference. Thirty-Fifth IAS Annual Meeting and World Conference on Industrial Applications of Electrical Energy (Cat. No. 00CH37129) (Vol. 2, pp. 1268-1274). IEEE.
[46] Holakooie, M. H., Ojaghi, M., & Taheri, A. (2016). Full-order Luenberger observer based on fuzzy-logic control for sensorless field-oriented control of a single-sided linear induction motor. ISA transactions, 60, 96-108.
[47] Alessandri, A., & Zaccarian, L. (2015, July). Results on stubborn Luenberger observers for linear time-invariant plants. In 2015 European Control Conference (ECC) (pp. 2920-2925). IEEE.
[48] Andrieu, V. (2014). Convergence speed of nonlinear Luenberger observers. SIAM Journal on Control and Optimization, 52(5), 2831-2856.
[49] Li, Y., & Sanfelice, R. G. (2013, June). A coupled pair of Luenberger observers for linear systems to improve rate of convergence and robustness to measurement noise. In 2013 American Control Conference (pp. 2497-2502). IEEE.
[50] Friedland, B. (1996). Full-order state observer. department of electrical and computer engineering, New Jersey Institute of Technology, NEWARY, NEW JERSEY, USA.
[51] Kreisselmeier, G. (1977). Adaptive observers with exponential rate of convergence. IEEE transactions on automatic control, 22(1), 2-8.
[52] Kumar, R., Das, S., Syam, P., & Chattopadhyay, A. K. (2015). Review on model reference adaptive system for sensorless vector control of induction motor drives. IET Electric Power Applications, 9(7), 496-511.
[53] Sugimoto, H., & Tamai, S. (1987). Secondary resistance identification of an induction-motor applied model reference adaptive system and its characteristics. IEEE Transactions on Industry Applications, (2), 296-303.
[54] Teja, A. R., Verma, V., & Chakraborty, C. (2015). A new formulation of reactive-power-based model reference adaptive system for sensorless induction motor drive. IEEE Transactions on Industrial Electronics, 62(11), 6797-6808.
[55] Kumar, R., Das, S., & Chattopadhyay, A. K. (2016). Comparative assessment of two different model reference adaptive system schemes for speed-sensorless control of induction motor drives. IET Electric Power Applications, 10(2), 141-154.
[56] Ohnishi, K., Ueda, Y., & Miyachi, K. (1986). Model reference adaptive system against rotor resistance variation in induction motor drive. IEEE Transactions on Industrial Electronics, (3), 217-223.
[57] Xiao, J., Li, B., Gong, X., Sheng, Y., & Chai, J. (2010, June). Improved performance of motor drive using RBFNN-based hybrid reactive power MRAS speed estimator. In The 2010 IEEE International Conference on Information and Automation (pp. 588-593). IEEE.
[58] Maiti, S., & Chakraborty, C. (2010). A new instantaneous reactive power based MRAS for sensorless induction motor drive. Simulation Modelling Practice and Theory, 18(9), 1314-1326.
[59] Aymen, F., Novak, M., & Lassaad, S. (2018). An improved reactive power MRAS speed estimator with optimization for a hybrid electric vehicles application. Journal of Dynamic Systems, Measurement, and Control, 140(6), 061016.
[60] Zheng, H., Zhao, J., & Liu, L. (2016). Improved mutual MRAS speed identification based on back-emf. Journal of Electrical Engineering and Technology, 11(3), 769-774.
[61] Kashif, M., & Singh, B. (2022, January). BEMF-MRAS Based Sensorless PMSM for Solar Irrigation Pump with Ancillary Load Services. In 2022 IEEE International Conference on Power Electronics, Smart Grid, and Renewable Energy (PESGRE) (pp. 1-5). IEEE.
[62] Haron, A. R., & Idris, N. R. N. (2006, November). Simulation of MRAS-based speed sensorless estimation of induction motor drives using MATLAB/SIMULINK. In 2006 IEEE International Power and Energy Conference (pp. 411-415). IEEE.

[63] Brandstetter, P., Dobrovsky, M., Kuchar, M., Dong, C. S. T., & Vo, H. H. (2017). Application of BEMF-MRAS with Kalman filter in sensorless control of induction motor drive. Electrical Engineering, 99(4), 1151-1160.
[64] Brandstetter, P., Dobrovsky, M., Petrtyl, O., Dong, C. S. T., & Vo, H. H. (2016, May). Sensorless control of induction motor drive using BEMF-MRAS with Kalman filter. In 2016 ELEKTRO (pp. 121-126). IEEE.
[65] Yin, Z., Li, G., Zhang, Y., Liu, J., Sun, X., & Zhong, Y. (2016). A speed and flux observer of induction motor based on extended Kalman filter and Markov chain. IEEE Transactions on Power Electronics, 32(9), 7096-7117.
[66] Zhang, Y., Zhao, Z., Lu, T., Yuan, L., Xu, W., & Zhu, J. (2009, September). A comparative study of Luenberger observer, sliding mode observer and extended Kalman filter for sensorless vector control of induction motor drives. In 2009 IEEE Energy Conversion Congress and Exposition (pp. 2466-2473). IEEE.
[67] Zerdali, E., Yildiz, R., Inan, R., Demir, R., & Barut, M. (2021). Improved speed and load torque estimations with adaptive fading extended Kalman filter. International Transactions on Electrical Energy Systems, 31(1), e12684.
[68] Chenchen, W., & Yongdong, L. (2008, February). A novel speed sensorless field-oriented control scheme of IM using extended Kalman filter with load torque observer. In 2008 Twenty-Third Annual IEEE Applied Power Electronics Conference and Exposition (pp. 1796-1802). IEEE.
[69] Habibullah, M., & Lu, D. D. C. (2015). A speed-sensorless FS-PTC of induction motors using extended Kalman filters. IEEE Transactions on Industrial Electronics, 62(11), 6765-6778.
[70] Tiwari, V., Das, S., & Pal, A. (2017, November). Sensorless speed control of induction motor drive using extended Kalman filter observer. In 2017 IEEE PES Asia-Pacific Power and Energy Engineering Conference (APPEEC) (pp. 1-6). IEEE.
[71] Et-Taaj, L., Boulghasoul, Z., Elbacha, A., & El Kharki, A. (2021, July). Robust sensorless induction motor control based on extended kalman filter observer. In 2021 International Congress of Advanced Technology and Engineering (ICOTEN) (pp. 1-9). IEEE.
[72] Alonge, F., Cangemi, T., D'Ippolito, F., Fagiolini, A., & Sferlazza, A. (2014). Convergence analysis of extended Kalman filter for sensorless control of induction motor. IEEE Transactions on Industrial Electronics, 62(4), 2341-2352.
[73] Zerdali, E. (2018). Adaptive extended Kalman filter for speed-sensorless control of induction motors. IEEE Transactions on Energy Conversion, 34(2), 789-800.
[74] Allaoui, S., Chafaa, K., Laamari, Y., & Athamena, B. (2015, December). Induction motor state estimation using tuned Extended Kalman Filter. In 2015 4th International Conference on Electrical Engineering (ICEE) (pp. 1-5). IEEE.
[75] Efimov, D., Zolghadri, A., & Simon, P. (2010, October). Improving fault detection abilities of extended Kalman filters by covariance matrices adjustment. In 2010 Conference on Control and Fault-Tolerant Systems (SysTol) (pp. 131-136). IEEE.
[76] Dhaouadi, R., Mohan, N., & Norum, L. (1991). Design and implementation of an extended Kalman filter for the state estimation of a permanent magnet synchronous motor. IEEE Transactions on Power Electronics, 6(3), 491-497.
[77] Saha, M., Ghosh, R., & Goswami, B. (2013). Robustness and sensitivity metrics for tuning the extended Kalman filter. IEEE Transactions on Instrumentation and Measurement, 63(4), 964-971.
[78] Laamari, Y., Chafaa, K., & Athamena, B. (2015). Particle swarm optimization of an extended Kalman filter for speed and rotor flux estimation of an induction motor drive. Electrical Engineering, 97(2), 129-138.
[79] Valappil, J., & Georgakis, C. (2000). Systematic estimation of state noise statistics for extended Kalman filters. AIChE Journal, 46(2), 292-308.
[80] Barut, M., Bogosyan, S., & Gokasan, M. (2007). Speed-sensorless estimation for induction motors using extended Kalman filters. IEEE Transactions on Industrial Electronics, 54(1), 272-280.
[81] MESBAHI Abdelouahed, «contribution aux techniques d'estimation et d'observation appliquées au machines a synchrones et synchrones a aimants permanants», thèse de doctorat (2013)
[82] S. Chavez Velazquez, R.Alejos Palomares, A.Nava Segura, « Speed estimation for an Induction motor using the extended Kalman filter. » Electronics, Communications and Computers, CONIELECOMP. 14th International Conference, 2004.
[83] S. Yanxia, W. Dinghui, S. Xiaoping, "High Performance Direct Vector Control of an Asynchronous Motor based on EKF", 2010 IEEE
[84] A. Kheldoun, « Amélioration des Performances d'un Variateur de Vitesse par Moteur Asynchrone Contrôlé

par la Méthode à Flux Orienté », Thèse de doctorat, Université de Boumerdès. 2007.

Chapter IV
Improving torque of induction motor using different DTC structures

IV.1 Introduction

Direct Torque Control (DTC) is an advanced and simple control method in Alternating Current (AC) drive systems, to achieve high performance torque control. Conventional DTC uses a hysteresis band controller, whose control action has no difference between large torque error and small torque error. This results in a high torque ripple and variable switching frequency. This chapter aims to improve the conventional DTC performance by using space vector SVPWM with different controllers, to minimize torque error, and achieve constant switching frequency and better motor performance. These techniques can significantly reduce torque ripple and improve dynamic response in comparison with conventional DTC. The validity of these techniques is confirmed by the simulation results.

IV.2 DTC control parallel structure with different controllers

IV.2.1 Classical DTC with hysteresis controller

The direct torque control strategy, originally proposed by Takahashi, is based on the principles developed in chapter one. Using a judicious choice of the inverter's appropriate voltage vector, this method consists in controlling the stator flux magnitude and the torque directly and simultaneously [1].

Choosing the voltage vector depends on the desired variation in stator flux magnitude, the desired rotation speed evolution and consequently the torque as well [2].

Flux and torque are estimated using the supply voltages and currents, then compared to their respective references by two- or three-level hysteresis comparators [3] [4]. Therefore, the voltage vector choice is made according to the comparator's state and the stator flux position as well in the complex plane [5]. This strategy shows that the complex plan is divided into six sectors of 60º. Decomposition into twelve sectors is possible but it does not bring additional improvements in the DTC structure with a two-level inverter [6].

The structure control block diagram is shown in figure (IV.1). Hysteresis band controllers are used to regulate flux and torque.

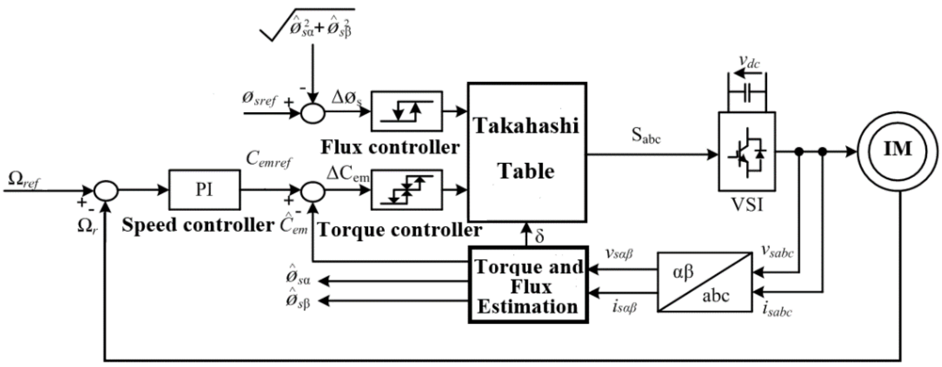

Figure IV. 1: General structure of the Classical Direct Torque Control (CDTC).

IV.2.2 DTC-SVPWM with three PI controllers

This method retains the basic idea of the classic DTC method [7]. This is accomplished by using the stator flux orientation method [8]. Thus, the PI regulators and the SVPWM method can both produce and impose control voltages [9].

This control structure has the advantages of vector control and conventional DTC by overcoming the problems of the latter [10]. PI controllers and vector modulation techniques are used to achieve fixed switching frequency and less torque and flux ripple [11].

The structure control block diagram is shown in figure (IV.2). Two PI controllers are used to regulate flux and torque.

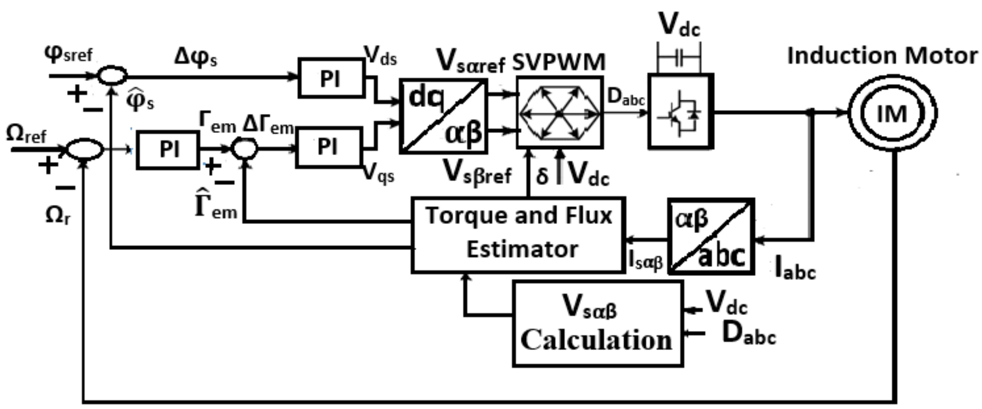

Figure IV. 2: DTC-SVPWM of an induction motor.

In this arrangement, there are two proportional integral (PI) type controllers, which adjust the torque and stator flux magnitude instead of the hysteresis band. The two PI controllers produce the control voltages to control the motor-side voltage source inverter [12]. A PI controller controls torque, where Takahashi tables and hysteresis have been eliminated. Compared to FOC (Field Oriented Control) vector control, this DTC control is not required by using a decoupling mechanism, and only PI controllers can adjust the magnitudes of stator flux and torque [13].

IV.2.3 DTC-SVPWM with two PI controllers and fuzzy logic controller speed

In this chapter, we aim to construct a more robust DTC control by replacing the PI controller for the speed regulation loop with the fuzzy logic controller (FLC). The FLC was designed using the fuzzy control toolbox provided in Matlab, with Mamdani's min max decision inference engine.

The signals for the error and the variation in speed error are used as inputs to the speed controller, and an output is taken to provide the electromagnetic torque reference [14].

The structure control block diagram is shown in figure (IV.3). Where the fuzzy logic controller instead of the classical PI controller adjusts the speed.

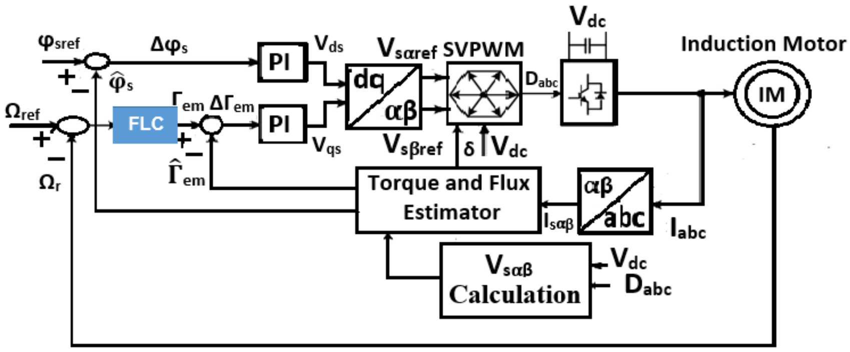

Figure IV. 3: DTC-FLC control functional diagram.

IV.2.4 DTC-SVPWM with a fractional order PI (FOPI) controller speed

We keep the same studied system illustrated in Fig. III.2, only the PI controller is changed to a fractional order PI (FOPI) controller for speed, torque and flux control [15].

The FOPI control algorithm like that in a conventional PI controller focused on the error value calculation, which corresponds to the difference between the quantity measured and that of the desired reference [16] [17]. The FOPI controller is similar in structure to the classic PI controller, which tries to minimize the error by adjusting process control inputs, but the FOPI controller considers non-integer integration orders to determine the control action [18].

The structural control block diagram is shown in figure (IV.4).

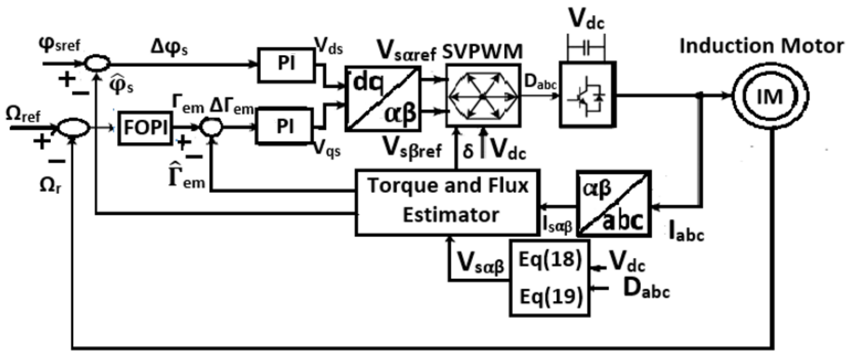

Figure IV. 4: DTC-FOPI controller.

IV.3 Control of speed, stator flux, and electromagnetic torque

IV.3.1 Decoupling

There are different decoupling techniques: decoupling by state feedback, static decoupling or compensation decoupling, which we will now present [19].

IV.3.1.1 Compensation decoupling

The purpose of compensation is to decouple the d and q axes. Through this decoupling, it is possible to define the regulators' coefficients by simply writing the equations of the machine and the regulator part [20]. By considering the slow dynamics of the flux at low speed ($\frac{d\psi_{rd}}{dx} = 0$) compared to the currents [21], then the voltage equations can be written by introducing the Laplace operator s as follows [22]:

$$\begin{cases} v_{sd} = \left(R_s + s\sigma L_s\right) i_{sd} - \omega_s \sigma L_s i_{sq} \\ v_{sq} = \left(R_s + s\sigma L_s\right) i_{sq} + \omega_s \dfrac{L_m}{L_r} \psi_r + \omega_s \sigma L_s i_{sd} \end{cases} \quad \text{(IV.1)}$$

Then, the new control variables v_{sd}^*, v_{sd}^* are written as follows:

$$\begin{cases} v_{sd}^* = \left(R_s + s\sigma L_s\right) i_{sd} = v_{sd} + \omega_s \sigma L_s i_{sq} = v_{sd} + e_{sd} \\ v_{sq}^* = \left(R_s + s\sigma L_s\right) i_{sq} = v_{sq} - \left(\omega_s \dfrac{L_m}{L_r} \psi_r + \omega_s \sigma L_s i_{sd}\right) = v_{sq} - e_{sq} \end{cases} \quad \text{(IV.2)}$$

With: * designating the reference variable control.

Thus, the actions on the d and q axes are decoupled as represented in the figure diagram (IV.5).

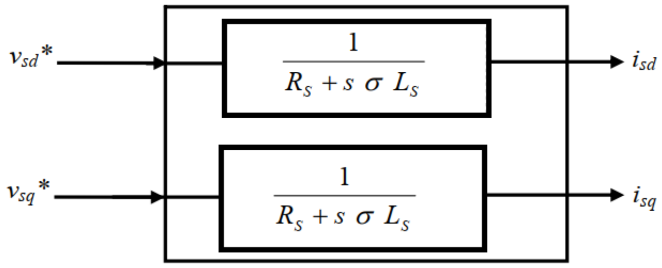

Figure IV. 5: New control acquired.

The voltages v_{sd} and v_{sq} are then reconstituted from the voltages v_{sd}^*, v_{sq}^* figure (IV.6):

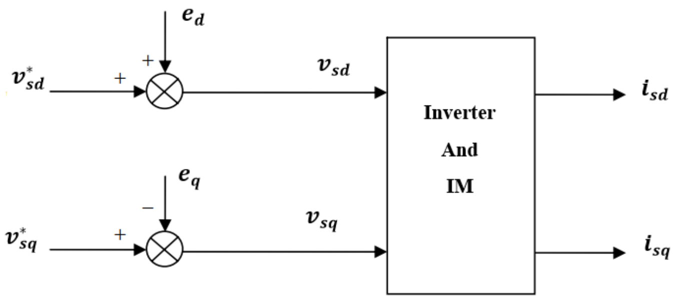

Figure IV. 6: Reconstruction of voltages v_{sd} and v_{sq}.

IV.3.2 Stator flux evolution rule

The generally accepted model for the DTC implementation is that with a stationary reference frame α, β, this model is given by the following equations system [23]:

$$\begin{cases} \mathbf{v_s} = R_s \mathbf{i_s} + \dfrac{d\Psi_s}{dt} \\ 0 = R_r \mathbf{i_r} + \dfrac{d\psi_{\mathbf{r}}}{dt} - j\omega \mathbf{\Psi_r} \end{cases} \quad \text{(IV.3)}$$

Where:

$$\mathbf{v_s} = v_{s\alpha} + jv_{s\beta}, \mathbf{i}_s = i_{s\alpha} + ji_{s\beta}, \mathbf{\Psi}_s = \psi_{s\alpha} + j\psi_{s\beta} \quad \text{(IV.4)}$$

$$\mathbf{i}_r = i_{r\alpha} + j i_{r\beta}, \boldsymbol{\psi}_r = \psi_{r\alpha} + j\psi_{r\beta} \tag{IV.5}$$

From (IV.3)

$$\boldsymbol{\psi}_{\mathbf{s}} = \int_0^t \left(\mathbf{v}_{\mathbf{s}} - R_s \mathbf{i}_{\mathbf{s}}\right) dt \tag{IV.6}$$

Knowing that during a sampling period $[0,T_s]$, the control sequence $(S_a\ S_b\ S_c)$ of the converter is fixed, the equation (IV.6) can be written as follows [24]:

$$\boldsymbol{\psi}_{\mathbf{s}}(t) = \boldsymbol{\psi}_{\mathbf{s}0} + \mathbf{v}_{\mathbf{s}} T_s - R_s \int_0^{T_s} \mathbf{i}_{\mathbf{s}} dt \tag{IV.7}$$

Or:

$$\boldsymbol{\Psi}_{\mathbf{s}}(t) = \boldsymbol{\psi}_{\mathbf{s0}} + \frac{2}{3} V_{\text{dc}} \left(S_a + aS_b + a^2 S_c\right) - R_s \int_0^{T_s} \mathbf{i}_{\mathbf{s}} dt \tag{IV.8}$$

Where: $a = e^{j2\pi/3}$, ψ_{s0} is the flux vector at $t = 0$, and with the assumption that the resistance R_s remains constant [25].

And if we ignore, as a first approximation the voltage drop due to the stator resistance, the stator flux vector at the time $(t + \Delta t)$ is deduced from the flux vector at time t by the following vector summation, within one inverter switching period (where v_s being fixed):

$$\boldsymbol{\Psi}_{\mathbf{s}}(t+\Delta t) = \boldsymbol{\Psi}_{\mathbf{s}}(t) + \mathbf{v}_{\mathbf{s}} \Delta t \tag{IV.9}$$

The equation (IV.9) can be reduced to the following recurrence equation:

$$\boldsymbol{\psi}_{\mathbf{s}}(n+1) \approx \boldsymbol{\psi}_{\mathbf{s}}(n) + \mathbf{v}_{\mathbf{s}} T_s \tag{IV.10}$$

Where:

$\psi_s(n)$ The stator flux vector at sampling time t_n.

$\psi_s(n+1)$ The stator flux vector at sampling time t_{n+1}.

Therefore, the variation of the stator flux due to the application of a voltage vector during a control period is:

$$\Delta\psi_s(n) \approx v_s T_s \approx \psi_s(n+1) - \psi_s(n) \tag{IV.11}$$

The equation (IV.11) shows that the trajectory of ψ_s follows the direction of the voltage vector v_s, such that, if the latter is nonzero, the extremity of the vector v_s follows the direction of ψ_s, and if v_s is zero voltage, then ψ_s is fixed.

To better illustrate the behavior of the stator flux module, we will represent it in a rotating frame, d, q where it coincides with the axis d ,figure (IV.7) [26].

We can rewrite the equation (IV.3), knowing that:

$$|\boldsymbol{\psi}_{\mathbf{s}}| = \sqrt{\psi_{sd}^2 + \psi_{sq}^2} \tag{IV.12}$$

$$\frac{d|\psi_s|}{dt} = \frac{d\psi_{sd}}{dt} = v_{sd} - R_s i_{sd}, \quad \left(\psi_{sq} = 0\right) \tag{IV.13}$$

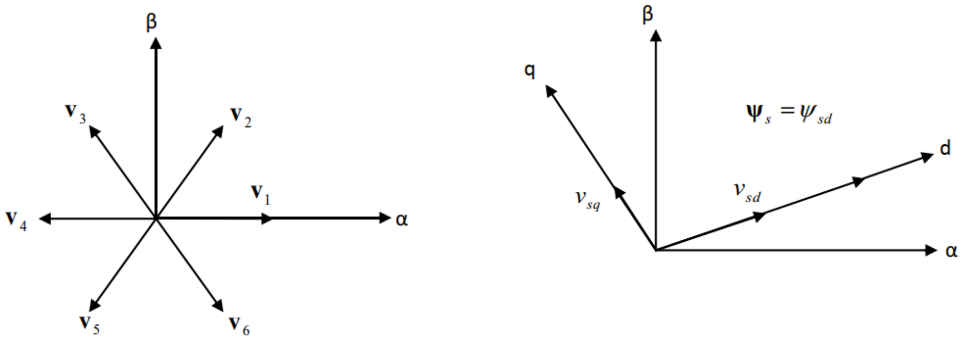

Figure IV. 7: Orientation of the d-axis according to the stator flux direction.

By neglecting the stator ohmic voltage drop due to the resistance, the variation of the stator flux modulus becomes:

$$\frac{d\psi_{sd}}{dt} = v_{sd} \tag{IV.14}$$

From equation (IV.14), we find that the change in the stator flux magnitude is proportional to the stator voltage radial component, i.e., when an active voltage vector is applied, the projection of this voltage on the flux axis allows its magnitude variation [27].

If a zero voltage sequence is applied, we find that the variation of the stator flux magnitude is zero.

$$\frac{d\psi_{sd}}{dt} = 0 \tag{IV.15}$$

We can see in figure (IV.7) that the vectors (V_1 , V_2 , V_6) have a positive radial component V_{sd} , this means that these vectors increase the stator flux magnitude. On the other hand the vectors (V_3 , V_4 , V_5) have a negative radial component V_{sd} which has the effect of reducing the stator flux magnitude [28].

Figure (IV.8) shows two situations of the stator flux variation, when two different voltages are applied.

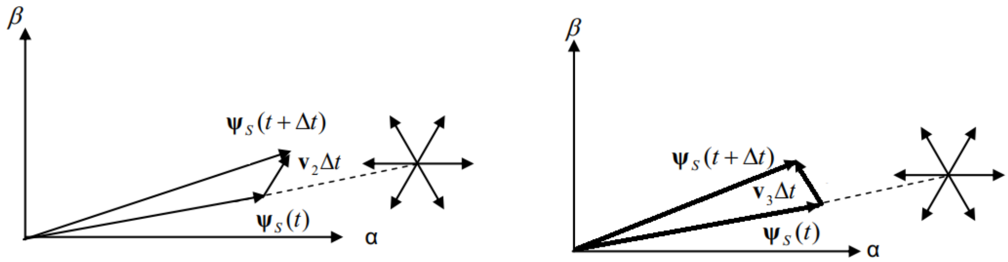

Figure IV. 8: Evolution of stator flux vector in terms of an applied voltage vector.

IV.3.3 The electromagnetic torque evolution rule

The torque is expressed by [26]:

$$T_e = K_t^{'}\left(\mathbf{\Psi_s} \times \mathbf{\Psi_r}\right) = K_t^{'} \cdot \left|\mathbf{\Psi_s}\right| \cdot \left|\mathbf{\Psi_r}\right| \cdot \sin\delta \tag{IV.16}$$

With:

$$K_t' = p\frac{3}{2}\frac{L_m}{\sigma L_s L_r} \tag{IV.17}$$

$|\psi_s|$: Stator flux magnitude.

$|\psi_r|$: Rotor flux magnitude.

δ: Angle between the stator flux and rotor flux vectors, figure IV.9.

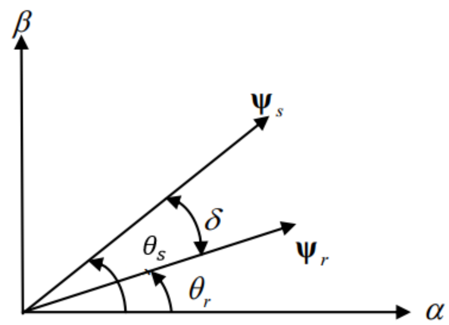

Figure IV. 9: angle δ illustration.

We can immediately see that the torque depends, on the magnitude of the two vectors ψ_s and ψ_r as well as on the angle δ.

Assuming that the stator flux is maintained within a predetermined hysteresis band, this allows us to assume that, it follows its reference ($\psi_s = \psi_{sref}$), and that the rotor flux evolution is slow compared to that of the stator flux [29], the expression (IV.16) now becomes:

$$T_e = K_t' \cdot |\mathbf{\Psi}_{\text{sref}}| \cdot |\mathbf{\Psi}_{\mathbf{r}}| \cdot \sin(\delta + \Delta\delta) \tag{IV.18}$$

Figure IV.10 illustrates the evolution of the angle δ, for two different voltage vectors.

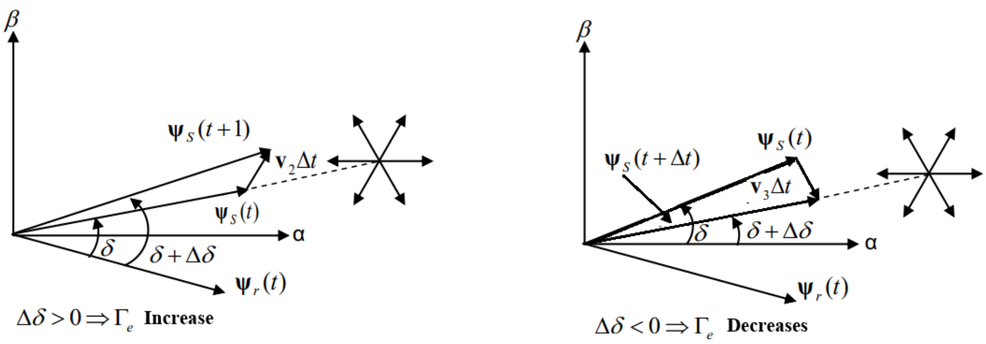

Figure IV. 10: Evolution of the angle in terms of applied voltage vector.

Therefore, to fix the stator flux magnitude, it is necessary to impose a circular trajectory at the end of the flux vector. For this, the applied voltage vector must always be perpendicular to the flux vector. However, as there are only eight possible voltage vectors, two of which are zero, this results in the stator flux, by the radial component application, which acts on the stator flux magnitude, and of a transverse component, which acts on the angular difference between the stator and rotor fluxes, thus on the torque.

The vectors (V_2 , V_3 , V_4) have a positive transverse component, so it is these vectors that increase the torque more or less depending on the speed and the flux phase. On the other hand, the vectors (V_5 , V_6 , V_1) have a negative transverse component that enables the torque to be decreased. The application of zero vectors amounts to blocking the position of the stator flux vector for a duration corresponding to the control period, while the rotor flux vector is continuing its course according to its inertia, thus catching up with the stator flux vector [30]. Therefore, the action obtained is a decrease in torque while maintaining the stator flux magnitude unchanged if the speed is positive and an increase in torque if it is negative.

IV.3.4 Stator flux hysteresis controller

In order to achieve adequate dynamic performance, the two-level hysteresis controller is the simplest and most suitable solution for direct torque control. The hysteresis band is used to evaluate the flux error where the flux controller's output is given by the logical variable d_φ[0, 1], indicating the overshoot and undershoot of the flux's magnitude [31].

Thus, by using the following equation, the two-level hysteresis comparator enables the detection of the control band overshoots [32]:

$$e_\psi = \left|\psi_s^* - \hat{\psi}_s\right| < \Delta H_\psi \tag{IV.19}$$

Where ΔH_ψ is the hysteresis band of the controller.

The sign error between the reference flux ψ_s^* and the estimated flux $\hat{\psi}_s$ defines which voltage vector should be used.

$$\begin{cases} d_\varphi = 1 & for \quad e_\varphi > \Delta H_\varphi \\ d_\varphi = 0 & for \quad e_\varphi < \Delta H_\varphi \end{cases} \tag{IV.20}$$

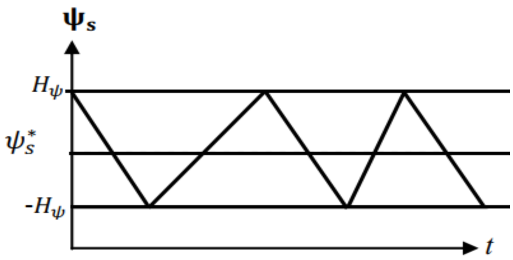

Figure IV. 11: Magnitude flux evolution.

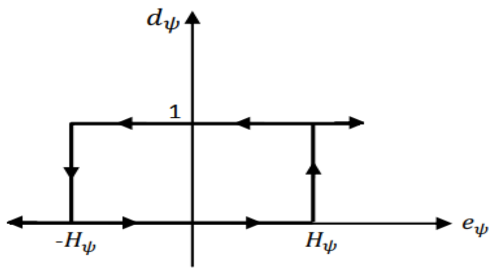

Figure IV. 12: Two-level hysteresis controller.

IV.3.5 Electromagnetic torque hysteresis controller

IV.3.5 .1 Two-level hysteresis comparator

This controller is identical to that used for stator flux magnitude control. It only enables torque control in one rotational direction. Therefore, only the vectors V_{i+1} and V_{i+2}can be chosen to cause the flux to evolve. As a result, the torque decrease is only achieved by the null vector selection [33].

With this corrector, it is necessary to cross two machine phases in order to reverse the machine's rotational direction [34] [35]. However, this controller is easier to implement.

IV.3.5 .2 Three-level hysteresis comparator

It allows the motor to be controlled in both rotational directions, either for positive or negative torque, figure (IV.13) [36]. The corrector output, represented by the boolean variable tc indicates directly whether the torque magnitude must be increased in absolute value, i.e. $tc = 1$ for a positive setpoint and $tc = -1$ for a negative setpoint, or decreased $tc = 0$.

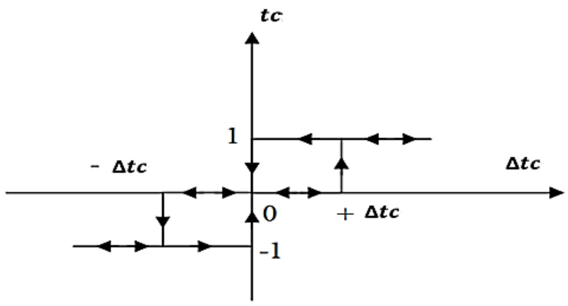

Figure IV. 13: Three-level hysteresis torque comparator.

Three-level comparator allows operation in all four quadrants without requiring structural modifications [37].

IV.3.6 Speed regulation in DTC control

DTC of the induction motor has the ability to operate without a speed control loop [38]. Therefore, it does not require information on the rotation speed. This can classify the DTC as a speed sensorless control for many industrial applications. On the other hand, since many applications necessitate speed control, the speed regulation loop is required.

Rotation speed regulation typically involves the use of proportional-integral (PI) controllers [39]. It is performed by comparing the reference value and the actual measured value of the rotational speed. Then the comparison error becomes the input of the PI controller, which has calculated gains. The most common approach for calculating these gains is pole placement [40].

The dynamic equation and the transfer function using the speed loop's Laplace transform are given as follows [41]:

$$J\frac{\mathrm{d}\Omega}{\mathrm{dt}} = \mathrm{T_e} - \mathrm{T_r} - \mathrm{f_v}\Omega \tag{IV.21}$$

$$G_\Omega(s) = \frac{\Omega(s)}{\mathrm{T_e}(s) - \mathrm{T_r}(s)} = \frac{1}{Js + \mathrm{f_v}} \tag{IV.22}$$

The transfer function of the PI controller is defined by:

$$PI = K_p s + \frac{K_i}{s} \tag{IV.23}$$

Where:

k_p: The proportional gain of the PI controller.

k_i: The integral gain of the PI controller.

S: The Laplace operator.

Figure (IV.14) shows the operating principle diagram of the speed control loop:

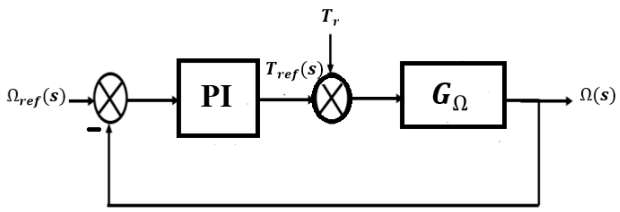

Figure IV. 14: Block diagram of the regulation speed.

Taking into account that the load torque is a perturbation. The open loop speed control's global transfer function has now become:

$$G_\Omega(s) = \frac{1}{js+f_v}\left(K_p s + \frac{K_i}{s}\right) \tag{IV.24}$$

The transfer function in a closed loop is as follows:

$$G_\Omega(s) = \frac{\Omega(s)}{\Omega^*(s)} = \frac{K_p s + K_i}{Js^2 + \left(K_p + \mathrm{f_v}\right)s + K_i} \tag{IV.25}$$

By member-to-member identification, the canonical form of the second-order system given in (IV.23) is used as the denominator of the equations (IV.24), which are as follows:

$$G(s) = \frac{1}{s^2 + 2\xi\omega_n s + \omega_n^2} \tag{III.26}$$

Where:

ω_n: Natural frequency.

ξ : The damping coefficient is usually equal to 1 in gains calculations.

We obtain:

$$\begin{cases} \dfrac{J}{K_i} = \dfrac{1}{\omega_n^2} \\ \dfrac{K_p + \mathrm{f_v}}{J} = 2\xi\omega_n \end{cases} \tag{IV.27}$$

IV.3.7 Control of stator flux with PI controller

Figure (IV.15) shows the block diagram of an induction motor that is simplified and doesn't include the rotor equation, on the $d - q$ frame where the stator flux is orientated.

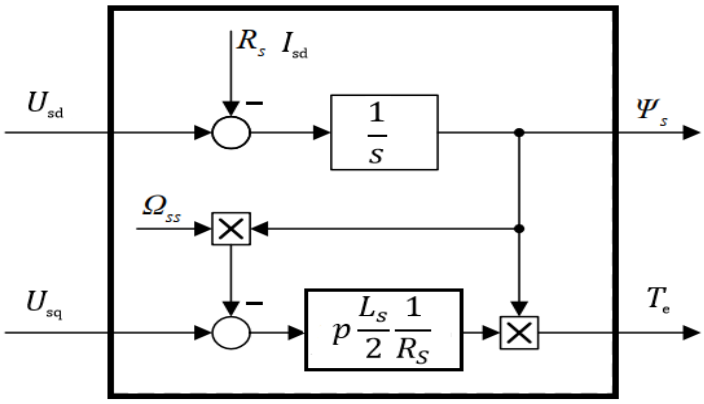

Figure IV. 15: Simple block diagram of induction motor.

The literature [42, 43, 44] proposes various control structures based on the aforementioned induction motor model. One of them is a technique that used two PI controllers shown in figure (IV.2).

The flux and torque control loops for the technique shown in figure (IV.2) are presented in figure (IV.16) by taking into account a straightforward model of IM (figure IV.15). The IM model is illustrated in Fig. IV.16 by the bold line.

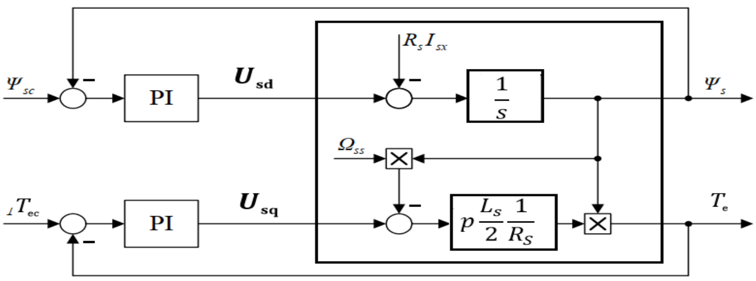

Figure IV. 16: Induction motor control loops with two PI controllers.

The PI controller's transfer function is given as follows:

$$G_R(s) = \frac{U(s)}{E(s)} = K_p\left(1 + \frac{1}{sT_i}\right) = K_p\frac{1+sT_i}{sT_i} \tag{IV.28}$$

Where:

K_p: Proportional gain.

T_i: Controller integrating time.

The figure below represents the PI controller scheme.

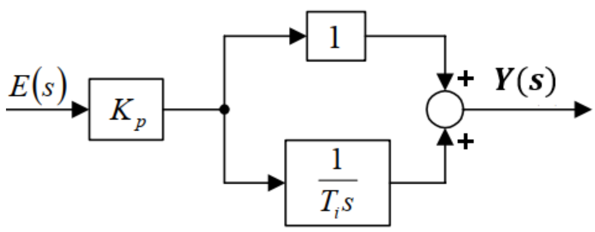

Figure IV. 17: PI controller's block diagram.

Figure (IV.18) illustrates the flux control loop's block diagram. The model shown in figure

(IV.16) serves as the foundation for this control loop. The voltage drop across the stator resistance is ignored [45]. In the stator flux control loop, the inverter delay is taken into consideration.

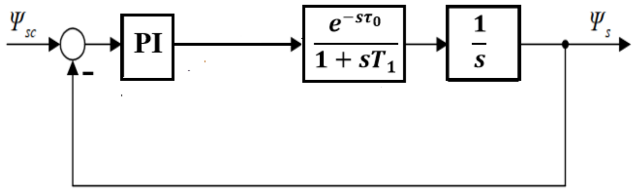

Figure IV. 18: Control loops of the stator flux magnitude.

The symmetry criterion can be used for flux controller parameter design [46]. The plant transfer function can be expressed as follows in compliance with the symmetry criterion:

$$G(s) = \frac{e^{-s\tau_0}}{s(1+sT_1)} \tag{IV.29}$$

Where:

τ_0: The inverter's dead time.

T_1: Sum of small time constants.

The following formulas can be used to get the ideal controller parameters [50]:

$$K_{p\psi} = \frac{1}{2(T_1+\tau_0)} = \frac{1}{2T_s} \tag{IV.30}$$

$$T_{i\psi} = 4(T_1+\tau_0) = 4T_s \tag{IV.31}$$

By taking $T_1 = T_s$ and $\tau_0 = 0$, we obtain the values shown in the following table:

Table IV. 1: Determining the flux controller parameters.

T_s	$K_{p\psi}$	$T_{i\psi}$
10^{-4}	5000	0.00040
$2 * 10^{-4}$	2500	0.0008

IV.3.8 Control of electromagnetic torque with PI controller [47] [48] [49]

Based on the model presented in figure (IV.16), figure (IV.19) depicts the schematic diagram of the torque control loop.

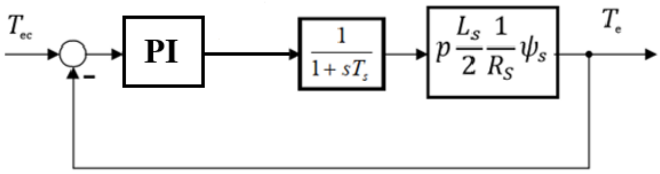

Figure IV. 19: Control loops of the torque.

In this situation, we use Ziegler Nichols tuning method to find the parameter of the torque controller. Starting with the initial values [51] [52] [53], such as $K_p = K_{pm} = 1$ and $T_i = 4T_s$.

Finally, we obtain the values shown in the following table:

Table IV. 2: Determining the torque controller parameters.

T_s	K_p	T_i
10^{-4}	20	0.0004
$2 * 10^{-4}$	12	0.0008

IV.3.10 Control of speed with FOPI controller [57] [58] [59]

The FO-PI controller is based on the same principles as a classic PI controller, except that in this case the control action is calculated using fractional order integrals, where α denotes the fractional order, which is a real number $\alpha \in (0,1)$ [54] [55].

The Control loop of speed with the FOPI controller is shown in figure (IV.20).

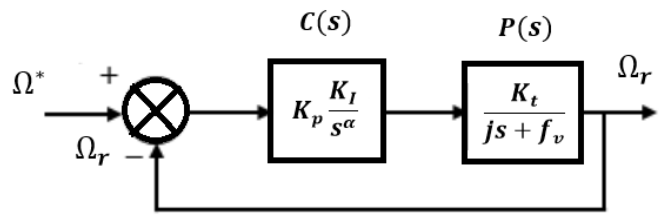

Figure IV. 20: Rotor speed control loops.

Here, we have taken into account the three specifications proposed to ensure the system's stability and robustness, which are [84], [85], [86]:

- The robustness of plant gain variation requires that the phase derivative with respect to frequency be zero, i.e., the Bode phase plot should be flat at the gain crossover frequency. it means that the system is more robust to get changes and the response overshoots are almost the same.

- The specification of gain crossover frequency:

$$|G(j\omega_c)|_{dB} = |C(j\omega_c)P(j\omega_c)|_{dB} = 0 \quad \text{(IV.32)}$$

-The phase margin specification:

$$\text{Arg}[G(j\omega_c)] = \text{Arg}[C(j\omega_c)P(j\omega_c)] = -\pi + \phi_m \quad \text{(IV.33)}$$

The equation $G(s)$ is the open-loop transfer function of the FO-PI controller design for induction motor speed control, shown by the block diagram in figure (IV.20), given by [56]:

$$G(s) = C(s)P(s) = \left(K_P + \frac{K_I}{s^\alpha}\right)\left(\frac{K_t}{js + f_v}\right) \quad \text{(IV.34)}$$

Where:

$$\begin{cases} P(s) = \left(\dfrac{K_t}{Js + f_v} \right) = \left(\dfrac{K}{T_m s + 1} \right) \\ C(s) = K_P + \dfrac{K_I}{s^\alpha} \end{cases} \tag{IV.35}$$

Where:

$K = \frac{K_t}{f_v}$ and $T_m = \frac{j}{f_v}$ the mechanical time constant.

Depending on the phase and gain of the FOPI controller, the open-loop frequency response $G(j\omega)$ is as follows:

$$G(j\omega) = C(j\omega) P(j\omega) \tag{IV.35}$$

With the phase and gain of the $G(s)$ are as follows:

$$C(j\omega) = K_P + K_I (j\omega)^{-\alpha} = K_P + K_I \omega^{-\alpha} \cos\left(\alpha \frac{\pi}{2}\right) - jK_I \omega^{-\alpha} \sin\left(\alpha \frac{\pi}{2}\right) \tag{IV.36}$$

$$\arg[C(j\omega)] = -\tan^{-1}\left(\frac{K_I \omega^{-\alpha} \sin\left(\alpha \frac{\pi}{2}\right)}{K_P + K_I \omega^{-\alpha} \cos\left(\alpha \frac{\pi}{2}\right)} \right) \tag{IV.37}$$

$$|C(j\omega)| = \sqrt{\left(K_P + K_I \omega^{-\alpha} \cos\left(\alpha \frac{\pi}{2}\right)\right)^2 + \left(K_I \omega^{-\alpha} \sin\left(\alpha \frac{\pi}{2}\right)\right)^2} \tag{IV.38}$$

The phase and the gain of the $P(s)$ are as follows:

$$P(j\omega) = \frac{K}{T_m (j\omega)^\alpha + 1} = \frac{K}{\left[1 + T_m \omega^\alpha \cos\left(\alpha \frac{\pi}{2}\right)\right] + jT_m \omega^\alpha \sin\left(\alpha \frac{\pi}{2}\right)} \tag{IV.39}$$

$$\arg[P(j\omega)] = -\tan^{-1}\left(\frac{T_m \omega^\alpha \sin\left(\alpha \frac{\pi}{2}\right)}{1 + T_m \omega^\alpha \cos\left(\alpha \frac{\pi}{2}\right)} \right) \tag{IV.40}$$

$$|P(j\omega)| = \frac{K}{\sqrt{\left(1 + T_m \omega^\alpha \cos\left(\alpha_{\frac{\pi}{2}}\right)\right)^2 + \left(T_m \omega^\alpha \sin\left(\alpha^{\frac{\pi}{2}}\right)\right)^2}} \tag{IV.41}$$

The phase of $G(j\omega)$ of (IV.35) can be expressed as follows:

$$\arg\left[G(j\omega_c)\right] = -\tan^{-1}\left(\frac{K_I \omega_c^{-\alpha} \sin\left(\alpha \frac{\pi}{2}\right)}{K_P + K_I \omega_c^{-\alpha} \cos\left(\alpha \frac{\pi}{2}\right)} \right) - \tan^{-1}\left(\frac{T_m \omega_c^{-\alpha} \sin\left(\alpha \frac{\pi}{2}\right)}{1 + T_m \omega_c^{-\alpha} \cos\left(\alpha \frac{\pi}{2}\right)} \right) = -\pi + \phi_m \tag{IV.42}$$

Where: ω_c and ϕ_m are desired cutoff frequency and phase margin respectively.

From (IV.42), the relation between K_I and α can be established as follows:

$$K_I = -\frac{D}{\omega_c^{-\alpha}\sin\left(\alpha\frac{\pi}{2}\right)+\omega_c^{-\alpha}\cos\left(\alpha\frac{\pi}{2}\right)D} \tag{IV.43}$$

Where:

$$D = \tan\left[\tan^{-1}\left(\frac{T_m\omega_c^{-\alpha}\sin\left(\alpha\frac{\pi}{2}\right)}{1+T_m\omega_c^{-\alpha}\cos\left(\alpha\frac{\pi}{2}\right)}\right)+\phi_m\right] \tag{IV.44}$$

The plant variation is obtained as follows:

$$\left(\frac{d\left(\arg\left(G\left(j\omega_c\right)\right)\right)}{d\omega}\right)_{\omega=\omega_c} = \left(\frac{K_I\alpha\omega_c^{\alpha-1}\sin\left(\alpha\frac{\pi}{2}\right)}{\omega_c^{2\alpha}+2K_I\omega_c^{\alpha}\cos\left(\alpha\frac{\pi}{2}\right)+K_I^2}\right)-E=0 \tag{IV.45}$$

Where:

$$E=\frac{T_m\alpha\omega_c^{\alpha-1}\left[\left(1+T_m\omega_c^{-\alpha}\cos\left(\alpha\frac{\pi}{2}\right)\right)\sin\left(\alpha\frac{\pi}{2}\right)-\left(T_m\omega_c^{-\alpha}\sin\left(\alpha\frac{\pi}{2}\right)\right)\cos\left(\alpha\frac{\pi}{2}\right)\right]}{\left(1+T_m\omega_c^{-\alpha}\cos\left(\alpha\frac{\pi}{2}\right)\right)^2+\left(T_m\omega_c^{-\alpha}\sin\left(\alpha\frac{\pi}{2}\right)\right)^2} \tag{IV.46}$$

From (IV.45), we can establish an equation about α and K_I in the following form,

$$K_I=\frac{-F\pm\sqrt{F^2-4E^2\omega_c^{-2\alpha}}}{2E\omega_c^{-2\alpha}} \tag{IV.47}$$

Where:

$$F=E\omega_c^{-\alpha}\cos\left(\alpha\frac{\pi}{2}\right)-\alpha\omega_c^{\alpha-1}\sin\left(\alpha\frac{\pi}{2}\right) \tag{IV.48}$$

K_p is obtained as follow:

$$|G(j\omega_c)|_{dB}=|C(j\omega_c)P(j\omega_c)|_{dB}=1 \tag{IV.49}$$

$$|G(j\omega_c)|_{dB}=\frac{K_P\sqrt{\left(1+K_I\omega_c^{-\alpha}\cos\left(\alpha\frac{\pi}{2}\right)\right)^2+\left(K_I\omega_c^{-\alpha}\sin\left(\alpha\frac{\pi}{2}\right)\right)^2}}{\sqrt{\left(1+T_m\omega_c^{\alpha}\cos\left(\alpha_{\frac{\pi}{2}}\right)\right)^2+\left(T_m\omega_c^{\alpha}\sin\left(\alpha^{\frac{\pi}{2}}\right)\right)^2}}=1 \tag{IV.50}$$

$$K_P=\sqrt{\frac{\left(1+T_m\omega_c^{\alpha}\cos\left(\alpha\frac{\pi}{2}\right)\right)^2+\left(T_m\omega_c^{\alpha}\sin\left(\alpha\frac{\pi}{2}\right)\right)^2}{\left(1+K_I\omega_c^{-\alpha}\cos\left(\alpha\frac{\pi}{2}\right)\right)^2+\left(K_I\omega_c^{-\alpha}\sin\left(\alpha\frac{\pi}{2}\right)\right)^2}} \tag{IV.51}$$

It is clear that equations (IV.48), (IV.49) and (IV.51) allow us to observe that α, K_P and K_I can be obtained together.

IV.3.11 Control of speed with fuzzy logic controller

IV.3.11.1 Fuzzy logic concept

Fuzzy logic is a technique used in artificial intelligence. It mirrored the empirical behavior of the human brain by appearing as a precise logic substitute. Prof. Lotfi A. Zadeh at the University of California, defined fuzzy logic's theoretical foundations in 1965 [60].

Then it was Mr. Mamdani's turn to try it out by incorporating it into the regulation of industrial operations (such as the steam engine regulation) in 1974 [61]. Fuzzy logic has been used since 1985 in numerous industries, including automation, robotics, road traffic management, air traffic control, and environmental protection (meteorology, climatology, seismology).

IV.3.11.2 Fuzzy Logic Control (FLC) Properties

In general, fuzzy logic controllers are typically used when a system's nonlinearity makes mathematical modeling of the system extremely challenging [62]. We can cite some of FLC's properties [63]:

- Accurate identification of system parameters.
- Under precisely defined conditions, the system behaves in a confusing characteristic.
- The system is described in a linguistic form but not in its analytical form.
- The conditions themselves are ambiguous.

IV.3.11.3 General Theory of fuzzy logic

Boolean set vs fuzzy set [64]

Let A be both a generic component of X and an object space (also known as the discourse universe or the universal set). A classical set A (A is a subset of X), is defined as a collection of elements or objects, so each may or may not belong to set A. By defining a characteristic function for each element of X, we can represent the classical set A by a set of ordered pairs $(x;\ 0)$ or $(x;\ 1)$ which respectively indicate $x \in A$ or $x \notin A$

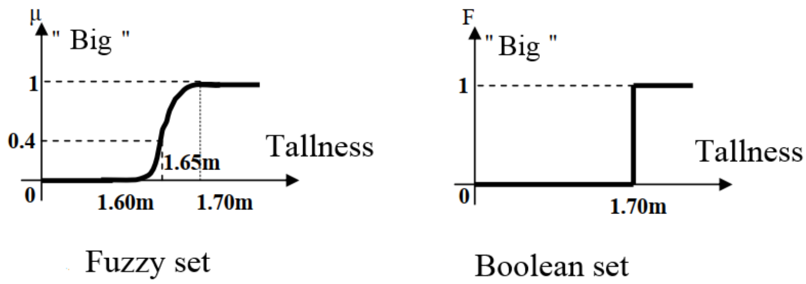

Figure IV. 21: Example of classical set and fuzzy set.

Despite being a crucial tool for engineering science, classical sets do not exactly replicate the ambiguous and abstract human ideas' nature (figure IV.21).

The degree to which an element belongs to a set is expressed via a fuzzy set. In other words, a fuzzy set A in X is defined as a set of ordered pairs if X is a collection of objects generally denoted by x:

$$A = \{(x, u_A(x)) | x \in X\} \tag{IV.52}$$

Where:

$u_A(x)$: is the membership function (MF) for the fuzzy set A

Each element of X is mapped to a membership grade (or membership value) between 0 and 1 using the membership function. A is reduced to a classical set, and $u_A(x)$ is the characteristic function of A, if the value of $u_A(x)$ is bounded to 0 or 1.

FUZZY SETS [65]

In traditional set theory, an entity can be classified as either belonging to or not belonging to a set. It is uncommon to come across items whose status is clearly defined in reality though. Where exactly does a tall person differ from a tall person on average, for instance? Professor L. Zadeh based his idea on observations of this nature. He described linguistic concepts of the following types as fuzzy sets: zero, huge, negative and small. These terms can be found in traditional sets as well. However, what differentiates these two set theories comes from the limits of sets. In fuzzy sets, it is allowed for a thing to partially belong to a certain set; this is called the membership degree. In conventional sets, the degree of membership is 0 or 1 whereas in the fuzzy sets theory, the membership degree can vary between 0 and 1 (we then speak of the membership function μ). A simple example of fuzzy sets is the people classification by age into three sets: young, middle, and old [66]. The way to establish this classification is shown in figure (IV.22).

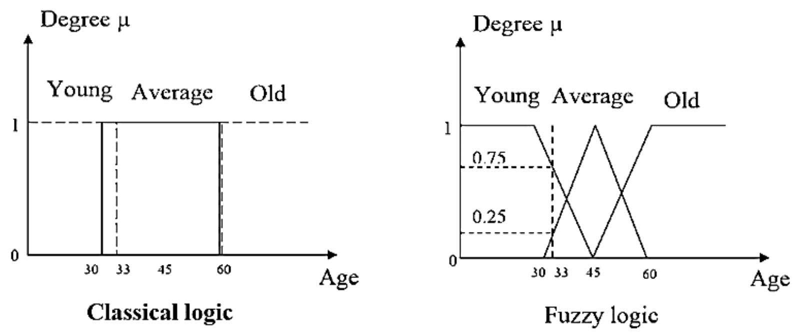

Figure IV. 22: Classification of humans according to their age.

- ✓ **Net variables**

Physical parameters known as "net variables" are those that may be measured with equipment and given a discrete or net value, such as a temperature of 35°C or an output voltage of 6 V.

- ✓ **Linguistic variables**

When the discourse universe is a continuous space, it is typical to divide X into a fuzzy set number whose membership functions roughly cover X. These fuzzy sets, which usually have names conforming to adjectives appearing in our daily linguistic usage, such as “big”, “average” or “small”, are called linguistic values. Therefore, the discourse universe X is often called the linguistic variable.

Theoretical operations of fuzzy sets [67] [68] [69]

The mathematics for this kind of set has been created since fuzzy sets were defined. The mathematics developed is very similar to that related to conventional set theory. The most basic operations on classical sets include: union, intersection, and complement. Additionally, there are standard operations, including addition, subtraction, division, and multiplication of two or more fuzzy sets.

Subset operation

Fuzzy set A is contained in fuzzy set B, in another way, A is a subset of B $(si\, u_A(x): \leq u_B(x))$.

Union operation

The union of two fuzzy sets A and B is another fuzzy set C, written as $C = A \cup B$. Where $C = A\ OR\ B$, where the linked membership function A and B is expressed by:

$$u_C(x) = max(u_A(x), u_B(x)) = u_A(x) \cup u_B(x) \quad \text{(IV.53)}$$

In another way, the union is the smallest fuzzy set containing both A and B.

The intersection operation

The intersection of two fuzzy sets A and B is a fuzzy set C, written as $C = A \cap B$.

Where: $C = A\ AND\ B$, where the linked membership function A and B is expressed by:

$$u_C(x) = min(u_A(x), u_B(x)) = u_A(x) \cap u_B(x) \quad \text{(IV.54)}$$

The intersection of A and B is the largest fuzzy set that is contained in A and B.

The following figure illustrates the intersection and union of two fuzzy sets A and B:

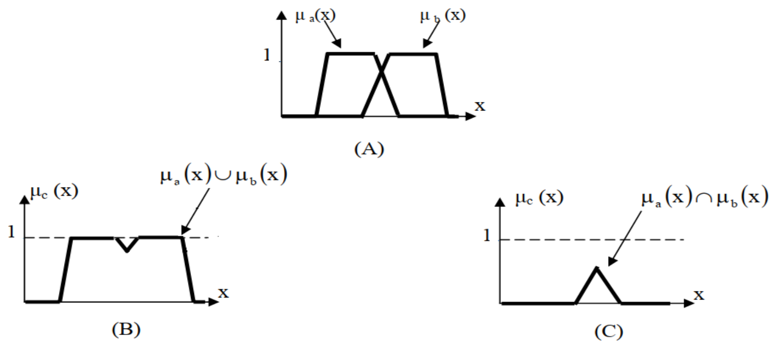

Figure IV. 23: Logical operators: (A) fuzzy sets a and b; (B) fuzzy sets $a \cup b$; (C) fuzzy sets $a \cap b$.

Complement operation

The complement of the fuzzy set A, denoted by $\bar{A}$ (A, $NOT\ A$), is defined as:

$$non(u_A(x)) = u_{\bar{A}}(x) = 1 - u_A(x) \quad \text{(IV.55)}$$

The following figure shows the complement of fuzzy sets A:

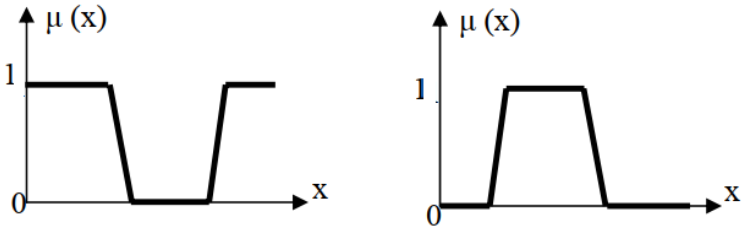

Figure IV. 24: Negation operation.

Membership function representations [70] [71] [72]

Any membership function characterizes the fuzzy set it belongs to completely. A mathematical function can be used to express a membership function in a useful and condensed manner.

Based on their preferences and prior knowledge, designers select a wide range of forms to create the fuzzy membership function. The graphic below illustrates the several classes of frequently employed membership functions:

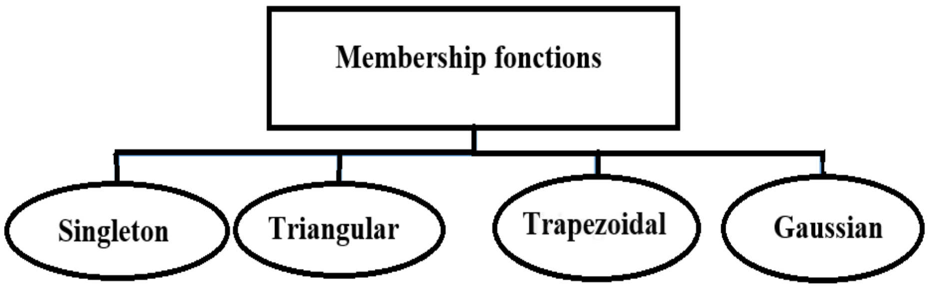

Figure IV. 25: Membership functions.

The diagram's membership functions can be represented as follows:

- **Singleton**

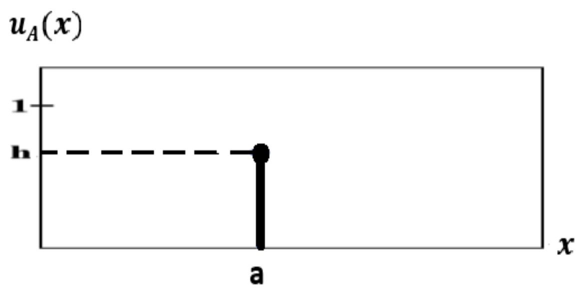

Figure IV. 26: Singleton type membership function.

Where:

$$u_A(x) = \begin{cases} h, x = a \\ 0, x \neq a \end{cases} \quad \text{(IV.56)}$$

❖ **Triangular**

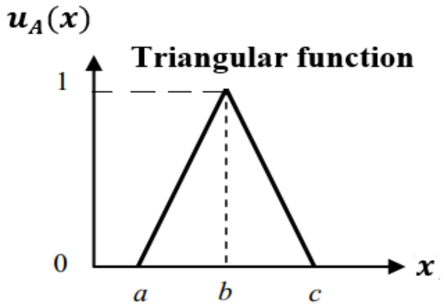

Figure IV. 27: Triangular membership function.

Where:

$$u_A(x) = \begin{cases} \frac{a-x}{a-b}, x \in [a,b] \\ \frac{x-c}{b-c}, x \in [b,c] \end{cases} \quad \text{(IV.57)}$$

❖ **Trapezoidal**

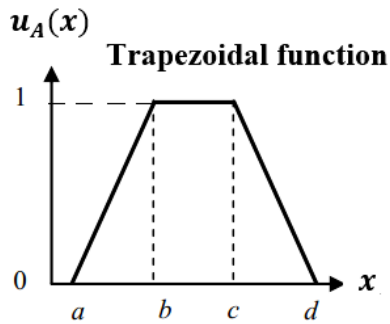

Figure IV. 28: Trapezoidal membership function.

Where**:**

$$u_A(x) = \begin{cases} \frac{x-a}{b-a}, x \in [a,b] \\ 1, \ x \in [b,c] \\ \frac{x-d}{c-d}, x \in [c,d] \end{cases} \quad \text{(IV.58)}$$

❖ **Gaussian**

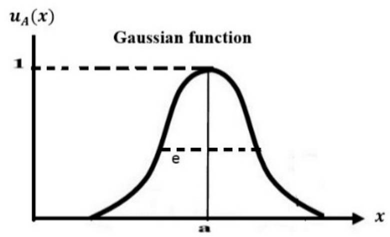

Figure IV. 29: Gaussian membership function.

Where**:**

$$u_A(x) = e^{-(\frac{x-a}{e})^2} \quad \text{(IV.59)}$$

The fuzzy controller's structure

Fuzzy logic controllers (FLCs) are an unusual type of control system that uses a knowledge-based methodology [73]. The FLC is presented as an alternative to conventional control strategies in automatic control systems [74]. The FLC provides linear and non-linear controllers. It offers simple control for several complex nonlinear control actions [74]. This means that it is able to control vague system data such as the absence of the poles and zeros of the system transfer function [75].

Lotfi A. Zadeh (1960) introduced fuzzy theory as an extension of conventional control theory. Fuzzy sets are constructed from elements with varying degrees of membership and are framed in accordance with a system's inaccuracy [75]. In this theory, a DTC-based induction motor drive uses the FLC as a speed regulator to investigate how this control performs better using the fuzzy logic controller [76].

There are basically three essential segments in a fuzzy logic controller:

- **Fuzzification**

Fuzzification consists in defining membership functions for the different physical input variables. This involves assigning to the input variable "crisp" the degrees of membership of its fuzzy sets. The expert operator defines the choice of the fuzzy sets number, the membership functions form, and their distribution over the discourse universe.

- **Inference system**

The following three paradigms make up a fuzzy logic controller's inference system.

1) Rules Base

The expert's knowledge of a given process is transformed into linguistic rules set of the following form:

If premise **then** conclusion

The rules can be represented in a matrix called an inference matrix.

The premise is a set of conditions linked together by fuzzy operators which apply to the membership functions. The most commonly used are: the intersection operator "AND", the union operator "OR", and the negation or complement operator "NOT".

2) Database

It consists of all the defined membership functions that are to be used by the rules.

3) Reasoning mechanism

It performs the inference procedure on the provided rules and data to provide a reasonable result. It is the software codes, which process the rules and body of knowledge according to a particular situation. It exercises a human brain type attribute to methodically perform inference steps for information processing.

- **Defuzzification**

The result obtained from the inference using one of the implication methods is formally a fuzzy value. The latter cannot be used directly to control the process. A transformation must be considered at the inference mechanism output to transform it into a strict quantity. This action is interpreted by the term **defuzzification**. There exist in the literature several solutions which carry out this operation, among them are the maximum value method, the average of the maxima, the center of gravity (barycenter), and the weighted heights.

The most frequently employed technique for fuzzy control is the gravity defuzzification center [81, 82]. It consists in calculating the surface's center of gravity formed by the membership function resulting from the rules aggregation.

If the output variable's membership functions take the shape of rectangles with "singleton" bars, we find a specific situation where "Sugeno's approach" is applicable.

IV.3.11. 4 Fuzzy controller design used for speed control [77] [78] [79] [80]

In our study, we will add a fuzzy controller to the speed regulation loop, which will be used for the DTC control instead of the PI regulator. The fuzzy control tools included in Matlab and the min max decision inference engine of Mamdani were used to create the FLC. The speed error $e(k)$ and the variation of speed error $de(k)$ signals are used as inputs to the speed controller, and an output is taken to provide the electromagnetic torque reference (figure IV.30). The values of these two quantities are expressed by:

$$e(k) = K_e(\Omega^*(k) - \Omega(k)) \qquad \text{(IV.60)}$$

$$de(k) = K_{de}(e(k) - e(k-1))/T_S \qquad \text{(IV.61)}$$

Where: T_S is the sampling period. K_e and $K_{de}$are the normalization gains or scaling factors.

The output quantity causes a variation in electromagnetic torque, and after integration and normalization, this variation produces the reference electromagnetic torque (${T_e}^*$).

Scale factors are very important to adjust fuzzy controller sensitivity and system stability, they allow the normalization of fuzzy controller inputs and output in the universe of speech range [83].

After several trials, the values of the scale factors are set in our study at:

$K_e = 0,3$, $K_{de} = 0,3$ and $K_s = 4$

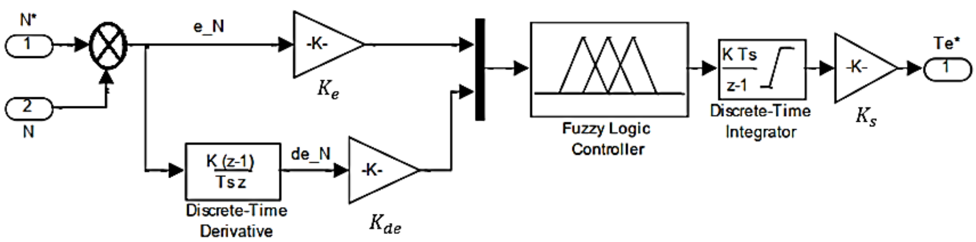

Figure IV. 30: FLC's schematic.

For each error, error change, and torque value, the membership value u_A is evaluated for all membership functions as shown in the following figure.

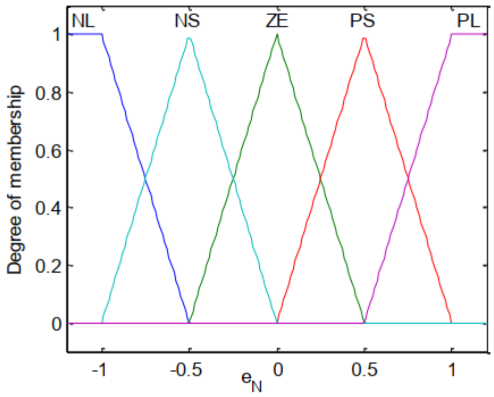

Figure IV. 31: The FLC's membership functions.

The fuzzy variable, which consists of five fuzzy sets, is represented by three triangular membership functions and two trapezoidal membership functions.

The different sets are defined by the following linguistic variables:

- NL : Negative Large.
- NS : Negative Small.
- ZE : Zero.
- PS : Positive Small.
- PL: Positive Large.

This leads to 25 control rules, structured as shown in the following table (Table. IV.2) where the inference method chosen is that of Mamdani:

Table IV. 3: Rules table for speed FLC.

	NL	NS	ZE	PS	PL
NL	NL	NL	NL	NS	ZE
NS	NL	NL	NS	ZE	PS
ZE	NL	NS	ZE	PS	PL
ZE	NS	ZE	PS	PL	PL
PL	ZE	PS	PL	PL	PL

IV.4 Simulation results

This paragraph presents an analysis of the simulation results for various DTC control methods used in this chapter.

The simulation system designed in the Matlab/Simulink environment enabled us to reproduce the behavior of various electrical and mechanical quantities.

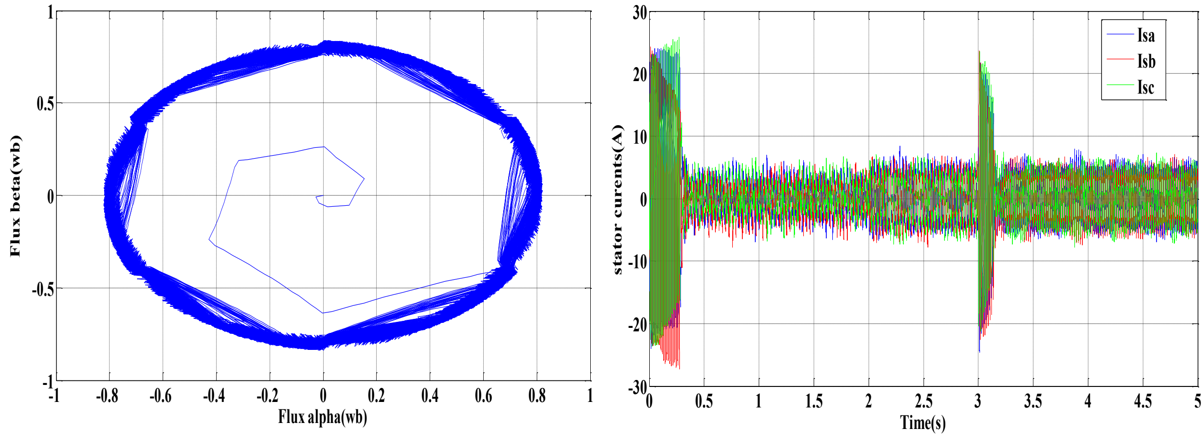

(a) **(b)**

Figure IV. 32: Conventional DTC simulation results: (a) Flux in the (α, β) reference, (b) Stator current

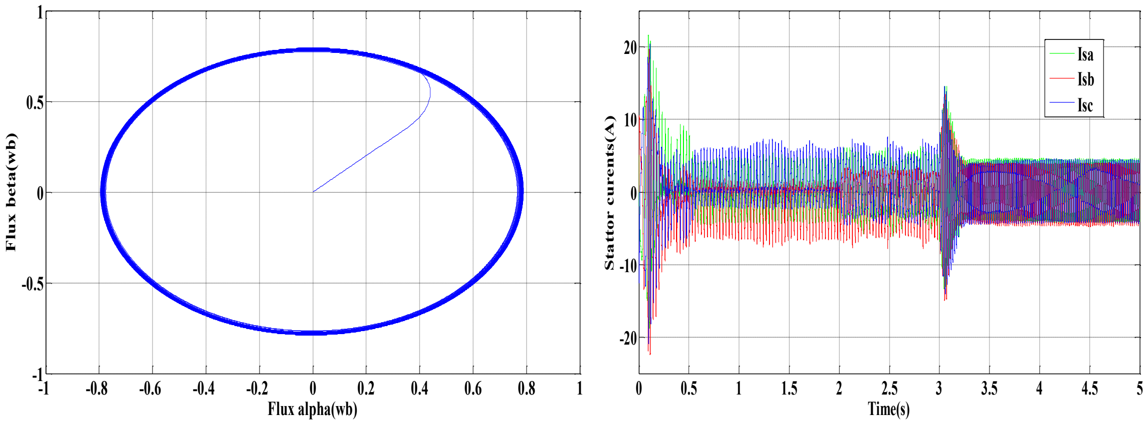

(a) (b)

Figure IV. 33: PI-DTC simulation results: (a) Flux in the (α, β) reference, (b) Stator currents.

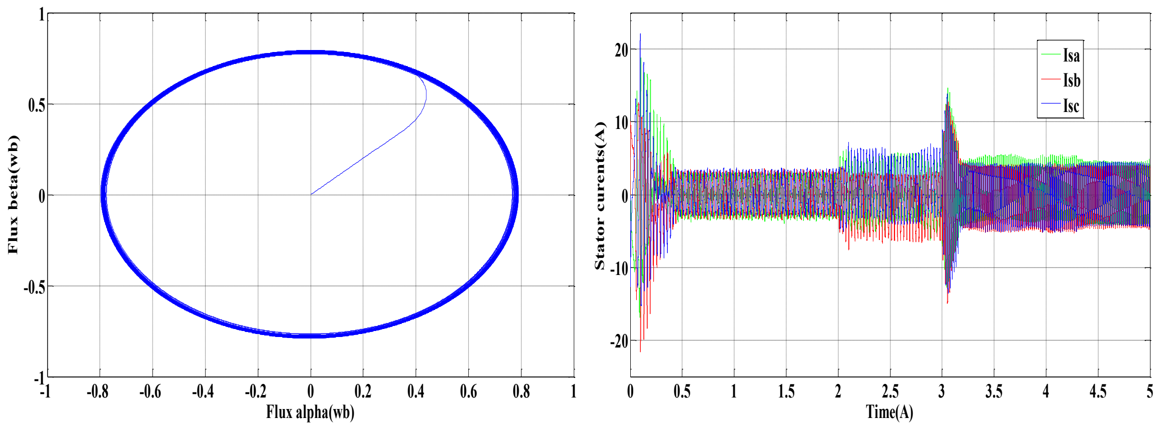

(a) **(b)**

Figure IV. 34: FOPI-DTC simulation results: (a) Flux in the (α, β) reference, (b) Stator currents.

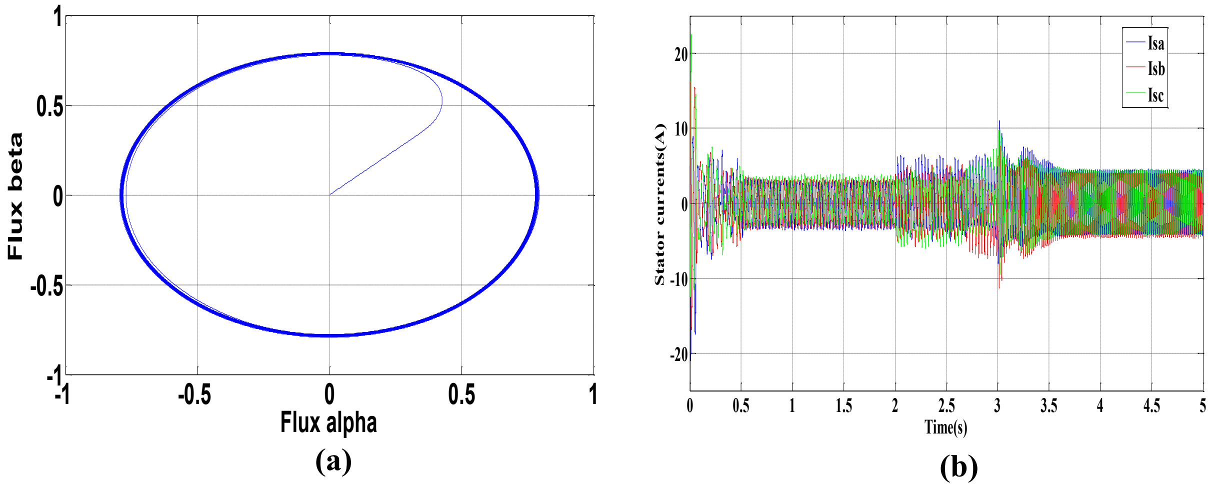

Figure IV. 35: Fuzzy-DTC simulation results: (a) Flux in the (α, β) reference, (b) Stator currents.

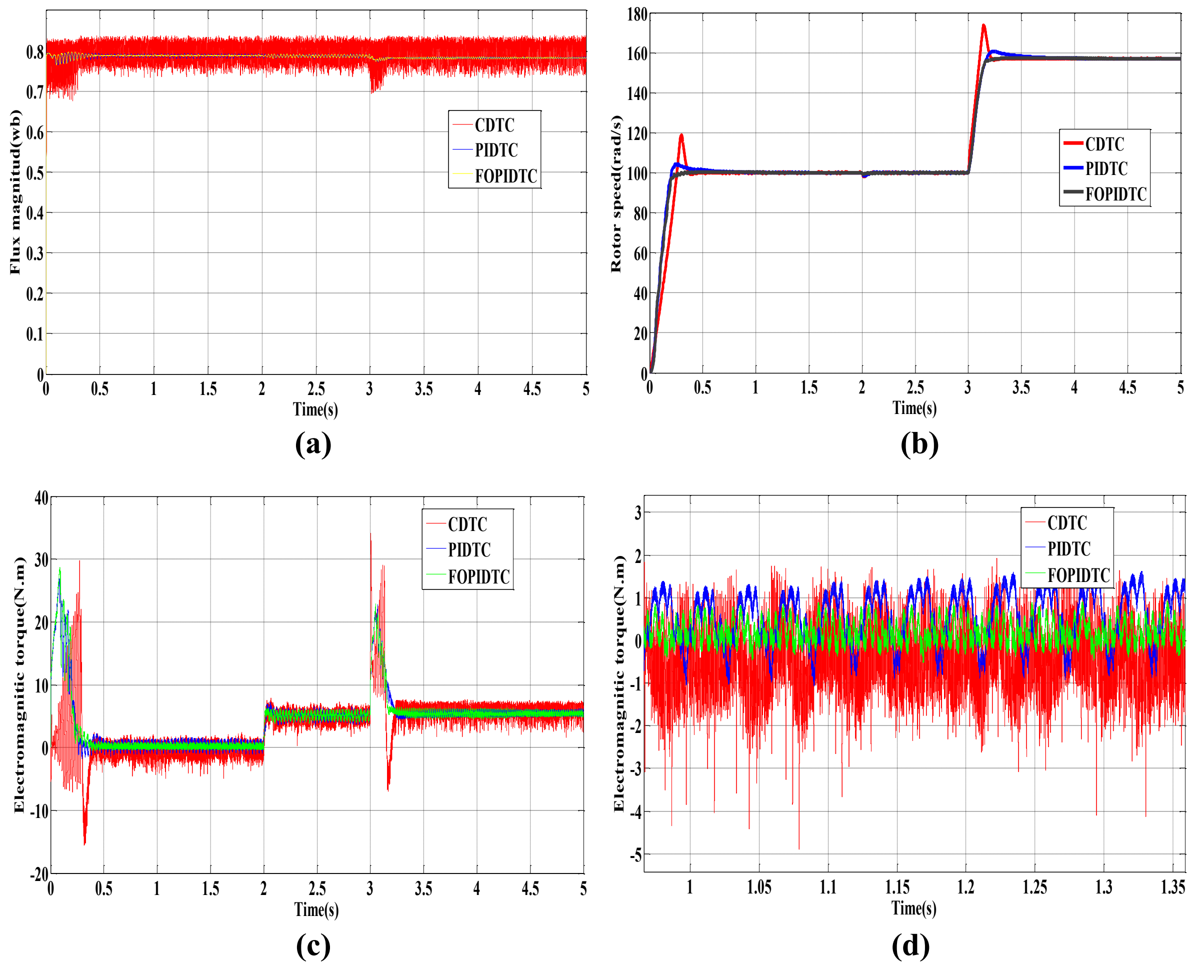

Figure IV. 36: Comparison of DTC simulation results: (a) Flux magnitude, (b) Rotor speed (c) Electromagnetic torque, (d) Zoom in electromagnetic torque

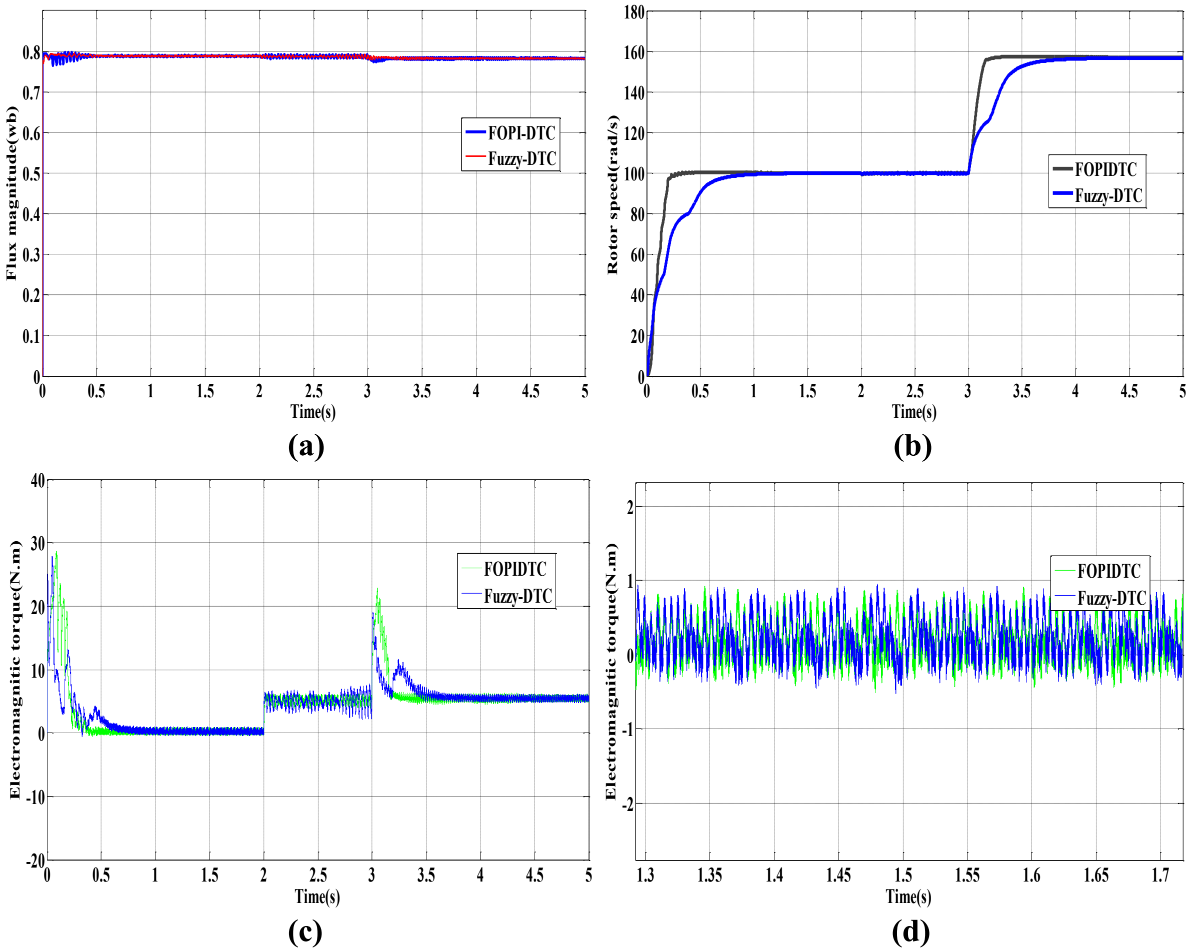

Figure IV. 37: Comparison between Fuzzy-DTC & FOPI -DTC: (a) Flux magnitude, (b) Rotor speed (c) Electromagnetic torque, (d) Zoom in electromagnetic torque

Figures (IV.32), (IV.33), and (IV.34) show the circular trajectory of the stator flux and the stator currents waveforms respectively for: conventional DTC, PI-DTC, FOPI-DTC and Fuzzy-DTC applied to a two-level inverter.

The stator flux modulus reaches the value of 0.8Wb. The plotting of the flux $\varphi_{s\alpha}$ of the direct axis α in terms of the flux $\varphi_{s\beta}$ of the quadratic axis β takes a circle form. However, poor quality for classical DTC compared to PI-DTC and FOPI-DTC control.

Through figures (IV.36) and (IV.37), we realize that the torque perfectly follows the set-point value and remains in the hysteresis band for the classical DTC control. However, ripples appear on the torque time response. For the FOPI-DTC and Fuzzy-DTC control, there is an obvious improvement in the torque quality. We also observe, in the same figure, the speed response at a step of 100 rad for t from 0 to 3 s and 157 rad with $t = 3\ to\ 5\ s$ which shows that the FOPI-DTC control has a high dynamic performance without overshoot at start-up and at the time of the speed variation.

IV.5. Conclusion

In this chapter, we have implemented a classical DTC control strategy that offers an accurate and fast response to the electromagnetic torque and the stator flux. However, the major drawbacks of this control are related to the presence of significant ripples in the torque, and the variation of the switching frequency due to the hysteresis comparator uses. In addition, a nonlinear control approach by FLC, and two linear approaches PI and FOPI have been implemented to control the induction motor’s variable speed. Finally, the simulation results of the DTC control are presented, where we found that these three approaches have made it possible to overcome the problem linked to the classic DTC in terms of robustness vis-à-vis the variations of the parameters of the motor.

References

[1] Toliyat, H. A., & Xu, H. (2000, February). A novel direct torque control (DTC) method for five-phase induction machines. In APEC 2000. Fifteenth Annual IEEE Applied Power Electronics Conference and Exposition (Cat. No. 00CH37058) (Vol. 1, pp. 162-168). IEEE.
[2] Mekrini, Z., & Seddik, B. (2016, September). Control of complex dynamical systems based on Direct Torque Control of an asynchronous machine. In 2016 5th International Conference on Multimedia Computing and Systems (ICMCS) (pp. 537-542). IEEE.
[3] Escalante, M. F., Vannier, J. C., & Arzandé, A. (2002). Flying capacitor multilevel inverters and DTC motor drive applications. IEEE Transactions on Industrial Electronics, 49(4), 809-815.
[4] El Ouanjli, N., Derouich, A., El Ghzizal, A., Motahhir, S., Chebabhi, A., El Mourabit, Y., & Taoussi, M. (2019). Modern improvement techniques of direct torque control for induction motor drives-a review. Protection and Control of Modern Power Systems, 4(1), 1-12.
[5] I. Takahashi, T. Noguchi, "A new quick response and high efficiency control strategy of an induction motor," IEEE Trans.Ind.Appl., vol. IA-22, Sept./Oct. 1986, pp. 820–827.
[6] Ismail El Hassan, "Commande haute Performance d'un moteur asynchrone sans capteur de vitesse par control directe du couple", Thèse de Doctorat, INP de Toulouse 1999.
[7] Kumar, A., Fernandes, B. G., & Chatterjee, K. (2004, November). Simplified SVPWM-DTC of 3-phase induction motor using the concept of imaginary switching times. In 30th Annual Conference of IEEE Industrial Electronics Society, 2004. IECON 2004 (Vol. 1, pp. 341-346). IEEE.
[8] Campos, R. D. F., de Oliveira, J., Marques, L. C. D. S., Nied, A., & Seleme, S. I. (2007, May). SVPWM-DTC strategy for single-phase induction motor control. In 2007 IEEE International Electric Machines & Drives Conference (Vol. 2, pp. 1220-1225). IEEE.
[9] Zhao, Y. T., Liu, Y. C., & Ren, J. J. (2012). Study on direct torque control applied in the electrical propulsion ship. In Advanced Materials Research (Vol. 354, pp. 1252-1256). Trans Tech Publications Ltd.
[10] Inan, R., & Demir, R. (2019, June). Improved speed-sensorless input/output linearisation-based SVPWM-DTC of IM. In 2019 1st Global Power, Energy and Communication Conference (GPECOM) (pp. 222-226). IEEE.
[11] Zheng, Z., Xue, X., & Xu, B. (2011, September). Direct torque control of asynchronous motor based on space vector modulation. In 2011 International Conference on Electronics, Communications and Control (ICECC) (pp. 1440-1443). IEEE.
[12] Kumar, V., & Rao, S. S. (2010, November). Reduction of torque ripple in direct torque control of induction motor using constant switching frequency operation. In 7th Mediterranean Conference and Exhibition on Power Generation, Transmission, Distribution and Energy Conversion (MedPower 2010) (pp. 1-6). IET.
[13] Ponce, H., Ibarra, L., Ponce, P., & Molina, A. (2014). A novel artificial hydrocarbon networks based space vector pulse width modulation controller for induction motors. American Journal of Applied Sciences, 11(5), 789.
[14] Arafa, O. M., Wahsh, S. A., Badr, M., & Yassin, A. (2020). Grey wolf optimizer algorithm based real time implementation of PIDDTC and FDTC of PMSM. International Journal of Power Electronics and Drive Systems, 11(3), 1640.
[15] Chandra Sekhar, O., Lakhimsetty, S., & Bhat, A. H. (2021). A comparative experimental analysis of fractional order PI controller based direct torque control scheme for induction motor drive. International Transactions on Electrical Energy Systems, 31(1), e12705.
[16] Kasbi, A., & Rahali, A. (2021). Adaptive FOPI controller based on the fuzzy supervisory for wind power conversion system equipped by a doubly fed induction generator. International Transactions on Electrical Energy Systems, 31(8), e12923.
[17] Ahmed, W. A. E. M., Adel, M. M., Taha, M., & Saleh, A. A. (2021). PSO technique applied to sensorless field-oriented control PMSM drive with discretized RL-fractional integral. Alexandria Engineering Journal, 60(4), 4029-4040.
[18] D. M. Kumar, H. K. Mudaliar, M. Cirrincione, U. Mehta, and M. Pucci, "Design of a Fractional Order PI (FOPI) for the Speed Control of a High-Performance Electrical Drivewith an Induction Motor," ICEMS 2018 - 2018 21st Int. Conf. Electr. Mach. Syst., pp.
[19] S. Khojet El Khil "Commande Vectorielle d'une Machine Asynchrone Doublement Alimentée (MADA) ", Thèse de Doctorat, INP de Toulouse 2006.
[20] Descusse, J., & Moog, C. H. (1985). Decoupling with dynamic compensation for strong invertible affine non-

linear systems. International Journal of Control, 42(6), 1387-1398.
[21] Ramón Blasco Giménez "High Performance Sensorless Vector Control of Induction Motor Drives", Thèse de Doctorat Nottingham 1995.
[22] Mihai Comanescu "Flux and Speed Estimation Techniques for Sensorless Control of Induction Motors ", Thèse de Doctorat Université de l'état d'Ohio USA 2005.
[23] Jun Zhang, "Direct Torque Controlled Induction Machines for Integrated Starter/Alternator System", Ph. D thesis, The University of New South Wales, 2006.
[24] Krim, S., Gdaim, S., Mtibaa, A., & Mimouni, M. F. (2019). Contribution of the FPGAs for complex control algorithms: sensorless DTFC with an EKF of an induction motor. International Journal of Automation and Computing, 16(2), 226-237.
[25] Esandi, I., Juankorena, X., Lopez, J., & Marroyo, L. (2009, March). Alternative protection system for wind turbines with doubly fed induction generator. In 2009 International Conference on Power Engineering, Energy and Electrical Drives (pp. 501-506). IEEE.
[26] Leboeuf, N., Boileau, T., Nahid-Mobarakeh, B., Takorabet, N., Meibody-Tabar, F., & Clerc, G. (2015). Effects of imperfect manufacturing process on electromagnetic performance and online interturn fault detection in PMSMs. IEEE transactions on Industrial electronics, 62(6), 3388-3398.
[27] Sandulescu, P., Meinguet, F., Kestelyn, X., Semail, E., & Bruyère, A. (2013). Control strategies for open-end winding drives operating in the flux-weakening region. IEEE Transactions on Power Electronics, 29(9), 4829-4842.
[28] Gao, Y., & Parsa, L. (2007, February). Modified direct torque control of five-phase permanent magnet synchronous motor drives. In APEC 07-Twenty-Second Annual IEEE Applied Power Electronics Conference and Exposition (pp. 1428-1433). IEEE.
[29] Jamel Belhadj, "Commande directe en couple d'une machine asynchrone- Structures d'observation - Application aux systèmes multimachines-multiconvertisseurs" Thèse de Doctorat, Université de Tunis El-Manar, École Nationale d'Ingénieurs de Tunis 2001.
[30] Buja, G. S., & Kazmierkowski, M. P. (2004). Direct torque control of PWM inverter-fed AC motors-a survey. IEEE Transactions on industrial electronics, 51(4), 744-757.
[31] Casadei, D., Grandi, G., Serra, G., & Tani, A. (1994, September). Effects of flux and torque hysteresis band amplitude in direct torque control of induction machines. In Proceedings of IECON'94-20th Annual Conference of IEEE Industrial Electronics (Vol. 1, pp. 299-304). IEEE.
[32] MAHFOUD, S., DEROUICH, A., EL OUANJLI, N. A. J. I. B., & EL MAHFOUD, M. O. H. A. M. M. E. D. (2022). Enhancement of the Direct Torque Control by using Artificial Neuron Network for a Doubly Fed Induction Motor. Intelligent Systems with Applications, 13, 200060.
[33] Casadei, D., Grandi, G., Serra, G., & Tani, A. (1994, September). Effects of flux and torque hysteresis band amplitude in direct torque control of induction machines. In Proceedings of IECON'94-20th Annual Conference of IEEE Industrial Electronics (Vol. 1, pp. 299-304). IEEE.
[34] Kang, J. K., Chung, D. W., & Sul, S. K. (1999, May). Direct torque control of induction machine with variable amplitude control of flux and torque hysteresis bands. In IEEE International Electric Machines and Drives Conference. IEMDC'99. Proceedings (Cat. No. 99EX272) (pp. 640-642). IEEE.
[35] Rekioua, D., & Rekioua, T. (2009, December). DSP-controlled direct torque control of induction machines based on modulated hysteresis control. In 2009 International Conference on Microelectronics-ICM (pp. 378-381). IEEE.
[36] Bıçak, A., & Gelen, A. (2021). Sensorless direct torque control based on seven-level torque hysteresis controller for five-phase IPMSM using a sliding-mode observer. Engineering Science and Technology, an International Journal, 24(5), 1134-1143.
[37] Allirani, S., Lakshmi, N. S., & Vidhya, H. (2020). Performance analysis on direct torque controlled induction motor drive with varying hysteresis controller bandwidth. International Journal of Power Electronics and Drive Systems, 11(3), 1165.
[38] Lee, J. H., Kim, C. G., & Youn, M. J. (2002). A dead-beat type digital controller for the direct torque control of an induction motor. IEEE Transactions on Power Electronics, 17(5), 739-746.
[39] Alsofyani, I. M., & Idris, N. R. N. (2015). Simple flux regulation for improving state estimation at very low and zero speed of a speed sensorless direct torque control of an induction motor. IEEE Transactions on power electronics, 31(4), 3027-3035.

[40] Pragati, A., Ganthia, B. P., & Panigrahi, B. P. (2021). Genetic algorithm optimized direct torque control of mathematically modeled induction motor drive using PI and sliding mode controller. In Recent Advances in Power Electronics and Drives (pp. 351-366). Springer, Singapore.
[41] Tang, Y., & Lin, G. (2010, August). Direct torque control of induction motor based on self-adaptive PI controller. In 2010 5th International Conference on Computer Science & Education (pp. 1230-1234). IEEE.
[42] C. Lascu, I. Boldea, F. Blaabjerg, "Variable-Structure Direct Torque Control-A Class of Fast and Robust Controllers for Induction Machine Drives", IEEE Transactions on Industrial Electronics, Vol. 51, Issue: 4, Aug. 2004, pp.785-792.
[43] Y. Xue, X. Xu, T.G. Habetler, D.M. Divan, "A low cost stator flux oriented voltage source variable speed drive", Conference Record of the 1990 IEEE Industry Applications Society Annual Meeting, Vol.1, 7-12 Oct. 1990, pp.410-415.
[44] Z. Yan, C. Jin, V. Utkin, "Sensorless Sliding-Mode Control of Induction Motors", IEEE Transactions on Industrial Electronics, Vol. 47, Issue: 6, Dec. 2000, pp.1286-1297.
[45] Zemmit, A., Messalti, S., & Harrag, A. (2018). A new improved DTC of doubly fed induction machine using GA-based PI controller. Ain Shams Engineering Journal, 9(4), 1877-1885.
[46] M. P. Kazmierkowski, H. Tunia, "Automatic Control of Converter Fed Drives", ELSEVIER Amsterdam-London-New York-Tokyo, 1994.
[47] Costa, B. L. G., Graciola, C. L., Angélico, B. A., Goedtel, A., & Castoldi, M. F. (2018). Metaheuristics optimization applied to PI controllers tuning of a DTC-SVM drive for three-phase induction motors. Applied Soft Computing, 62, 776-788.
[48] Benbouhenni, H. (2019). Torque ripple reduction of DTC DFIG drive using neural PI regulators. Majlesi Journal of Energy Management, 8(2), 21-26.
[49] Rashag, H. F., Tan, N. M., Koh, S. P., Abdalla, A. N., Chong, K. H., & Tiong, S. K. (2014). DTC-SVM based on PI torque and PI flux controllers to achieve high performance of induction motor. Research Journal of Applied Sciences, Engineering and Technology, 7(4), 875-891.
[50] H. Li, Y. Luo, and Y. Chen, “A fractional order proportional and derivative (FOPD) motion controller: Tuning rule and experiments,” IEEE Trans. Control Syst. Technol., vol. 18, no. 2, pp. 516–520, 2010.
[51] Hägglund, T., & Åström, K. J. (2002). Revisiting the Ziegler-Nichols tuning rules for PI control. Asian Journal of Control, 4(4), 364-380.
[52] Meshram, P. M., & Kanojiya, R. G. (2012, March). Tuning of PID controller using Ziegler-Nichols method for speed control of DC motor. In IEEE-international conference on advances in engineering, science and management (ICAESM-2012) (pp. 117-122). IEEE.
[53] Bhatti, S. A., Malik, S. A., & Daraz, A. (2016, January). Comparison of PI and IP controller by using Ziegler-Nichols tuning method for speed control of DC motor. In 2016 International Conference on Intelligent Systems Engineering (ICISE) (pp. 330-334). IEEE.
[54] Machado, J. A. (2009). Calculation of fractional derivatives of noisy data with genetic algorithms. Nonlinear Dynamics, 57(1), 253-260.
[55] Hamamci, S. E., & Koksal, M. (2010). Calculation of all stabilizing fractional-order PD controllers for integrating time delay systems. Computers & Mathematics with Applications, 59(5), 1621-1629.
[56] Duarte-Mermoud, M. A., Mira, F. J., Pelissier, I. S., & Travieso-Torres, J. C. (2010, June). Evaluation of a fractional order PI controller applied to induction motor speed control. In IEEE ICCA 2010 (pp. 573-577). IEEE.
[57] Kumar, V., Rana, K. P. S., & Mishra, P. (2016). Robust speed control of hybrid electric vehicle using fractional order fuzzy PD and PI controllers in cascade control loop. Journal of the Franklin Institute, 353(8), 1713-1741.
[58] Mosaad, M. I. (2020). Direct power control of SRG-based WECSs using optimised fractional-order PI controller. IET Electric Power Applications, 14(3), 409-417.
[59] Mahvash, H., Taher, S. A., Rahimi, M., & Shahidehpour, M. (2019). Enhancement of DFIG performance at high wind speed using fractional order PI controller in pitch compensation loop. International Journal of Electrical Power & Energy Systems, 104, 259-268.
[60] Zadeh, L. A. (Ed.). (2013). Computing with words in Information/Intelligent systems 1: Foundations (Vol. 33). Physica.
[61] Lv, H., Zhang, S., Sun, Q., Chen, R., & Zhang, W. J. (2021). The dynamic models, control strategies and applications for magnetorheological damping systems: a systematic review. Journal of Vibration Engineering &

Technologies, 9(1), 131-147.
[62] Lewis, F. L., Tim, W. K., Wang, L. Z., & Li, Z. X. (1999). Deadzone compensation in motion control systems using adaptive fuzzy logic control. IEEE Transactions on Control Systems Technology, 7(6), 731-742.
[63] Jager, R. (1995). Fuzzy logic in control. Rene Jager.
[64] Ansari, A. Q. (1998). The basics of fuzzy logic: A tutorial review. COMPUTER EDUCATION-STAFFORD-COMPUTER EDUCATION GROUP-, 88, 5-8.
[65] JERRY M. MENDEL, 'Fuzzy Logic Systems for Engineering: A Tutorial', Procceding of the IEEE, Vol.83, No.3 March 1995.
[66] M. TA Cao « Commande Numérique de Machines Asynchrones par Logique Floue » Thèse de Doctorat, Departement de Génie Electrique et de Génie Informatique, Faculté des Sciences et de Génie Université Laval Québec, 1997.
[67] Chen, G., & Pham, T. T. (2000). Introduction to fuzzy sets, fuzzy logic, and fuzzy control systems. CRC press.
[68] Dubois, D., & Prade, H. (Eds.). (2012). Fundamentals of fuzzy sets (Vol. 7). Springer Science & Business Media.
[69] Ganesh, M. (2006). Introduction to fuzzy sets and fuzzy logic. PHI Learning Pvt. Ltd..
[70] Bai, Y., & Wang, D. (2006). Fundamentals of fuzzy logic control—fuzzy sets, fuzzy rules and defuzzifications. In Advanced fuzzy logic technologies in industrial applications (pp. 17-36). Springer, London.
[71] Sadollah, A. (2018). Introductory chapter: which membership function is appropriate in fuzzy system?. In Fuzzy logic based in optimization methods and control systems and its applications. IntechOpen.
[72] Zadeh, L. A. (1996). Knowledge representation in fuzzy logic. In Fuzzy Sets, Fuzzy Logic, and Fuzzy Systems: Selected Papers by Lotfi a Zadeh (pp. 764-774).
[73] Albertos, P., Sala, A., & Olivares, M. (1998, September). Fuzzy logic controllers. Advantages and drawbacks. In VIII international congress of automatic control (Vol. 3, pp. 833-844). Laxenburg, Austria: International Federation of Automatic Control.
[74] Lee, J. (1993). On methods for improving performance of PI-type fuzzy logic controllers. IEEE transactions on fuzzy systems, 1(4), 298-301.
[75] Guclu, R., & Yazici, H. (2008). Vibration control of a structure with ATMD against earthquake using fuzzy logic controllers. journal of sound and vibration, 318(1-2), 36-49.
[76] Patyra, M. J., Grantner, J. L., & Koster, K. (1996). Digital fuzzy logic controller: design and implementation. IEEE Transactions on Fuzzy Systems, 4(4), 439-459.
[77] Khuntia, S. R., Mohanty, K. B., Panda, S., & Ardil, C. (2009). A comparative study of PI, IP, fuzzy and neuro-fuzzy controllers for speed control of DC motor drive.
[78] Xia, C., Guo, P., Shi, T., & Wang, M. (2004, August). Speed control of brushless DC motor using genetic algorithm based fuzzy controller. In Proceeding of the 2004 International Conference on Intelligent Mechatronics and Automation, Chengdu, China, 3rd edn. A Treatise on Electricity and Magnetism (Vol. 2, pp. 68-73).
[79] Monicka, J. G., Sekhar, N. G., & Kumar, K. R. (2011). Performance evaluation of membership functions on fuzzy logic controlled ac voltage controller for speed control of induction motor drive. International Journal of Computer Applications, 13(5), 8-12.
[80] Oh, W. S., Kim, Y. T., Kim, C. S., Kwon, T. S., & Kim, H. J. (1999, November). Speed control of induction motor using genetic algorithm based fuzzy controller. In IECON'99. Conference Proceedings. 25th Annual Conference of the IEEE Industrial Electronics Society (Cat. No. 99CH37029) (Vol. 2, pp. 625-629). IEEE.
[81] Baghli L., "Contribution à la commande de la machine asynchrone, utilisation de la logique floue, des réseaux de neurones et des algorithmes génétiques", Thèse de Doctorat, Nancy, France, 1999.
[82] Abdelghani El Ougli, "Intégration des techniques floues à la synthèse de contrôleurs adaptatifs ", Thèse de doctorat national, Université Sidi Mohamed Ben Abdellah, Fès, Maroc, 2009.
[83] Leonid Reznik, "Fuzzy Controllers", Butterworth-Heinemann, Newnes, 1997, ISBN: 0 7506 3429 4.
[84] W. Chunyang, F. U. Weicheng, and S. H. I. Yaowu, "Tuning Fractional Order Proportional Integral Differentiation Controller for Fractional Order System," Control Conf. (CCC), 2013 32nd Chinese, vol. 2, pp. 552–555, 2013.
[85] Y. Luo, Y. Q. Chen, C. Y. Wang, and Y. G. Pi, "Tuning fractional order proportional integral controllers for fractional order systems," J. Process Control, vol. 20, no. 7, pp. 823–831, 2010.
[86] Lachtar, S. (2020). Contribution au diagnostic de la machine asynchrone commandée en vue de minimiser les efforts radiaux (Doctoral dissertation, Université Mohamed Khider-Biskra).

General conclusion

General conclusion and future perspectives

The work done in this thesis has focused on improving the classical direct torque control to reduce the torque ripple of an induction machine fed by a voltage inverter. We were particularly interested in the vector modulation technique for direct flux and torque control (DTC-SVPWM). First, the DTFC-SVM method is able to work with a constant frequency of the power converter. This operation is ensured by the use of a vector PWM modulation technique for which, at each modulation period, two active voltage vectors and a zero voltage vector are applied. With this technique, torque and flux oscillations are reduced.

Therefore, to achieve these objectives, we started in the first part with an art state representation, followed by the development of the mathematical model and study of different PWM techniques used for induction machine control. Combining DTC with Space Vector Pulse Width Modulation (SVPWM) is a highly effective technique against torque ripple.

The third part of this thesis was devoted to the different strategies used to estimate the unmeasured quantities of the motor with our proposed estimator.

The last part represents a study on the DTC-SVPWM with different controllers such as; hysteresis controller, PI controller, fuzzy logic, and fractional order PI controllers, and their effects on torque ripple. The simulation and experimental results obtained for these different types of control show a considerable reduction of the ripples on the torque and flux responses for the DTC-SVPWM control, with a two-level inverter, in front of the classical DTC control; which reduces the ripples on the torque and consequently a clear improvement on the current quality.

From perspectives, we can propose the continuity of the following studies:

- ❖ Realization of an experimental bench with the DSP-type microcontroller for the validity of the obtained results for all the controls used.
- ❖ Use the DTC-SVPWM with DSP microcontroller in embedded systems such as electric cars.

Appendix

A.1 Experimental setup's description:

At LEESI laboratory of the University of Adrar, an experimental setup shown in figure A.1 below is used to validate the estimation algorithms, explained in Chapter III.

This experimental setup is built around a dSPACE 1104 signal processor, it contains also:

An induction motor with a tachometer generator for rotor speed measurement, it is powered by a voltage source inverter operating in pulse width modulation based on IGBT transistors, a DC bus current and voltage sensor card is built to safely transmit the analog values to the dSpace card. The latter is connected to a computer containing a software development tool (Real-Time Interface to Simulink RTI1104 7.5), for inputting and debugging algorithms intended for real-time processing.

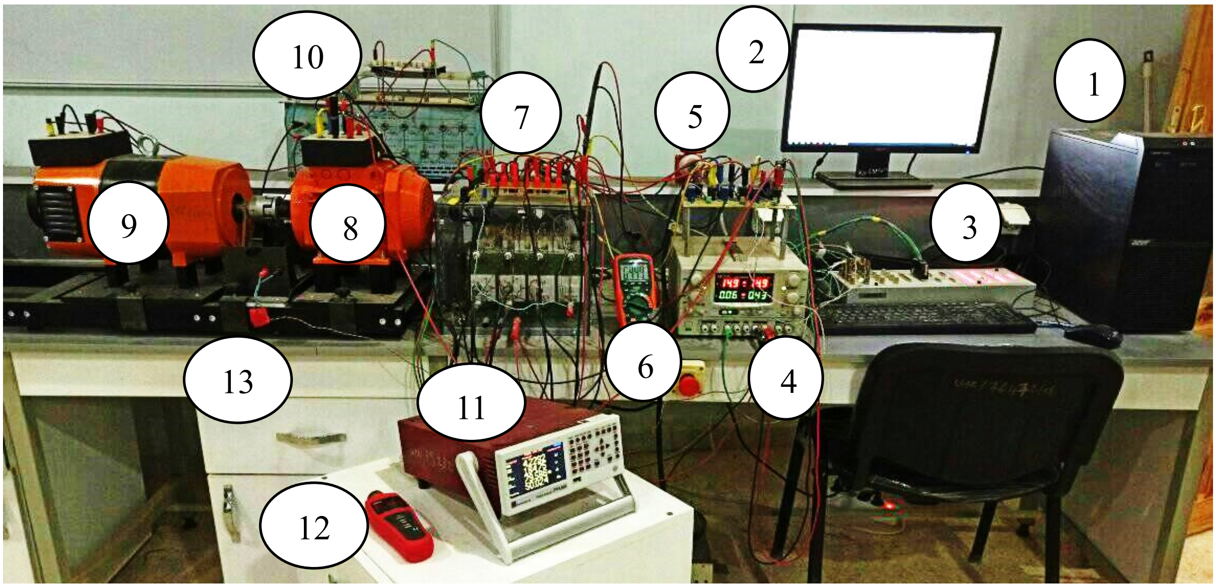

Figure A. 1: Experimental setup.

1. PC, 2. PC screen, 3. dSPACE 1104, 4.DC power supply, 5. Current and voltage sensor, 6.Multimeter, 7. Voltage inverter, 8. Induction motor, 9.DC machine, 10.load, 11.Power analyzer, 12 Tachometer, 13. Tachometer generator (speed sensor).

A.2 dSPACE 1104:

The DS1104 R&D Controller Board converts a Computer into a development system, allowing for fast control prototyping. The board is compatible with almost any Computer that has a free PCI or PCIe slot [1].

Figure A. 2: dSPACE 1104 Controller Board.

Figure A.2 depicts the dSpace DS1104 controller board. The DS1104's main CPU is an MPC8240 with a 250 MHz PowerPC 603e core. It has 8 MByte of boot flash memory for software and 32 MByte of synchronous DRAM (SDRAM) memory.

dSPACE 1104 interface board shown in figure A.3 contain the element below:

1. ADC ports, 2. DAC ports, 3. Digital I/O, 4. Slave I/O for PWM, 5. INC ports, 6. Light indicators.

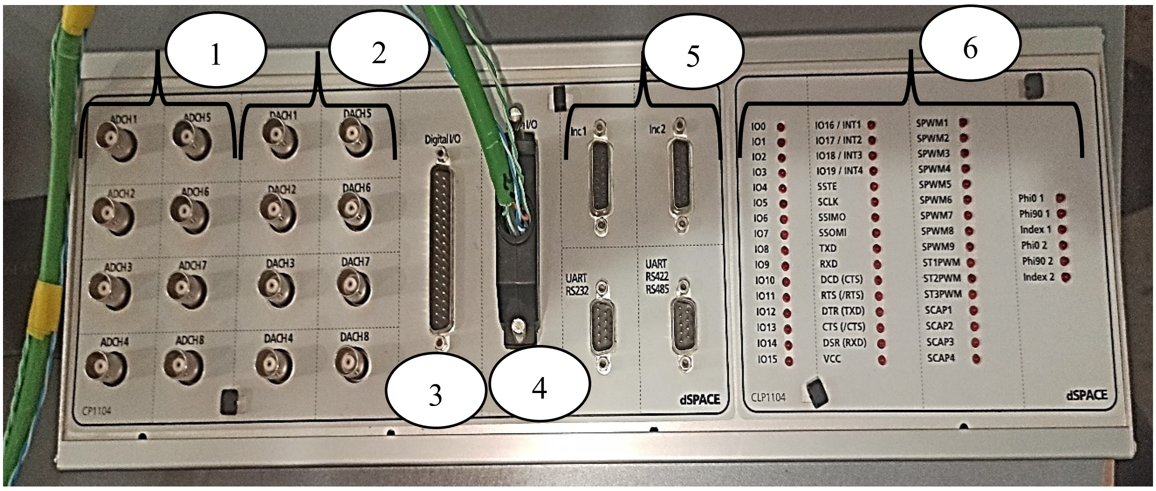

Figure A. 3: dSPACE 1104 interface board.

A.3 Characteristics of induction machine:

The characteristics of the induction machine used given by the manufacturer are:

TABLE A.1
INDUCTION MOTOR PARAMETERS

Symbol	Quantity	Value (SI)
P	Nominal power	1.1 (*KW*)
N_s	Nominal speed	1437 (*rpm*)
R_s	*stator resistance*	4.8 (Ω)
R_r	Rotor *resistance*	*5.4* (Ω)
L_s	*Stator* inductance	0.5636 (*H*)
L_r	Rotor inductance	0.5636 (*H*)
L_m	Magnetizing inductance	0.4915 (*H*)
J_L	Inertia	0.0023 ($kg.m^2$)
p	Number of poles pairs	2

A.4 Sensors module :

The design of a "sensor card" module presented in the figure below can deliver an image voltage proportional to the three real currents of the induction machine and the DC bus voltage.

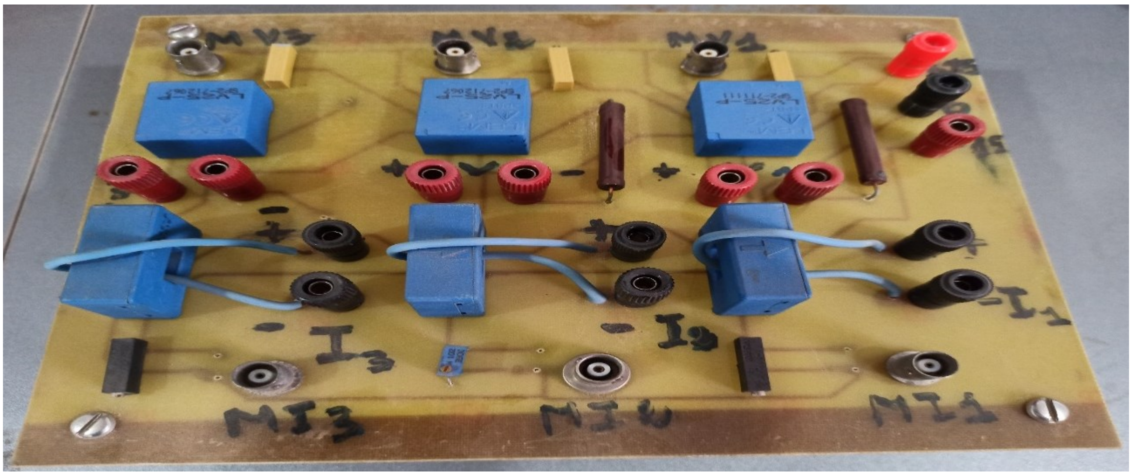

Figure A. 4: Top view of the sensor board.

A.4.1 Current sensor:

LEM's LA25-NP current sensors can resist a maximum current of 36 A. These sensors are used to measure the currents, which cross the stator phases of the induction machine.

A resistor is used between the ground and the sensor output where the voltage will be proportional to the input current between the terminals of this resistor to have a voltage at its terminals.

Figure A.5 describes the current sensor pinout.

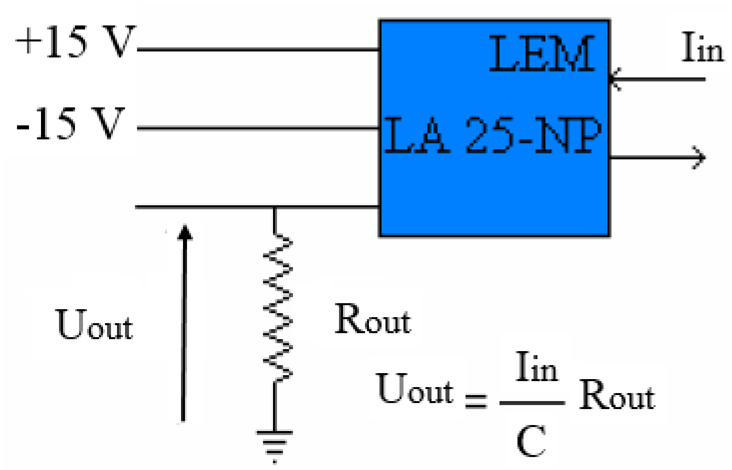

Figure A. 5: The current sensor pinout.

A.4.2 Voltage sensor:

LEM's LV25-P voltage sensors can resist a maximum current of 10 mA. These sensors are used to measure the stator phase voltages of the induction machine.

To limit the maximum input current to 10 mA, these sensors are connected to the phases by a high value resistor (Figure A.6).

Figure A.6 describes the voltage sensor pinout.

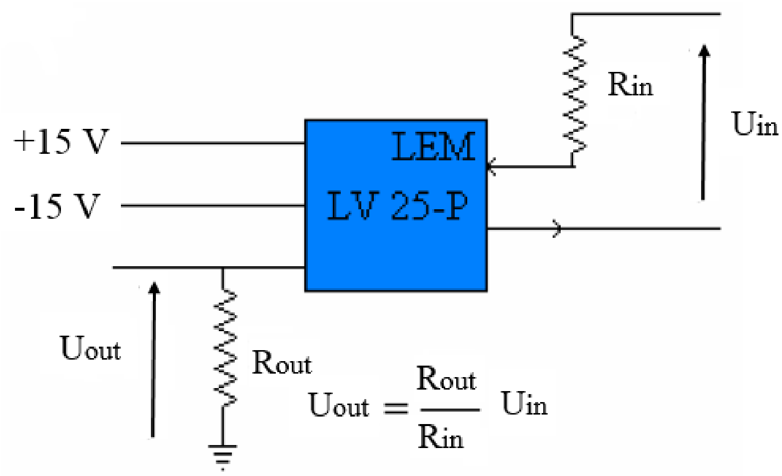

Figure A. 6: The voltage sensor pinout.

References

[1] https://www.dspace.com/fr/fra/home/products/hw/singbord/ds1104.cfm#179_24555.